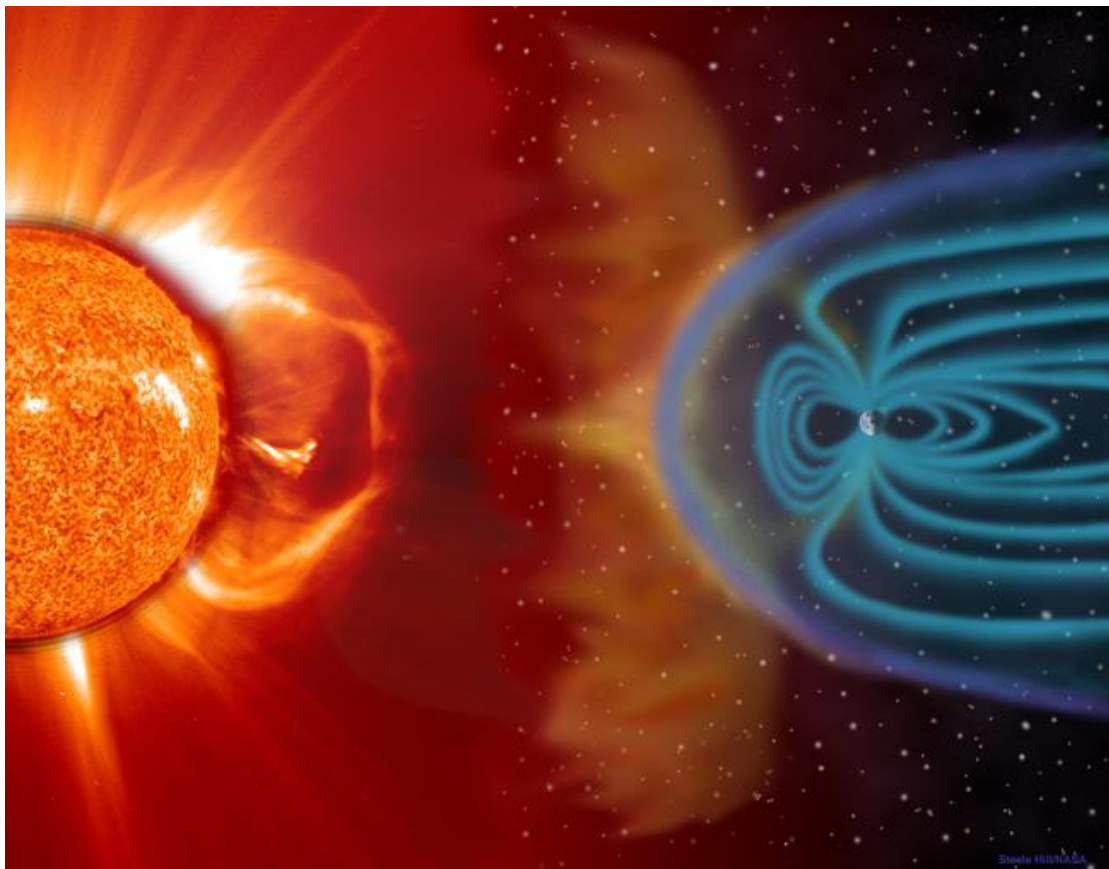


**A LOW FREQUENCY RADIO TELESCOPE
FIRST RESULTS OF SOLAR OBSERVATIONS**



Ioannis Myserlis

Aristotle University of Thessaloniki
Department of Physics
Section of Astrophysics, Astronomy and Mechanics
DIPLOMA THESIS
February 2011

**A LOW FREQUENCY RADIO TELESCOPE
FIRST RESULTS OF SOLAR OBSERVATIONS**

Ioannis Myserlis

Supervisors:

**Professor John H. Seiradakis, Aristotle University,
Thessaloniki, Greece**

**Professor Ulrich Klein, University of Bonn, D-53121,
Bonn, Germany**

Aristotle University of Thessaloniki
Department of Physics
Section of Astrophysics, Astronomy and Mechanics

Abstract

This Diploma thesis is divided into four chapters.

Chapter one is a short introduction to the science of Radio Astronomy. It includes a brief history of the first steps of Radio Astronomy and a description of the basics of radio telescopes. Finally new developments of low frequency Radio Astronomy are mentioned.

In the second chapter, I describe the sources of the radio sky that we should be able to observe with the 20.1 MHz radio telescope that we constructed. At these meter-wavelength frequencies the ionosphere can obscure our observations and a description of its influence is also included in this chapter.

In the third chapter, I describe the whole procedure of the construction of our radio telescope. The antenna and receiver we used are based on the NASA's Radio Jove project design with a few changes. I describe also the software we used for the system to work as a monitoring station that collects data continuously. Finally, the chapter includes a description of the calibration procedure that we followed to make the system work not only in a qualitative but also in a quantitative manner.

In the last chapter, I describe the actual observations we conducted with our radio telescope and the method we used to verify them with other observations in the same or different frequencies. I also describe the natural or manmade interference that made our observations at this frequency difficult.

Thessaloniki, February 2011

Table of Contents

Chapter 1: Introduction	1
1.1 Radio Astronomy	1
1.2 A brief history of Radio Astronomy	4
1.3 Radio telescopes	10
1.4 Low frequency Radio Astronomy.....	17
Chapter 2: Thesis target radio sources	19
2.1 The radio sun.....	19
2.2 The quiet sun	23
2.3 The disturbed sun	24
2.3.1 The slowly varying component	24
2.3.2 The rapidly varying component	24
2.4 Influence of the ionosphere	28
2.5 Jovian decametric radiation	29
Chapter 3: Technical Aspects	35
3.1 Antenna description and characteristics	35
3.2 Receiver design and specifications.....	42
3.3 Software.....	48
3.4 System calibration	52
3.4.1 Frequency calibration	52
3.4.2 The antenna temperature calibration.....	55
Chapter 4: Observations and Results	59
4.1 Verification of an observation.....	59
4.2 Sources of interference.....	64
4.3 Solar observations	65
4.4 Jovian observations.....	73
4.5 Conclusions.....	76

Acknowledgements

There are many people I would like to thank for their help without which I couldn't write this Diploma thesis.

First of all, I would like to thank my parents for everything they did for my upbringing and education and for their support on every decision I take in life.

Everything I could write would be too little for my Supervisor Professor John H. Seiradakis of the Aristotle University of Thessaloniki (AUTH). His guidance and advice were vital for every part of this project. I would like to thank him for being there every time I wanted his help and for the sharing of my joy every time I conducted a successful observation. I would also like to thank my second supervisor Professor Ulrich Klein of the Argelander Institute for Astronomy (AIfA) of the University of Bonn, Germany, for his help on the project and his guidance for the construction of the receiver which was done during my stay in Bonn with the ERASMUS exchange program.

This thesis included a lot of technical work for the construction and installation of the low frequency radio telescope. None of this would be done without the help of the staff of the Electronics Lab of the Argelander Institute for Astronomy (AIfA) and especially Philipp Muller whose advice was crucial for every part of the receiver construction. I couldn't construct and set up the antenna without the help of Evangelos Tsorlinis of the Aristotle University of Thessaloniki (AUTH) and also I couldn't calibrate the receiver without the vital ideas of Professor Theodoros Laopoulos of the Electronics Lab of the Aristotle University of Thessaloniki.

There are many friends and colleagues I would like to thank for their help and support on the project, especially Vasillis Karamanavis, John Vakoulis and Alexandros Dimaratos for their help to set up the antenna. I would like to express my appreciation for many staff members of the Physics Department of the Aristotle University of Thessaloniki (AUTH), the Argelander Institute for Astronomy (AIfA) and the Max Planck Institute for Radioastronomy (MPIfR), Bonn because they helped me with my thesis and my stay in Germany. To name a few, I would like to thank Manolis Angelakis of the MPIfR for his help during my stay in Bonn, John Morgan for the discussions we had on radio interferometry, Kosmas Lazaridis and John Antoniadis for their advices and ideas on the project.

Finally, I would like to thank everyone (and there are many) who were interested and had the patience to hear about this project and share their ideas with me and also the captain of my company at the 646 Mechanized Infantry Battalion, Neofytos Kaltsidis, because without his help I couldn't write this diploma thesis during my military duty service at Komotini, Greece.

Chapter 1

Introduction

1.1 Radio Astronomy

Radio Astronomy is the branch of Astronomy that studies the sky in the radio window of the electromagnetic spectrum. Although it is a relatively new kind of Astronomy, it is also the first one that expanded our horizons in different wavelengths than the optical window in which we conducted all our astronomical observations until then. This is the reason why we consider the birth of Radio Astronomy a huge breakthrough in the history of Astronomy, since it helped us understand and look out for different views of the universe and hence explain the physical phenomena that we observe better.

When we take a look at the electromagnetic spectrum in relationship to Earth's atmospheric opacity, as it is shown in Figure 1.1 below, it is easy to understand why the radio window was the first to broaden our perspective in the universe after the optical one.

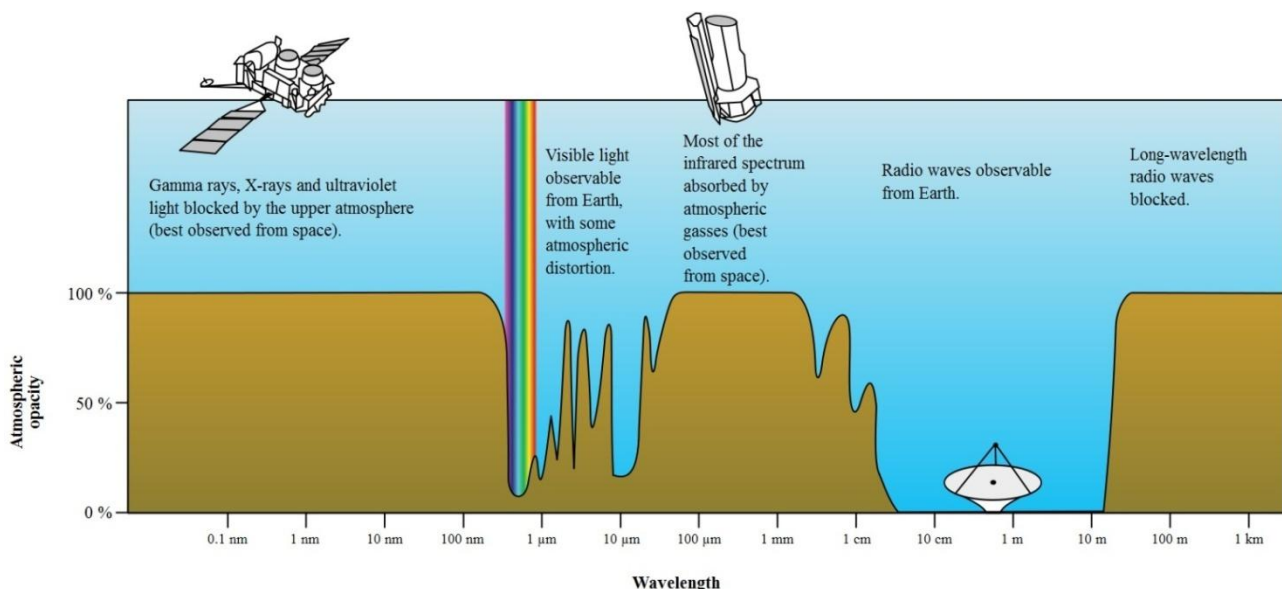


Figure 1.1: Electromagnetic spectrum showing relative opacity of the Earth's atmosphere and ionosphere.

It is the main part of the electromagnetic spectrum that can be viewed from the surface of the Earth. Observations in other parts of the electromagnetic spectrum require high

altitude constructions or even satellites that fly in orbit, away from the obscuring effects of Earth's atmosphere and ionosphere.

The radio window extends from about 1 cm to 10 m in wavelength but these limits are not well defined. Because of some relatively transparent bands in the millimeter region, especially at high altitudes, and occasional ionospheric “holes” at decameter wavelengths, the limits of the radio window can be extended to 1 mm and 100 m respectively. Observations in such a variety of wavelengths demand also a variety of radio telescopes. That is the reason why low frequency radio telescopes are so much different than high frequency ones. The short-wavelength limit of the radio window is defined by the Earth's atmosphere. It is a function of the atmospheric composition, cloud coverage and mainly the percentage of water vapour that is present in the atmosphere at the time and place of the observation. The long-wavelength limit of the radio window depends on the electron density of the ionosphere. This electron density is mainly a function of solar activity and time of the day.

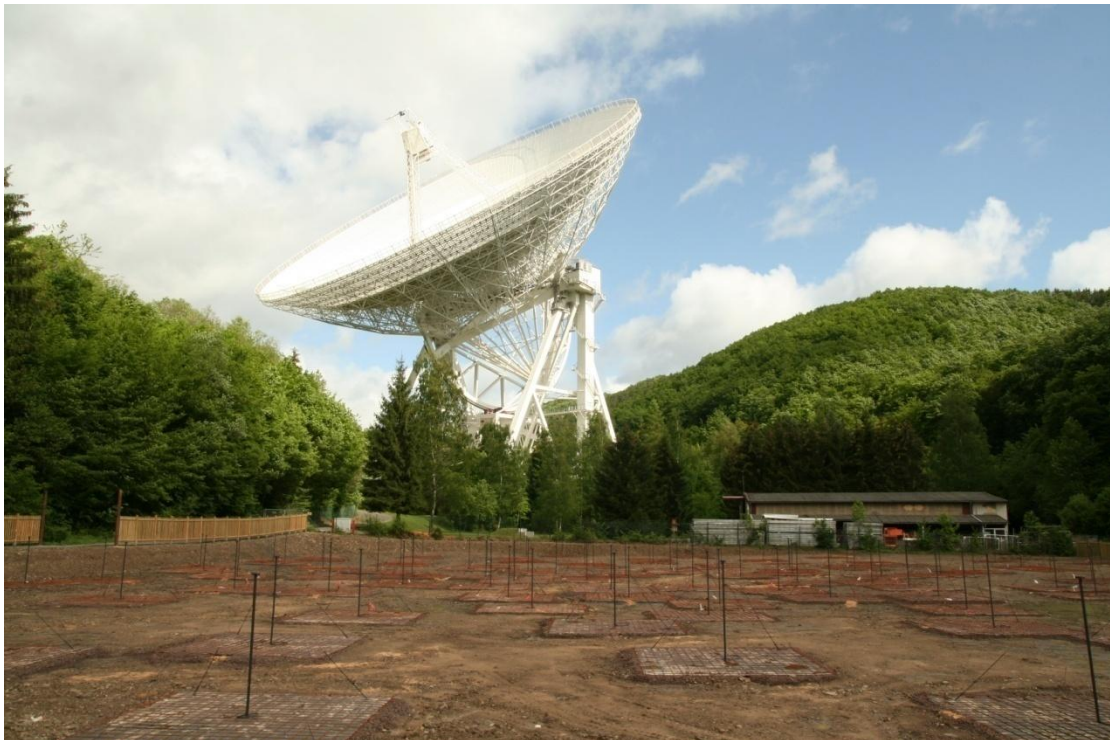


Figure 1.2: The Effelsberg observing site near Bonn, Germany. We can see the difference between a high frequency radio telescope in the background and a low frequency one in the foreground of the photograph.

Today, all around the globe, there are many radio telescopes that cover many parts of the radio window of the electromagnetic spectrum. Also, there is a considerable effort going on to build new and more capable radio telescopes especially for receiving radio waves at the limits of the radio window. Such projects are the A.L.M.A. (Atacama Large Millimeter Array) project at the short wavelength limit and the L.O.F.A.R. (Low Frequency Array) project at the long wavelength limit. The observations that we carried out for this thesis were conducted with a low frequency telescope that we constructed which can receive radio waves at a small bandwidth of frequencies around 20.1 MHz.



Figure 1.3: Three of the antennas that are being installed for the ALMA project.



Figure 1.4: A dipole antenna of the low frequency band of the LOFAR project.

1.2 A brief history of Radio Astronomy

The first radio astronomical observations were conducted by a young scientist named Karl G. Jansky in 1931 who was working for a completely different project at the time. Jansky was working in New Jersey, U.S.A. for the Bell Telephone Laboratories and he was assigned the task of studying the radio “static” that could affect transatlantic communications. To do that, Jansky built an antenna which could receive radio waves at the frequency of 20.5 MHz (wavelength $\lambda = 14.6\text{ m}$) with fair directivity. To study waves coming from every direction, Jansky placed his antenna on four wheels that could move on a circular track and thus rotate the antenna.

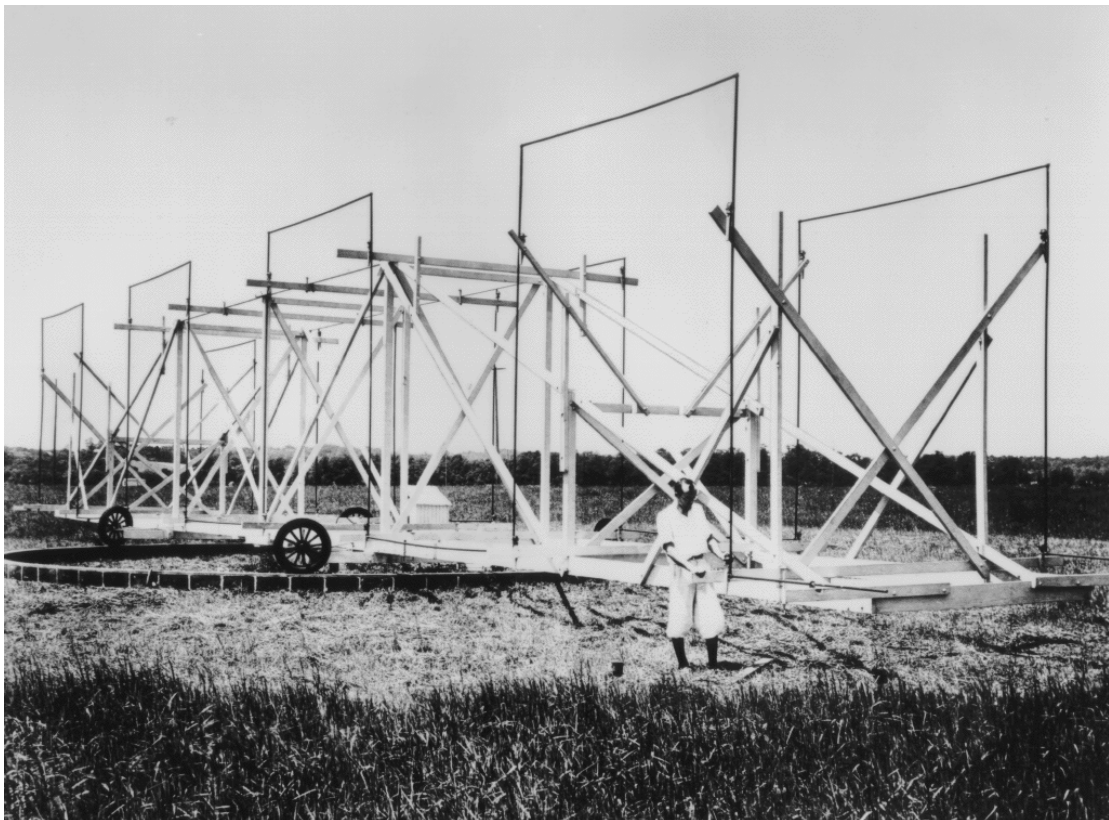


Figure 1.5: Karl G. Jansky with his famous antenna.

The results from Jansky’s experiment showed that his antenna was receiving three groups of static. The first one was coming from nearby thunderstorms, the second one from distant thunderstorms and finally there was a third group of static that its origin was unknown. This third group of static seemed to be periodic with a period of almost a day. This made Jansky suspect the sun as the signal’s origin, but later on a more precise look at the measurements showed that the static was delayed for about 4 minutes every day. This is a clear sign for an astronomer that the radiation’s origin is located outside our solar system. Furthermore, Jansky’s experiment showed that the third group of static, the “cosmic” static as he named it, was coming from a region in the sky which is in the vicinity of the galactic center. Today, we know that Jansky, with his famous experiment, discovered the synchrotron radiation that is emitted from relativistic

electrons spiraling in the galactic magnetic field. It is a pity that the experiment was conducted during a minimum of solar activity. If he continued his observations for a few years more, he would definitely discover radio waves coming from the sun too. Unfortunately, Bell Telephone Laboratories transferred Jansky in another research activity and many years passed for another radio observation to show up.

The person who took great interest in Jansky's discovery and continued his work some years later was Grote Reber. He was a radio engineer and an amateur astronomer living in Wheaton, Illinois. In 1937, Reber built a parabolic reflector antenna with a diameter of 9.5 meters in his backyard to continue the observations of the radio sky. At first, he built a high frequency receiver, working at 3.3 GHz, because at the time the only radiation mechanism known was the Planck's blackbody radiation emission. According to Planck's theory, the radiation that a blackbody of known temperature emits should be stronger at higher frequencies. That is why Reber expected to detect a stronger signal in higher frequencies and built such a receiver.

After getting negative results at that frequency, he built more receivers working in lower frequencies. Although he wasn't getting any positive results in any of them, he continued his work believing that he would start to get something at some point. Finally, at the frequency of 160 MHz his hard work started to pay off. Reber detected successfully radio waves emitting from the plane of the Galaxy in the sky. Although the angular resolution of his observations was relatively poor, about 12° , Reber successfully published the first map of the radio sky at 160 MHz.

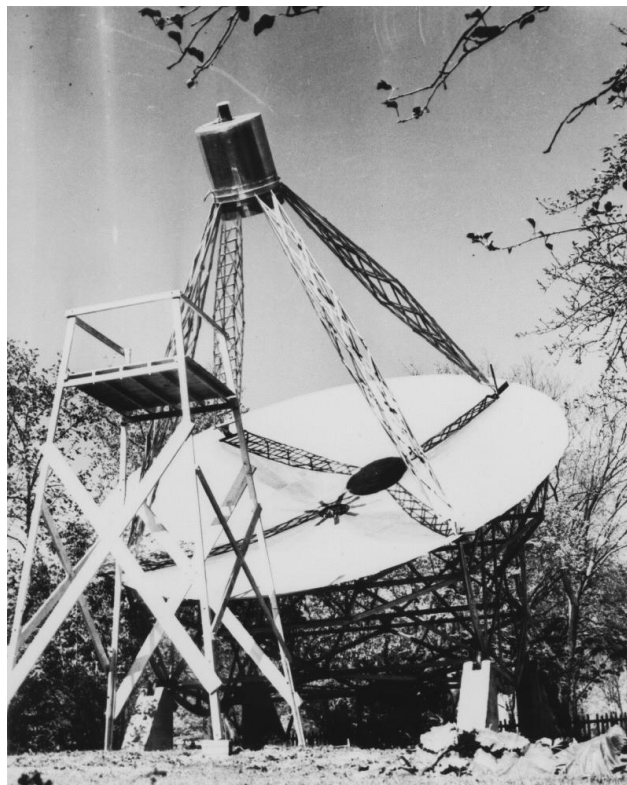


Figure 1.6: The parabolic reflector antenna that Grote Reber built in his backyard.

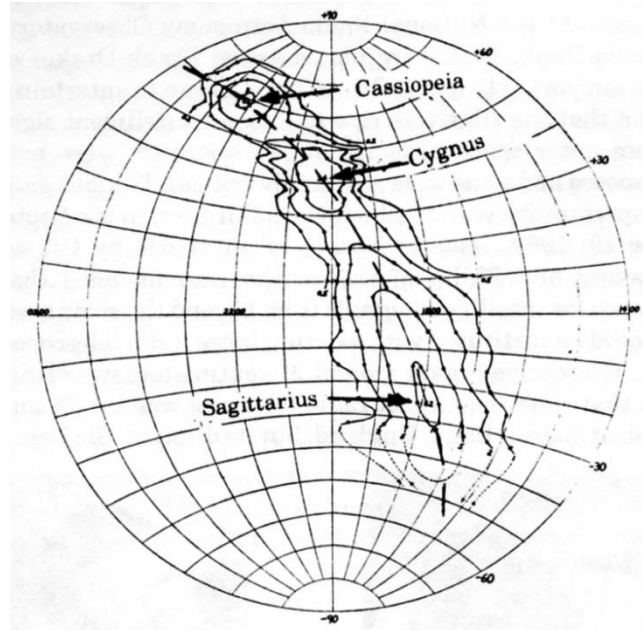


Figure 1.7: First map of the radio sky as produced by Grote Reber showing strong sources of radiation in Cassiopeia, in Cygnus and in Sagittarius, the center of the galaxy, the region from which Karl Jansky had detected radio emission.

The technological advancement that took place during World War II for military reasons played a role of great importance in the evolution of Radio Astronomy. For example, during World War II, British scientists under the guidance of Stanley Hey received strong interference at their radar system which they built to detect German aircrafts and V1 or V2 rockets. Later on, they realized that the interference was “static noise” coming from the sun.

Near the end of the War, in 1944, a young scientist from Leiden, Holland, named Hank van de Hulst, under the guidance of professor Jan H. Oort suggested that a monochromatic line radiation could be detected in radio waves. This line radiation has a rest frequency of 1420 MHz (wavelength $\lambda = 21.1 \text{ cm}$) and its emission is caused by a transition between two closely separated energy levels of the ground state of neutral hydrogen related to the electron – nucleus spin orientation. This transition is also called neutral hydrogen hyperfine structure.

The detection of this line emission on March 25 1951 by Ewen and Purcell at Harvard University marked a great moment of Radio Astronomy history. A radiowave line emission is a very powerful tool in the study of interstellar medium due to its insignificant absorption of radiowaves. The first observations that helped astronomers to study the structure of our Galaxy were conducted with the help of the 21cm line emission of its interstellar medium. This line emission also helps us understand the interaction of visibly unrelated galaxies.

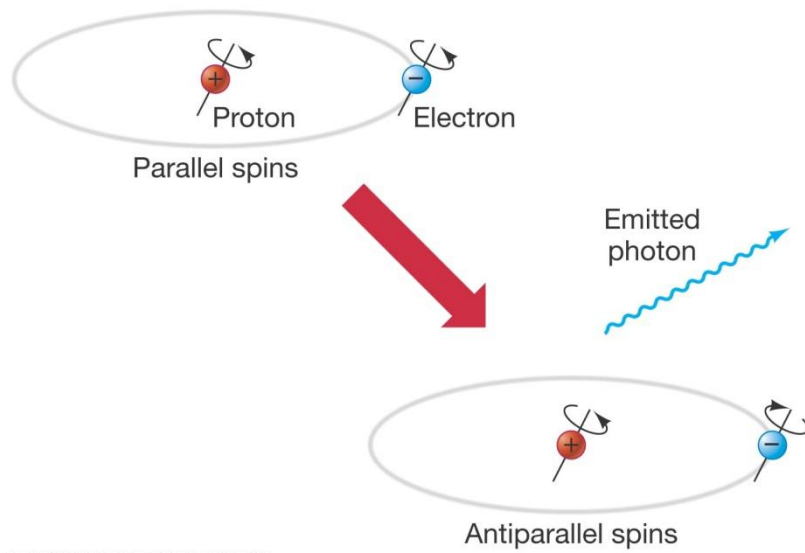


Figure 1.8: 21 cm line emission mechanism – Neutral Hydrogen’s hyperfine structure.

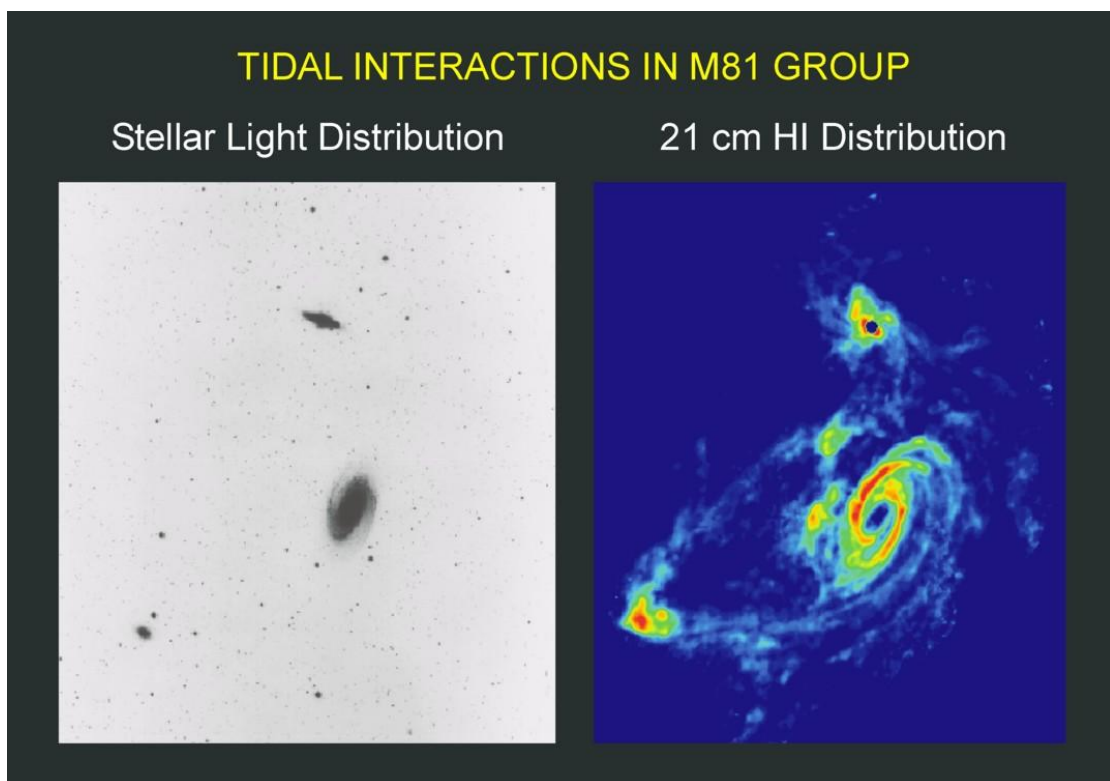


Figure 1.9: The streamers visible only in the 21 cm line emission clearly demonstrate that the M81 group is an interacting system of galaxies.

In the same year, Francis Graham Smith detected for the first time a radio “point source”, a radio source of small angular extent. Smith found this strong “point source” in the constellation of Cygnus using interferometric techniques. This source, which would later be named Cygnus A, is the third strongest radio source in the sky at the frequency of 178 MHz. Today we are capable to study the structure of many radio sources in the sky, including Cygnus A, with the help such interferometric or aperture synthesis techniques,.

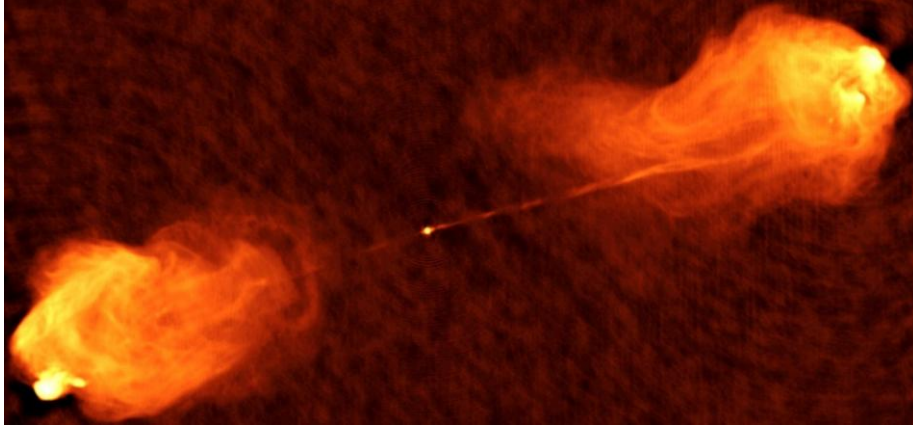


Figure 1.10: The radio galaxy Cygnus A.

The development of the science of Radio Astronomy was very rapid in the years that followed. Many countries contributed in this development, such as Australia, U.S.A., Soviet Union, France, Holland, India, Germany and Canada. Any new information we got from the radio sky contributed to many discoveries of modern Astronomy and Physics in general. Some of these great discoveries are listed below.

In 1963, a new kind of “stars” was discovered by optical astronomers who tried to detect strong radio sources in the optical window of the electromagnetic spectrum. These stars were named quasi-stars, or else quasars. Later on, it was found that quasars are in fact distant radio galaxies which are as old as the Universe itself.



Figure 1.11: A quasar as painted by an artist.

In 1967, Jocelyn Bell, a postgraduate student in the University of Cambridge, under the guidance of Antony Hewish discovered a new kind of stars using radio observations. These stars were named pulsars because of the repeating radio signals that they emit in the form of pulses, with high temporal precision. Pulsars helped us understand the physical phenomena that take place during the final stages of a star's life and also help us understand and test modern theories of Physics.

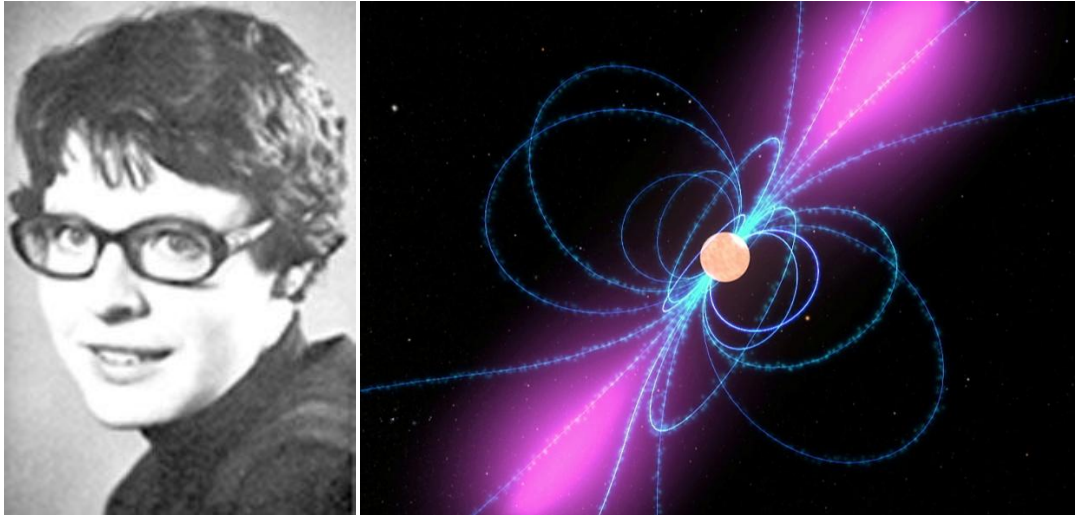


Figure 1.12: Young Jocelyn Bell and an artist's impression of a pulsar.

In 1965, Arno Penzias and Robert Wilson, accidentally discovered an isotropic radiowave radiation coming from anywhere in the sky while they were testing the antenna they built for satellite communication experiments. The spectrum of this radiation is almost identical to that of a blackbody with a temperature of 2.75 K and its maximum is located at the wavelength of 1 millimeter. The discovery of this radiation, known today as the Cosmic Microwave Background Radiation (CMBR), is the best observational proof of the Big Bang theory. It is considered to be the thermal radiation that was emitted from the Big Bang that created our Universe, the temperature of which is descending since then with a current value of 2.75 K.

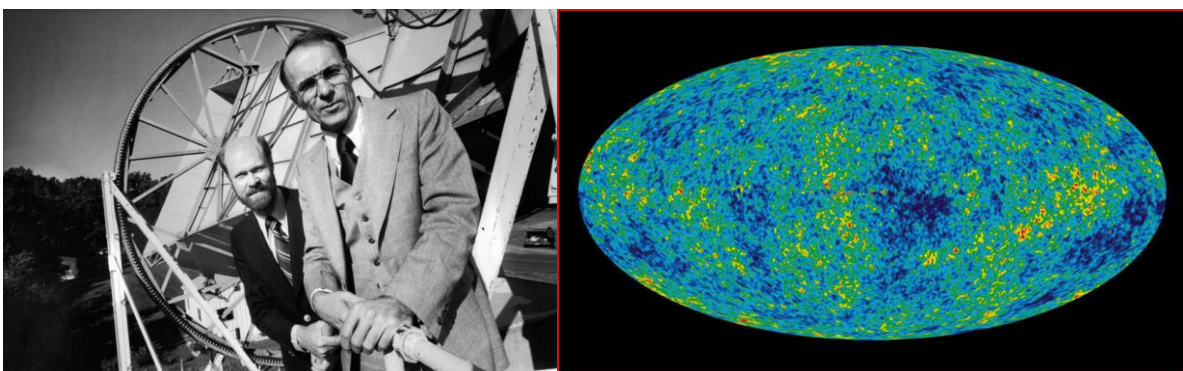


Figure 1.13: Arno Penzias and Robert Wilson with their antenna and a detailed image of the CMBR taken with the WMAP satellite.

These were only a few examples of the discoveries which were made using radio telescopes. It is crucial to understand that without the advancement of technology none of these would be possible. Every new development in the technology of radio antennas

helped in the detection of extremely faint extraterrestrial radio signals and also improved the resolving power of Radio Astronomy facilities. Today the radio sky has been successfully mapped in many frequencies and is continuously being observed, waiting for new amazing discoveries to come up. Finally, all these great discoveries were made possible using only a little bit of the energy we get from the Universe. Since the birth of Radio Astronomy, the whole amount of energy that has been gathered from all radio telescopes all around the globe is less than the energy that is carried from a falling snowflake!

1.3 Radio Telescopes

Radio telescopes are the devices which we detect radio signals with, coming from various celestial sources. The main parts of a radio telescope are the radio antenna, the transmission line and the receiver of the telescope. The antenna, through its feed, collects the power of the celestial radio signal and preamplifies it. The transmission line is usually a cable that transfers the preamplified signal to the receiver of the telescope where it is amplified again, detected and integrated over a predefined amount of time. Digital recording devices keep a log of the final output of the system for further use.

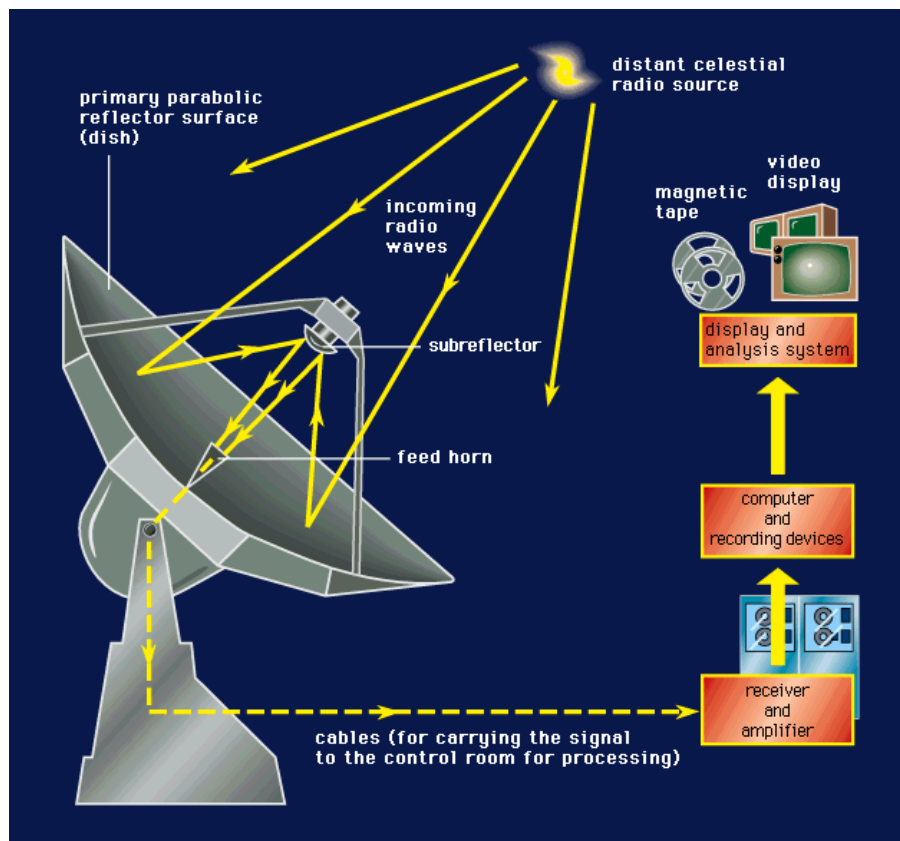


Figure 1.14: The structure of a Radio Telescope.

A radio telescope antenna collects celestial radio waves at its feed point. Its function is similar to that of the lens or mirror of an optical telescope. The collecting ability, or else the response, of an antenna as a function of the direction of the incident

radio wave is demonstrated by the antenna pattern. This pattern does not depend on the distance from the antenna as long as it is greater than the radius of its Fraunhofer region. The antenna pattern outside this region is called far-field pattern and is usually the case for radio telescope antennas since they detect signals coming from celestial bodies.

The antenna pattern of a radio telescope usually has a form similar to that in Figure 1.15. It is made up by a number of lobes. The largest lobe is called the main lobe of the radio telescope and it usually rests on its axis of symmetry. The rest of the lobes are called side and back lobes depending on their position in the antenna pattern. In order for a radio telescope to collect radio signals better, its main lobe should be as big as possible compared to its side and back lobes. The main lobe of modern radio telescopes is about 1000 times larger than their side lobes.

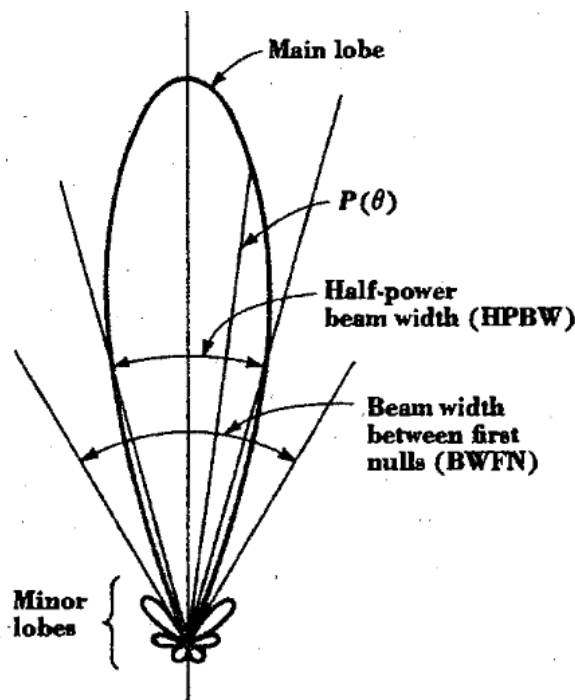


Figure 1.15: The antenna pattern of a radio telescope antenna.

Another important parameter of the antenna pattern is its main lobe's beam width. That is the angular extent of its main lobe. The narrower the beam width, the better for the radio telescope to detect two closely separated radio sources in the sky. The smallest angular distance of two celestial sources separately detected by a radio telescope is called the angular resolution of the telescope. The resolving power of a radio telescope is defined by the angular extent of the main lobe at half its power. This angle is called Half Power Beam Width (HPBW). In order to calculate the angular resolution of parabolic shaped antennas, we can use the Rayleigh criterion, also used for optical telescopes. So, the angular resolution of a parabolic antenna is

$$\theta_A = 1.22 \frac{\lambda}{D}$$

where λ is the observing wavelength, D is the diameter of the telescope and the angular resolution is measured in radians.

If we describe the antenna pattern of a radio telescope as a function of the angle between the direction of the incident radio wave and the main axis of the pattern, $P(\theta, \varphi)$, the total response of a radio telescope is given by the following integral

$$\Omega_A = \int_{4\pi} P(\theta, \varphi) d\Omega$$

where Ω_A , or the beam solid angle as it is called, is measured in rad^2 . The beam solid angle is defined as the angle through which all the power from a transmitting antenna would stream if the power were constant over this angle and equal to the maximum value of the antenna pattern. If we integrate the function of the antenna pattern over the main lobe only, we get the main beam solid angle Ω_M .

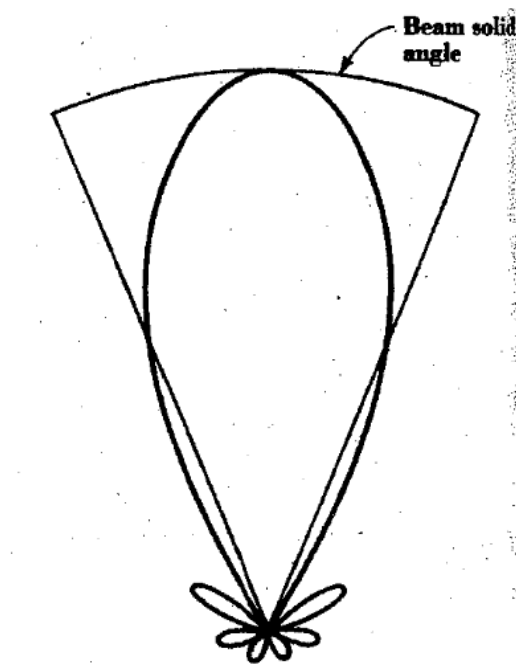


Figure 1.16: A comparison of the beam solid angle with the antenna pattern of a radio telescope.

Another useful quantity concerning radio telescope antennas is their directivity. It is equal to the solid angle of a sphere divided by the antenna beam solid angle

$$D = \frac{4\pi}{\Omega_A}$$

Directivity is defined as the ratio of the maximum radiation intensity to the average radiation intensity of a transmitting antenna. Using the electromagnetic theory, it is easy to derive the following equation for the beam solid angle of a radio telescope

$$\Omega_A = \frac{\lambda^2}{A_e}$$

where A_e is the effective aperture of the telescope, usually smaller than its geometric one. As a result, the directivity of a radio telescope can also be expressed by the following equation

$$D = \frac{4\pi}{\lambda^2} A_e$$

Finally, the gain of a radio telescope antenna is given by

$$G = k_{sys} D$$

where k_{sys} is the efficiency of our system, meaning the antenna's ability to transform the incoming radiation into signal power in the radio telescope receiver.

As mentioned above, radio telescope antennas receive electromagnetic radiation emitted from celestial radio sources. The strength of these sources is measured by their total flux density which is the power we receive from the source per unit area of collecting surface per unit bandwidth of receiving frequency. The flux density is measured in $Watts \cdot m^{-2} \cdot Hz^{-1}$ in the S.I. measuring system but this unit is extremely large compared to the power we receive from the celestial radio sources. It is better to use a smaller one and that's the reason why we have defined another unit called the Jansky (Jy) in memory of the father of Radio Astronomy. One Jansky is equal to $10^{-26} Watts \cdot m^{-2} \cdot Hz^{-1}$ by definition.

If the angular size of the source is bigger than our telescope's HPBW, we can resolve it. In this case, the radio telescope observes an extended radio source. This means that the flux density coming from a certain point of the source can be measured. This flux density is called brightness and it is easy to understand that the brightness distribution of a radio source is measured in $Watts \cdot m^{-2} \cdot Hz^{-1} \cdot rad^{-1}$.

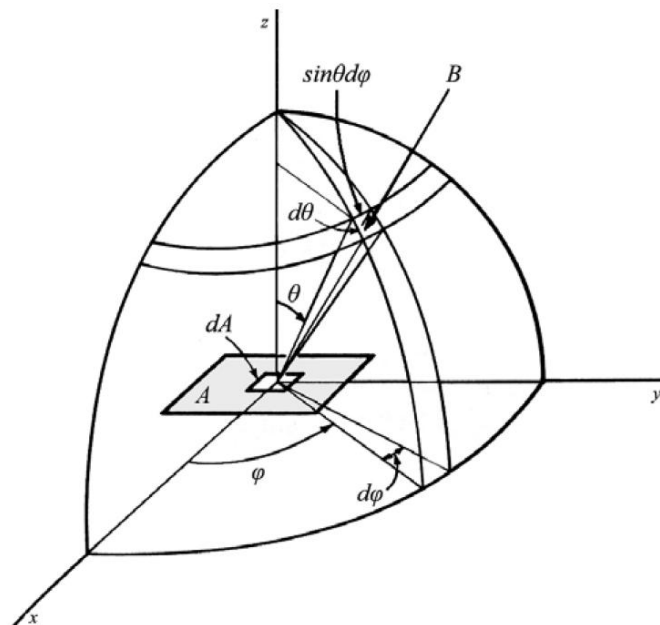


Figure 1.17: Basic quantities for the study of electromagnetic waves transmission.

Using the definitions above, it is now trivial to derive some useful equations. First, the total flux density of an extended source in a certain frequency is equal to

$$S_\nu = \iint B_\nu(\theta, \varphi) d\Omega$$

where $B_\nu(\theta, \varphi)$ is the brightness distribution of the source and the integration is over the total angular extend of the source. The flux density we get from the same radio source should be different for different radio telescopes because each antenna has its own response pattern. If we take into consideration the antenna pattern of the radio telescope, the flux density of the source is now equal to

$$S_\nu = \iint B_\nu(\theta, \varphi) P(\theta, \varphi) d\Omega$$

where $P(\theta, \varphi)$ is the antenna pattern of the telescope. The total power we receive from a celestial radio source per unit frequency is then

$$W_\nu = A_e \iint B_\nu(\theta, \varphi) P(\theta, \varphi) d\Omega$$

where A_e is the effective aperture of the telescope.

According to antenna theory, we can resemble a radio antenna with a resistor. The temperature of a resistor induces an electric current of intensity i due to the Brownian motion of its electrons. The mean value of this intensity is zero but the mean value of its square $\langle i^2 \rangle$ isn't. This means that the resistor produces some power which is related to its temperature. According to Planck's law, the power that is produced from a resistor of temperature T is

$$W dv = \frac{h\nu dv}{e^{h\nu/kT} - 1}$$

where h is Planck's constant, k is the Boltzmann's constant and dv is the frequency bandwidth. For radio astronomical sources the product $h\nu$ is always much smaller than the product kT , thus the denominator of the previous equation can be written as

$$e^{h\nu/kT} - 1 \approx 1 + \frac{h\nu}{kT} - 1 = \frac{h\nu}{kT}$$

So, the power that is produced from a resistor of temperature T , in low frequencies, is

$$W dv = kT dv$$

The equation above is an expression of the Nyquist theorem for thermal resistors and it is also valid for radio antennas.

This means that the antenna temperature T_A , which is also called noise temperature, is proportional to the power of the received signal and furthermore to the

flux density of the observed radio source. To avoid any confusion, the antenna temperature has nothing to do with the actual, physical temperature of the antenna and depends only on the radiation intensity that an antenna receives. It is convenient to describe the signal power we get from celestial radio sources in terms of antenna temperature. In theory, we could replace the antenna with a resistor and vary the temperature of the resistor until the noise power it produces matches the noise power from the celestial radio source. When the noise power levels match the value of the temperature of the resistor is equal to the corresponding antenna temperature.

The transmission line of a radio telescope delivers the signal received by the radio antenna to the receiver system of the radio telescope. It is usually in the form of coaxial cable and similar to the cables that radio engineers use for signal processing and transmission. A coaxial cable uses a metal core and a metal shield as the two wires of the transmission line separated by a layer of insulating material and has the geometry of a cylindrical capacitor.

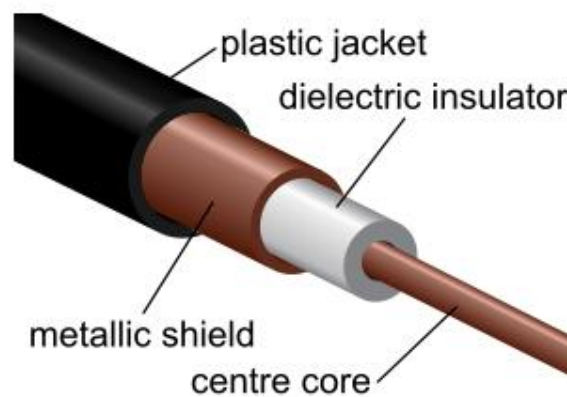


Figure 1.18: The structure of a coaxial cable.

The receivers of radio telescopes detect and measure the signal transmitted to them from radio antennas. The signal that a radio antenna receives from a celestial radio source is in the form of noise. This means that it has a frequency spectrum and random amplitude and phase variations. These variations have a Gaussian distribution around zero and when a receiver averages the signal in time without any processing, it wouldn't detect any information. The rectification of the incoming signal is the answer to this problem and it also ensures us that the output signal of the receiver is proportional to the power of the celestial radio source.

There are many radio telescope receiver types but the most common one is the superheterodyne receiver. The architecture of such a receiver is described as follows. First, the celestial signal power that a radio telescope antenna detects is amplified with a radio frequency amplifier which has usually a gain of 10-30 dB, because as it is mentioned above it is very weak. This weak signal is mixed with a strong local oscillator signal at a frequency ν_0 producing two output signals, one with a frequency $\nu_0 + \nu_{RF}$

and another with $\nu_0 - \nu_{RF}$, where ν_{RF} is the frequency of the received signal. To avoid high frequency capacitive end effects in the receiver electronics, the second signal is selected, with a low pass filter, for the following parts of the signal processing. This output signal is called intermediate frequency (IF) signal and its power is proportional to the power of the received signal. This intermediate frequency signal is amplified with a gain of 60-90 dB.

The amplifier of the IF signal is followed by a square law detector device. This means that the detector's DC output voltage amplitude is proportional to its input voltage amplitude squared. This is the point where the received signal is rectified. Finally, the signal power is integrated over a period of time and then recorded digitally. The receiver integrates the signal for a predetermined period of time. The length of this period is usually a few seconds and we compromise between too short a period for which the output noise is overwhelming and too long, causing loss of information due to smoothing out of the celestial radio source signal into the received noise. The receiver parts following the mixer are the same for almost all the receivers. If we want to detect signals in different frequencies we only have to change the local oscillator of the mixer.

In the following Figure, we can see the block diagram of a heterodyne receiver which shows its parts and how each one of them affects the celestial radio signal, from the time it is received by the radio antenna until it is recorded by the receiver

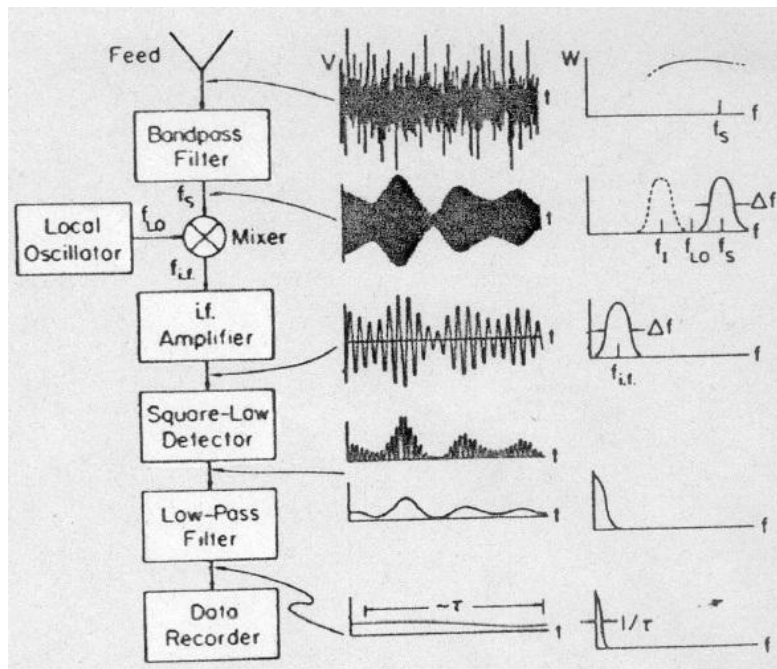


Figure 1.19: Modification of a radio-astronomical signal over various stages of a receiver.

1.4 Low frequency Radio Astronomy

Since the birth of Radio Astronomy, scientists have made only a few steps towards the exploration of the low radio frequency region of the electromagnetic spectrum. After the observations of Karl Jansky, low frequency radio astronomy has been overlooked because of the difficulty to achieve high angular resolution by the available Radio Astronomy facilities, the obscuring effects of the Earth's ionosphere and the rapid development of high frequency receiver systems after World War II. Recent developments in computer science have given us the opportunity to make the first big steps in this region of the electromagnetic spectrum and new experiments start to show up in research facilities all around the globe. Such an experiment is LOFAR (Low Frequency Array), which started in the Netherlands and is expected to give us very promising results.

New interferometric and aperture synthesis techniques are the key to achieve high angular resolution in such frequencies (10 – 300 MHz). Scattering low frequency antennas all around Europe help us lower the angular extent of the array's "main lobe" to satisfying levels. Such arrays are ideal for all-sky observations because of the huge main lobe of a single antenna but also for pinpoint observations on certain regions in the sky because of the small "main lobe" we can get after combining the received signal of all the antennas in the array with a method known as beam-forming.

Using low frequency Radio Astronomy we can explore new aspects of our Universe. One of the most interesting research projects of low frequency radio astronomy is the ability to observe the Universe as it was during the Epoch of Reionization. The 21cm line emission of the early Universe would be highly redshifted and if the redshift is of the order of 10, this line would be observed at a frequency of about 142 MHz. If we are able to observe this emission, theoretically we would be able to study the structure of our Universe as it was back in the Epoch of Reionization.

Another interesting science project is the observation of our sun in low frequencies and especially during periods of high solar activity. Solar observations in low frequencies help us understand the mechanism of solar flares that guide coronal mass ejections (CMEs) and furthermore study the connection of these observations to the solar wind. These observations would bring us a step closer in understanding and predicting space weather more accurately.

Finally, low frequency Radio Astronomy is the key to study galactic and intergalactic magnetism. Such studies would help us understand the importance of these magnetic fields in the evolution of our Universe and their contribution to cosmic energy. Answering these questions would get us closer to the solution of the dark energy problem. These are a few examples of the science we could do using low frequency observations. It is easy to understand that low frequency Radio Astronomy is an important tool in the exploration of our Universe.



Figure 1.20: The distribution of LOFAR stations all around Europe. Such great distances are required to achieve high angular resolution in low frequencies.

Chapter 2

Thesis target radio sources

2.1 The radio sun

The sun is located in the center of our solar system and it is its main energy source. The development of modern Astrophysics is based mainly on solar observations because it is the closest star to Earth and thus it can be studied in detail. The sun is a star of average size and it has a spectral type of G2V. It is a main sequence star, located towards its cooler end in the Hertzsprung – Russell diagram. The surface of the sun as seen by an optical telescope is called photosphere and has an angular diameter of about half a degree as seen from Earth. The solar atmosphere, which lies directly above the photosphere, can be divided into two parts. The chromosphere is the lower part of the solar atmosphere and it extends to a height of several thousand kilometers above the photosphere. The corona is the upper part of the solar atmosphere and it extends much higher than the chromosphere. Radio observations indicate that the corona extends much farther than a few million kilometers above the photosphere.

There are many visual surface features of the sun including sunspots, faculae and flocculi, granules and granulation, flares, spicules, prominences and filaments. Swabe, in 1843, discovered that these features of the solar surface vary greatly and these variations follow an 11-year cycle. Radio astronomers are especially interested in flares and eruptive prominences because their appearance is directly correlated with the occurrence of enhanced radio emission from the sun. This solar enhanced radio emission is also associated with the intense localized magnetic fields that appear around sunspot regions. These magnetic fields can reach a few thousand gauss in magnitude.

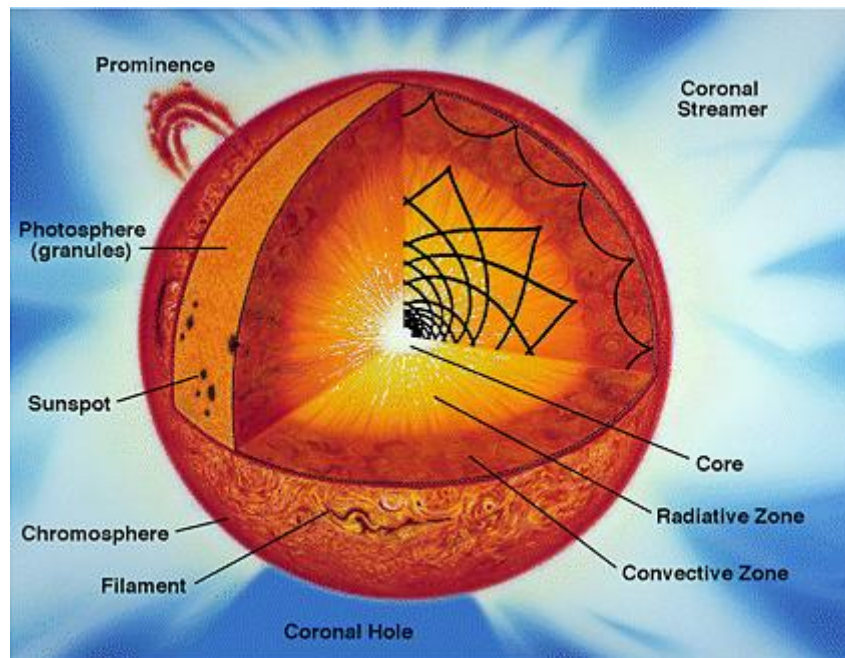


Figure 2.1: The structure of the sun and its atmosphere. Some of the sun's surface features can also be seen.

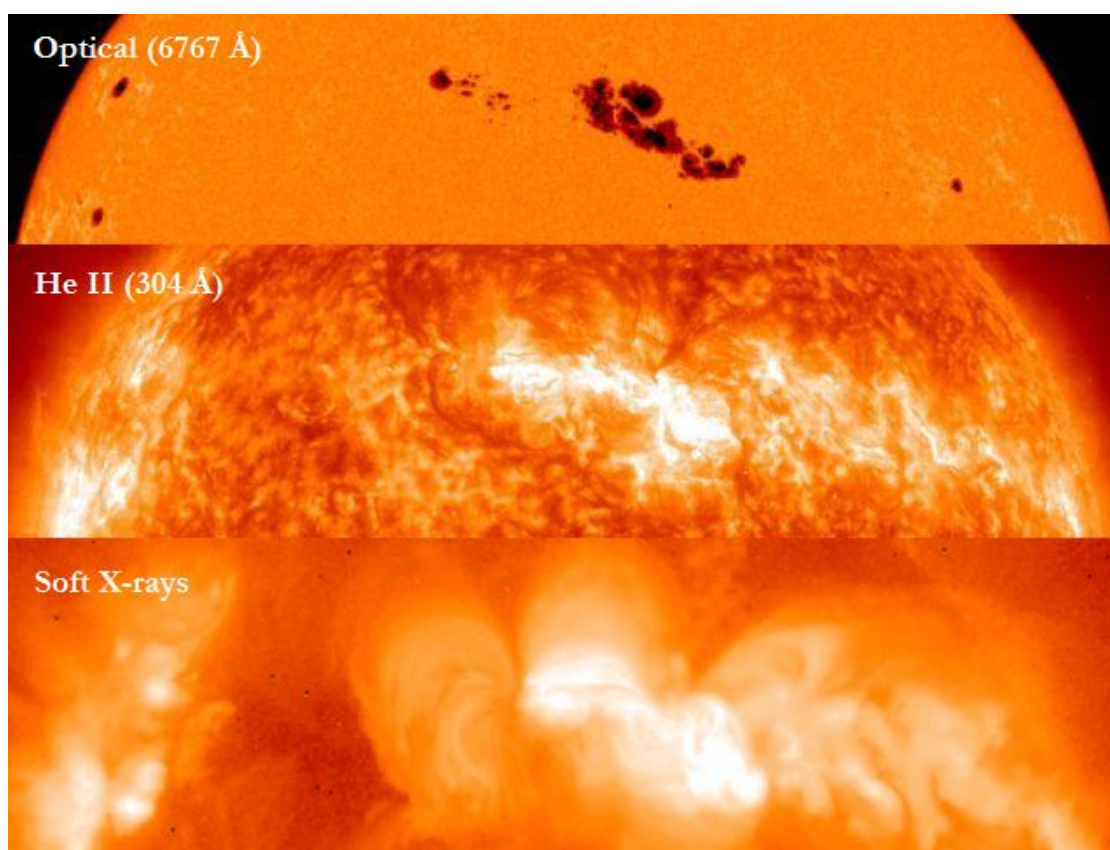


Figure 2.2: Photospheric features of the sun have a direct impact on its atmosphere as we can see in these pictures of the sun taken in different wavelengths.

The discovery of solar radio emission was done by Stanley Hey during World War II completely by chance. At first the strong interference that British radars received over the English Channel was thought to originate from German anti-radar jamming devices. Later on, the radar operators determined that the point of origin of this strong interference moved during the day, following the sun's trajectory in the sky. After these observations, Hey and his team concluded that the jamming effect must have been originated from the emission of electromagnetic radiation from the sun. At that time, the scientific community didn't welcome Hey's results, because they didn't agree with the the Planck's thermal radiation law. According to theory, the intensity of the solar "jamming" should be almost a million times weaker than it was observed.

According to Planck's radiation law, the power flux density of the radiation that a radiating thermal source emits, varies with frequency

$$B = \frac{2h\nu^3}{c^2} \frac{1}{e^{h\nu/kT} - 1}$$

Solar optical observations appear to have a spectrum similar to a Planck radiation curve for a blackbody at a temperature of 5800 K. However, radio observations of the sun can reach flux densities which correspond to Planck radiation curves for blackbodies with temperatures much greater than 5800 K, depending on solar activity. This means that the radiation emission mechanism for these frequencies is non-thermal, like synchrotron or cyclotron emission. A simplified solar spectrum can be seen in Figure 2.3. We can see that the spectrum follows the 5800 K Planck curve at wavelengths less than 1 cm but it is separated into two curves labeled as quiet sun and disturbed sun at wavelengths larger than 1 cm, according to solar activity. The quiet sun curve corresponds to the minimum background radiation received from the sun, while the disturbed-sun curve corresponds to the enhanced radio radiation received from the sun at times of high sunspot activity. It is clear that, the radiated energy of the sun during periods of high sunspot activity is greatly increased. This is indicated in Figure 2.3, where the disturbed-sun curve corresponds to equivalent blackbody temperatures up to 10^{10} K.

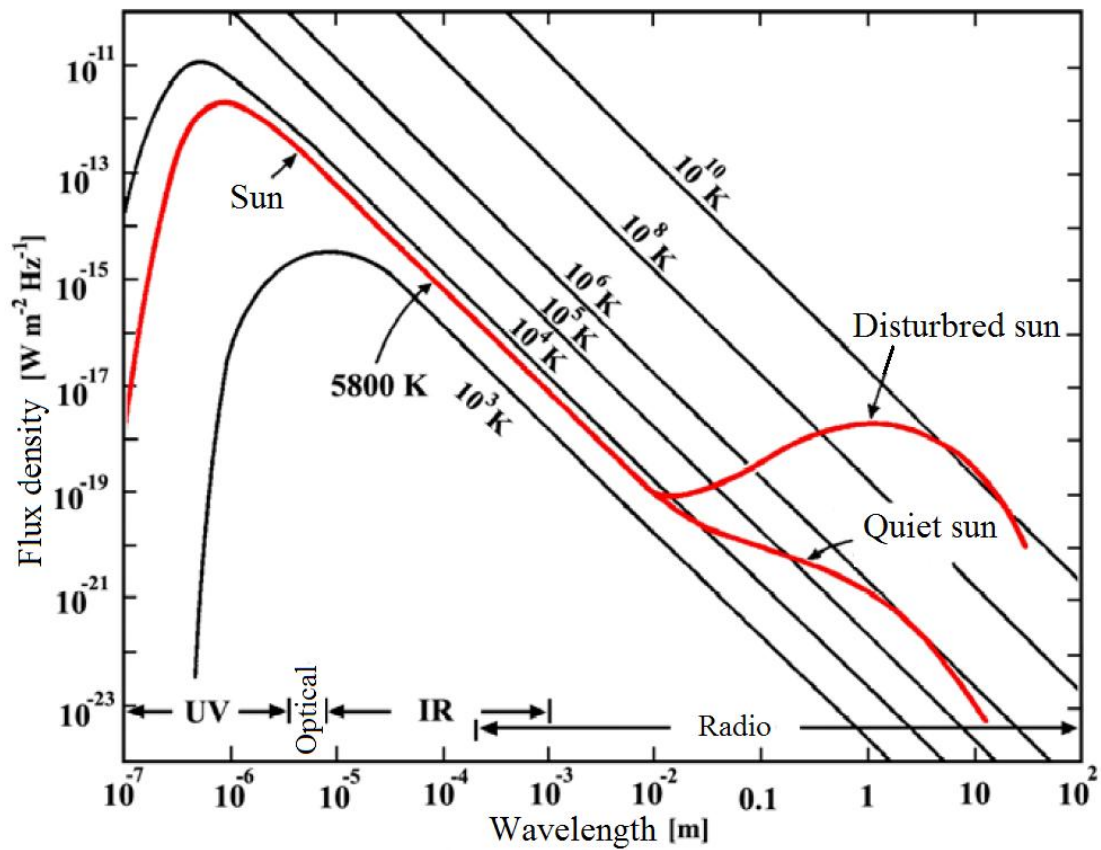


Figure 2.3: The spectrum of the sun over a big range of frequencies.

The solar radio emission can be divided into two categories, according to the solar activity during the sun's 11-year cycle, the emission from the quiet sun which corresponds to periods of little sunspot activity and the emission from the disturbed sun which corresponds to periods of high sunspot activity. Radiation from the disturbed sun can be divided into the slowly varying component which varies over periods of days, weeks or months and the rapidly varying component which varies over periods of seconds, minutes or hours.

2.2 The quiet sun

Due to the wide range of radio frequencies the sun appears in many different ways in the various regions of the radio window. At high radio frequencies we can observe regions of the solar atmosphere close to the photosphere while at low radio frequencies we can observe regions located high in the corona. Thus, at frequency ν the radiation is originated from a certain layer that corresponds to that frequency. The corresponding frequency of this layer is a function of the electron density and is given by

$$\nu = \frac{e}{2\pi} \sqrt{\frac{N}{\epsilon_0 m}}$$

where N is the electron density in electrons \cdot m $^{-3}$, ν is the observing frequency in Hz, ϵ_0 is the permittivity of vacuum ($8.85 \cdot 10^{-12}$ farad \cdot m $^{-1}$), m is the electron mass ($9.1 \cdot 10^{-31}$ kg) and e is its charge ($1.6 \cdot 10^{-19}$ Coulomb). The electron density of the solar atmosphere decreases with height and is given by

$$N = (1.55 \cdot r^{-6} + 2.99 \cdot r^{-16}) \cdot 10^{14}$$

where N is the electron density in m $^{-3}$ and r is the distance from the center of the sun in solar radii. This means that the layer of the solar atmosphere we can observe is located close to the photosphere for the highest frequencies and high in the corona for the lower frequencies.

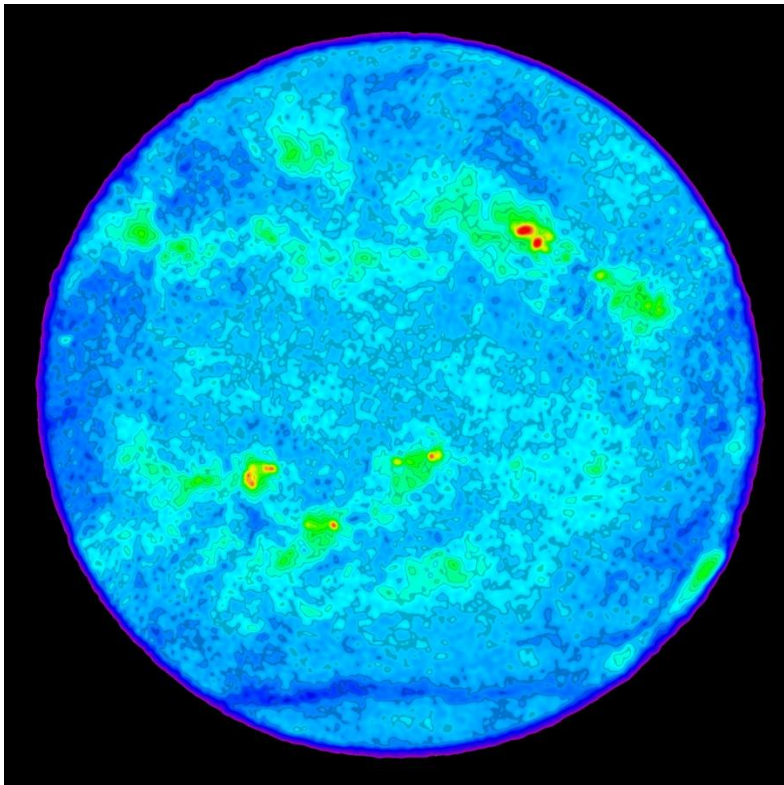


Figure 2.4: The quiet sun at $\nu=4.6$ GHz or about 8400 km over the surface of the sun. The brightest features (red) in this false-color image have brightness temperatures $T_b=10^6$ K and coincide with sunspots.

2.3 The disturbed sun

2.3.1 The slowly varying component

This component of solar emission is mainly observed in the 3 to 60 cm wavelength range. The slowly varying component originates in regions of the solar atmosphere located at distances up to 10^5 km above active regions of the photosphere. These regions of the solar atmosphere are related with these active regions of the photosphere and their spot groups. This association can be represented by the comparison of the picture of the sun in different frequencies. An example of this comparison can be seen in Figure 2.2.

2.3.2 The rapidly varying component

This component of the solar radio emission lasts from seconds to hours and is expressed mainly by radio bursts following the appearance of a solar flare in the lower layers of the solar atmosphere. The energy that is released by a solar flare can reach values of the order of 10^{25} joules and it is derived from the reconnection of solar magnetic field lines near sunspot areas. The rapidly varying component of the solar radio emission is very variable and depends on the observing frequency. On meter wavelengths the bursts may last from seconds to minutes. This component is less prominent in centimeter wavelengths but some bursts of one minute to one hour may be observed. It is common to observe this component of the solar radio emission first at higher frequencies and a while later at lower frequencies.

The classification of solar flares is based on the peak flux (in W/m^2) of 1 to 8 Å X-rays near Earth, as measured on the GOES spacecraft of the National Oceanic and Atmospheric Association (NOAA). There are five classes of flares, A, B, C, M or X. The peak flux is multiplied by ten for each class as compared by the previous one and X class flares have a peak flux of the order of $10^{-4} \text{ W}/\text{m}^2$. Furthermore, each class is divided by ten subclasses, from 1 to 9 in a linear scale. This means that an M2 flare is twice as powerful as an M1 flare, and is four times more powerful than a C5 flare.

As we mentioned above, the rapidly varying component of the solar radio emission is very variable but it appears that it can be classified into five principal types. Type I contains noise-storm bursts, type II slow-drift bursts, type III fast-drift bursts, type IV is a broadband continuum emission and type V is continuum emission at meter wavelengths. These types are associated with the events that follow the appearance of a solar flare. These events can be divided into two phases.

In phase one, which can be observed in all flares, strong radio bursts begin right after the flare which drift rapidly in frequency from around 500 MHz to lower frequencies. We classify these bursts as the fast-drift type III ones which have a frequency drift rate of the order of 20 MHz/sec. Type III emission is caused by plasma oscillations in the solar atmosphere which are driven by the ejection of an electron jet as a result of

the explosion of a flare in the solar chromosphere. The speed of this jet can reach velocity values of the order of 10^5 km/sec. This emission is usually accompanied by a continuum emission in the form of synchrotron radiation which is originated in the fast-rising electron jet trapped in the region's magnetic field. The latter type of emission is prominent in the meter wavelengths and it is classified as the type V emission of the rapidly varying component.

In large flares, there is a phase-two sequence of events which follow phase one. This phase-two sequence starts with slow-drift radio bursts which have a drift rate of the order of 20 MHz/min. This emission is caused by plasma oscillations of a shock front which rises in front of an expanding gas cloud rising at the flare location and is classified as type II emission. The speed of this shock front is of the order of 10^3 km/sec. These type II bursts are usually accompanied by a broadband, stable, continuum emission lasting for hours or days which is classified as type IV. Type IV emission is of the synchrotron type and originates from the gas cloud rising above the flare location which is trapped by the region's strong magnetic field.

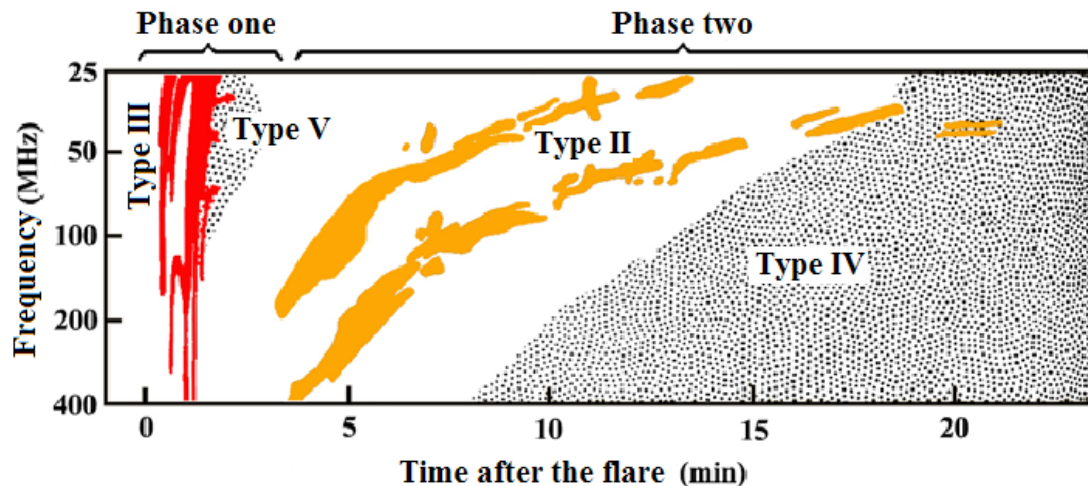


Figure 2.5: Dynamic radio-spectrum record of a large solar outburst.

For this thesis project, we obtained single-frequency (20.1 MHz) records of solar radiation like the one in Figure 2.6. In single-frequency records, it is difficult to classify the observed bursts, because we lack any frequency-drift information. For the record in Figure 2.6, it seems that the initial burst, which lasted for several minutes, consisted of type III and type V bursts, which are included in the phase one sequence of events. The second phase starts about 7 minutes later and is expressed by a slow-drift type II burst. A long-lasting emission appears in the record about 25 minutes after the start of the entire sequence, which is probably of the type IV emission and lasted for many hours. The sharp, short-duration spikes that appear on this type IV background are classified as type I emission. This is the method to study these observations and eventually the ones we obtained for this thesis project. After the successful observation of a solar burst we searched for records of the event in other wavelengths of the electromagnetic spectrum like the visual image of the flare or bursts of solar X-ray radiation. Finally, the different types of solar radio emission are summed up in the following table

Type	Duration	Bandwidth	Drift rate	Polarization	Mechanism	Temperature, K
Quiet Sun	Constant (or 11-year period)	Continuum		Random	Thermal	10^6
Slowly Varying component	Days or Months	Continuum		Random (CP at cm)	Thermal	$<2 \times 10^6$
Rapidly Varying component						
Phase 1: Type III	Seconds	100 MHz	20 MHz/sec	Random	Plasma	$>10^{11}$
Type V	Minutes	Continuum		Random	Synchrotron	10^{11}
Phase 2: Type II	Minutes	50 MHz	20 MHz/min	Random	Plasma	$>10^{11}$
Type IV	Hours	Continuum		Random to CP	Synchrotron	10^{11}
Type I	Seconds	5 MHz		Random to CP	?	10^9
Type I noise storm	Hours	50 MHz				

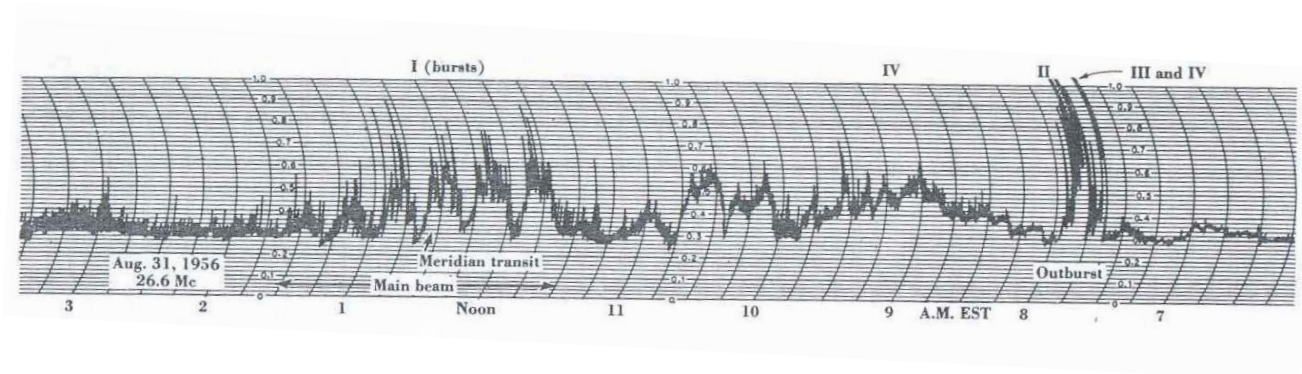


Figure 2.6: Single-frequency record of a solar outburst. Time runs from right to left.

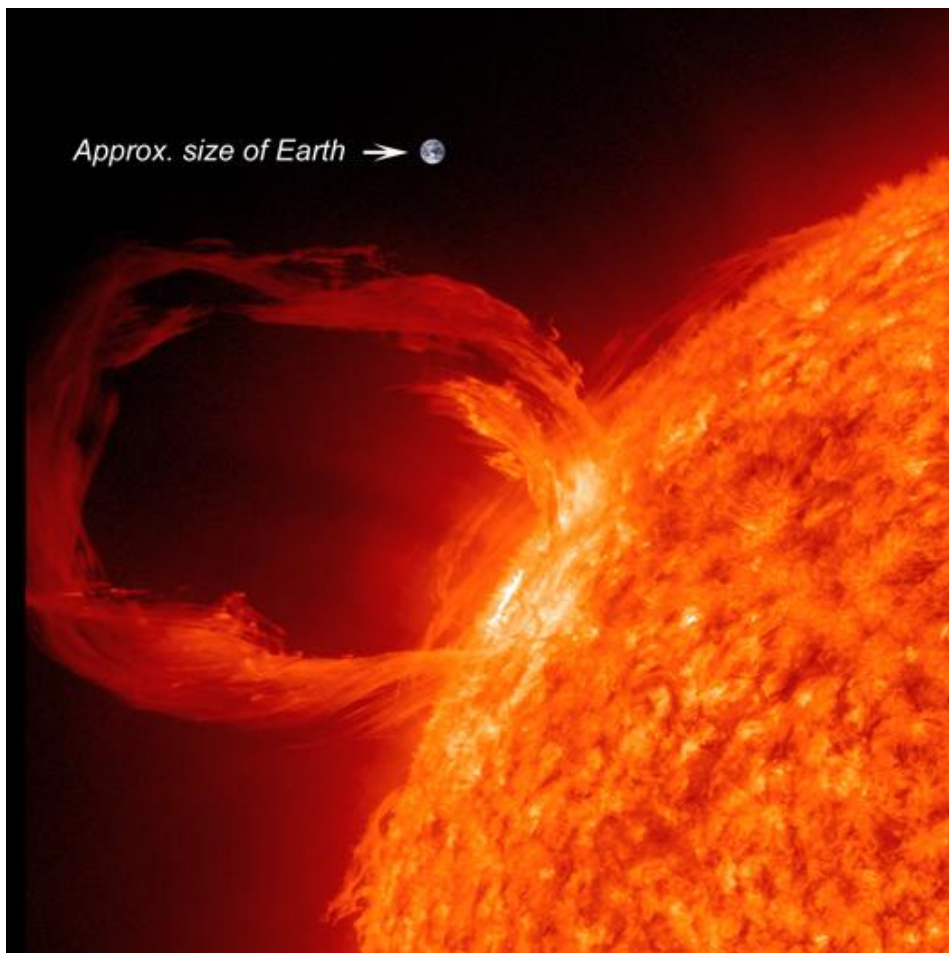


Figure 2.7: An image of the sun showing a large solar flare. The approximate size of Earth is also shown for comparison.

2.4 Influence of the ionosphere

The ionosphere is the layer of the Earth's atmosphere above 50 km where the intensity of solar ultraviolet and X-ray radiation is able to ionize atoms and molecules. The refractive index n , which is controlled by the number density of free electrons, determines the propagation of electromagnetic waves through the ionosphere. The structure and thickness of this layer of the atmosphere varies greatly over time. In general, the ionosphere consists of three distinct layers D, E and F. For the purposes of this thesis project, we conducted observations at the frequency of 20.1 MHz. At this frequency range, the lower two layers, D and E, cannot affect our observations because they inhibit observations at much lower frequencies than this.

The F layer is the highest layer of the ionosphere and it extends from an altitude of 160 km to more than 500 km. It is tenuous due to the low air density and highly ionized. The F layer has the ability to reflect the signals that reach it over a wide range of HF frequencies. This means that it can reflect terrestrial signals back to Earth and prevent the transmission of extraterrestrial signals. These effects are very effective at the 20.1 MHz frequency region. This aspect of the F layer has helped communication systems to work over great distances on Earth by continuous reflections of the signal on this layer and the Earth's surface. These effects also made our observations at some times of the day very difficult because the extraterrestrial signal could not pass through the ionosphere.

This ability of the F layer is highly variable and is a function of the angle and amount of solar incidence and the molecular content of the layer. This is the reason why for a certain period of time every day when the layer was highly ionized, strong manmade signals from around the world were reflected onto our radio telescope preventing solar radiation to be detected. We were even able to identify a shortwave radio station that was transmitting from Morocco and "blurred" our observations for a couple of hours every day because of this ability of the F layer.

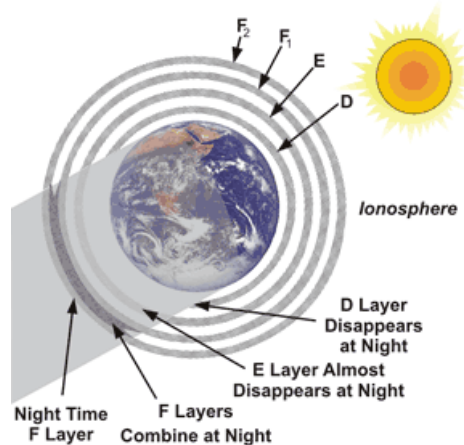


Figure 2.8: The layers of the ionosphere.

Using Maxwell's equations we can derive the characteristic frequency of any layer of the ionosphere below which propagation of radio waves is inhibited and the incident radio waves on that layer are reflected back to their region of origin. This limiting frequency is equal to the plasma frequency of the layer and is given by

$$v = \frac{e}{2\pi} \sqrt{\frac{N}{\epsilon_0 m}}$$

Thus, this characteristic frequency depends on the solar radiation intensity that is reaching Earth's atmosphere which changes its electron density. The variations of an atmosphere's layer electron density and hence its characteristic frequency are diurnal, seasonal and also follow the 11-year cycle of solar activity. For the northern hemisphere, the calculated extremes of the characteristic frequency are $v_{min} = 3 \text{ MHz}$ for an autumn night during solar activity minimum and $v_{min} = 24 \text{ MHz}$ for a spring day during solar activity maximum.

2.5 Jovian decametric radiation

Another target radio source that we were able to observe with our radio telescope is the Jupiter-Io system. Jupiter is the largest planet of our solar system and its mass is more than 300 times that of Earth. The mean rotational period of this giant is only $9^h.9$. The rotational period of Jupiter can be calculated by observing the characteristic belts on its surface gases. The rotational period of the gases near the planet's equator is $9^h50^m30^s$ (known as System I), while at the "temperate" zone of the planet it is calculated to be $9^h55^m40^s.6$ (System II). These differential rotation measurements indicate that Systems I and II refer to the planet's atmosphere and not its interior.

The first radio observations of Jupiter were conducted in 1950's when two American astronomers were testing a new antenna working at 22 MHz. The signals, which at first thought to be terrestrial manmade interference, were found to be radio emission coming from Jupiter. These decametric radiation signals are elliptically polarized and have a non-thermal spectrum. Statistical analysis of the signals showed that they have a periodicity almost equal to that of System II. Their period is $9^h55^m29^s.71$ and we believe that this is the rotational period of the planet and not its surface gasses. This rotational period was named System III.

Studies of the Jovian decametric radio emission showed that it is produced when certain longitudes of the planet are facing Earth. The distribution of the Jovian decametric radiation emission as a function of the Jovian longitude is shown in Figure 2.9. Regions 1, 2 and 3 of this Figure are more often known as B, A and C respectively.

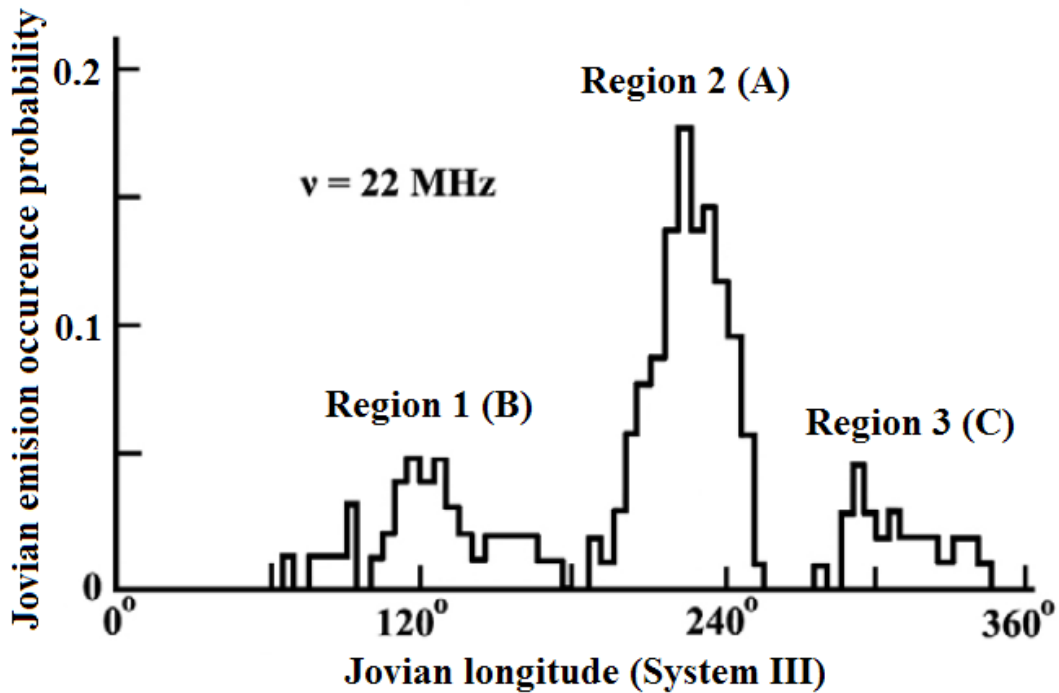


Figure 2.9: Occurrence probability of Jovian emission at 22 MHz as a function of Jovian longitude.

In the meantime, in 1956, scientists detected a thermal radio emission from Jupiter at the wavelength of 3 cm. The brightness temperature of this emission was found to be 140 K, almost equal to the temperature of the highest layers of the planet's atmosphere measured by infrared observations (130 K). This emission is observed in wavelengths smaller than 7 cm. The non-thermal decametric emission of Jupiter is observed at wavelengths greater than 7 cm and is highly polarized at the wavelength of 31 cm (25%). The inclination of the plane of polarization with respect to the planetary equator varies sinusoidally over the range $\pm 10^\circ$ as the planet rotates. These observations indicate the existence of a planetary magnetic field which has an axis with inclination of 10° with respect to the planet's rotational axis. Furthermore, interferometric measurements at 31 cm revealed that at this wavelength the non-thermal radio emission from Jupiter comes from a region that is about 3 times the planetary diameter in the equatorial plane and about one diameter along the direction perpendicular to that plane.

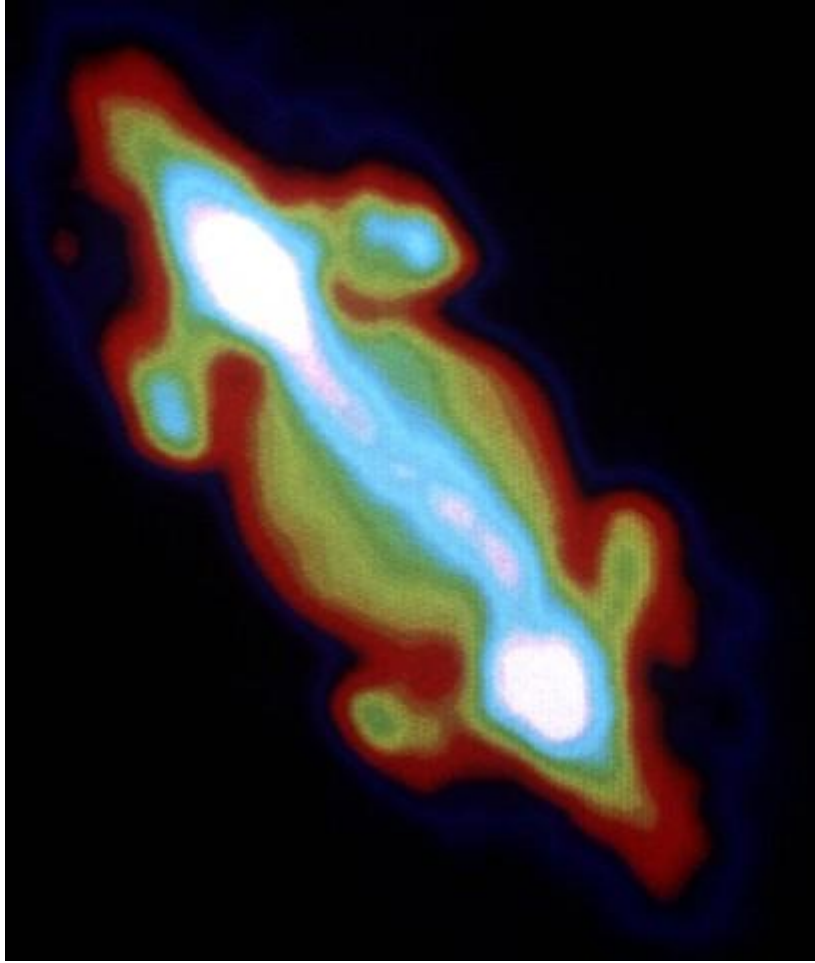


Figure 2.10: A VLA image of Jupiter. Most of the radio emission is synchrotron radiation from electrons in Jupiter's magnetic field.

The Jovian decametric emission has a cutoff frequency of 40.5 MHz. Using this information, we can calculate the intensity of the planet's magnetic field. If we consider the frequency of 40.5 MHz as the gyrofrequency of free electrons rotating in the planet's magnetic field we can calculate from the equation

$$\omega_g = \frac{e}{m} B$$

that the intensity of the field is 14.5 gauss. The spaceships Pioneer and Voyager 1 and 2 verified these calculations and also the magnetic field's axis inclination of 10° with respect to the planet's rotational axis.

The possibility to observe Jovian decametric radiation depends on the position of its Galilean satellite, Io. For example, the possibility to observe source B radiation is based on two conditions: (a) the Jovian Central Meridian Longitude (CML) to be within the source B longitude range and (b) the orbital phase of Io must be close to 90° from Superior Geocentric Conjunction (SGC). The CML is the meridian that is facing Earth at the time of observation and the SGC is the position of Io's trajectory which is behind Jupiter from our point of view. Io's orbital phase is the angle between SGC and Io's position at the time of observation.

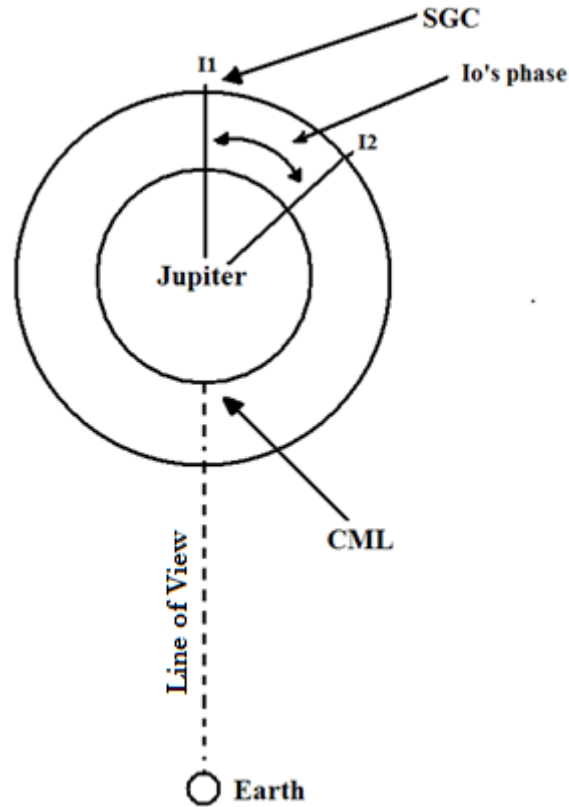


Figure 2.11: The Jupiter-Io system and our line of view of it.

There are also decametric emission components which are independent of Io's position. The following table summarizes the most common components of Jovian decametric emission in the frequency range from 15 to 40 MHz.

Source designation	Range of System III CML	Range of Io phase from SGC	Dominant circular polarization component
Io B	105°-185°	80°-110°	RH
Io A	200°-270°	205°-260°	RH
Non-Io A	230°-280°	0°-360°	RH
Io C	300°-20°	225°-260°	Mixed; more LH at lower freqs.

The system that we built for this thesis project was able to receive single-frequency information of the radio sky at the frequency of 20.1 MHz. Single-frequency records of Jupiter activity are very complex and a typical one recorded at 26.6 MHz can be seen in Figure 2.12. A single-frequency record of the Jovian decametric emission consists of discrete noise storms made up of repeated randomly-spaced radio bursts (L-bursts) which last from 1 to 6 seconds. These L-bursts are caused by scintillation of the Jovian radio emission due to drifts of plasma inhomogeneities through the interplanetary space. Jovian noise storms contain also another type of burst which is usually observed

during Io-related Jovian radio emission and is called S-burst. These bursts usually appear in short, rapid sequences and they last from about 5 to 50 msec. These bursts, unlike L-bursts, drift in frequency toward higher frequencies with drift rates of the order of 20 MHz/sec. This frequency-drift is caused by the motion of the source of each S-burst upwards from the Jovian ionosphere along the magnetic flux tube that passes through Io. The S-bursts drift upwards in frequency because their source passes through regions of ever lower magnetic field strength.

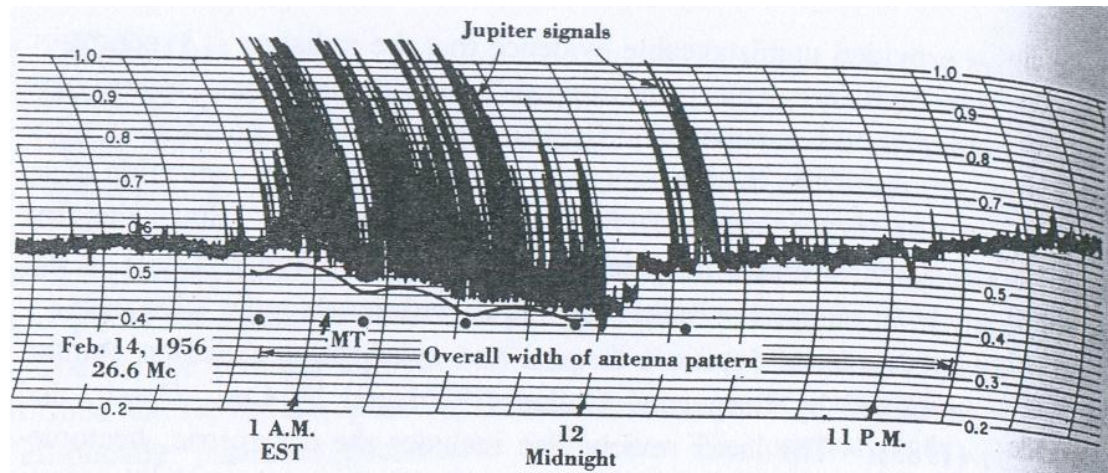


Figure 2.12: Jupiter radiation recorded in 26.6 MHz.

Io is a highly geologically active satellite and volcanic eruptions are very frequent. These eruptions fill the space around Io with atoms and molecules which can be ionized by solar radiation and thus trapped in Jupiter's magnetic field. The satellite's rotation around Jupiter creates a plasma torus which radiates the characteristic decametric radiation (Figure 2.13). The Jovian decametric radiation emission is generated near the electron gyrofrequency on magnetic field lines threading the plasma torus of its Galilean satellite, Io. As Io moves around its orbit, it produces Alfvén waves in the magnetized plasma of the Jovian magnetosphere. These MHD waves, in turn, form plasma condensations in the Jovian ionosphere which spiral along helical paths in magnetic flux tubes between hemispheres of the Jovian magnetosphere. The maximum observing frequency of the Io controlled Jovian radio emission corresponds to the maximum magnetic field at the base of the Io flux tube, near the Jupiter's surface gases, which is about 14 gauss. Thus, this magnetic cutoff frequency for the Jovian radio emission is given by

$$v_{max} = 2.8 \cdot B [MHz] = 2.8 \cdot 14 = 39.2 MHz$$

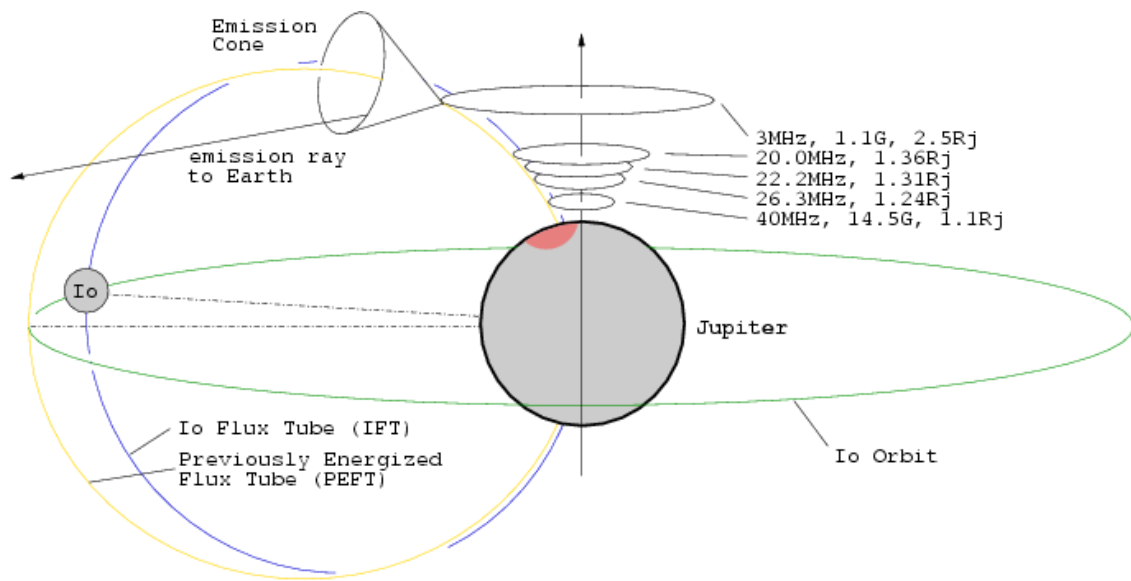


Figure 2.13: The Jovian decametric radiation emission mechanism. We can see the different points of origin for different frequencies of the radiation.

Chapter 3

Technical Aspects

The main goal of this thesis project was to build a low frequency radio telescope that monitors the sky at the frequency of 20.1 MHz. The two brightest celestial radio sources at this frequency are the sun during daytime and Jupiter during nighttime. The radio telescope that we built is based on NASA's Radio Jove Project but we made some alterations where it was needed. The Radio Jove Project started in 1999 and its main goal is to make Radio Astronomy popular. Anyone who takes part in this project is encouraged to build a simple radio telescope and observe Jupiter and the sun with it.

In this chapter I describe the infrastructure of the experiment which consists of a low frequency radio antenna, a receiver working at 20.1 MHz and the software to record and study our observations. A proper system calibration is of cardinal importance for all these parts to work together properly and gives us the opportunity to study the observations not only in a qualitative but also in a quantitative way.

3.1 Antenna description and characteristics

The antenna that we built for this thesis project is a phased array of two dipoles, based on the recommended design from the Radio Jove Project. The dipole is one of the simplest antennas and according to electromagnetic theory, its Poynting flux is given by the following equation

$$|\langle \vec{S} \rangle| = \frac{c}{4\pi} \cdot |\Re(\vec{E} \times \vec{H}^*)| = \frac{c}{4\pi} \cdot \left(\frac{I \cdot l}{2\lambda}\right)^2 \cdot \frac{\sin^2 \theta}{r^2}$$

The last term of the equation above indicates that the dipole antenna radiates or receives from a toroidal region oriented perpendicular to its axis and the flux of a radiating antenna decrease with distance squared. In other words, a dipole antenna is an isotropic radiator perpendicular to its axis but, on the contrary, it's unable to radiate or receive any radiation coming from the direction of its axis.

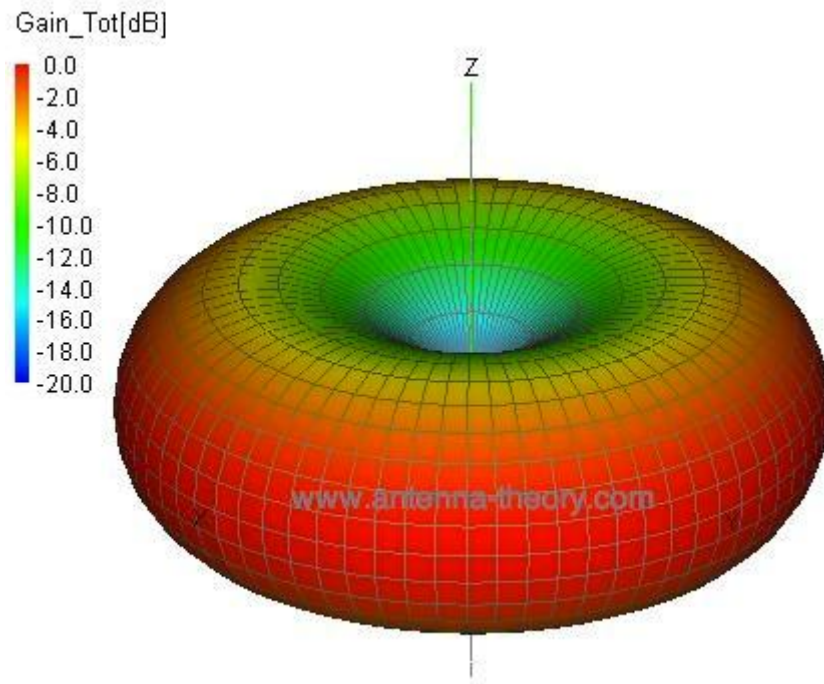


Figure 3.1: The antenna pattern of a single dipole. The dipole is located on the z-axis of the image.

A single dipole antenna consists of two pieces of wire and three insulators as shown in Figure 3.2. The most common type of dipole antenna is the halfwave dipole which has a length of half a wavelength of the receiving radiation ($\lambda/2$). This makes the dipole resonant at the observing frequency which means that of all the electromagnetic waves that reach the antenna the ones that have the resonant frequency are received better. In theory, the length of this antenna is exactly half a wavelength if we use infinitely thin wires, which is not the case in the real world. The length of a dipole antenna is somehow shorter than this due to capacitive end effects that are present in the wire of the antenna. The radio telescope that we built receives radiation at the frequency of 20.1 MHz (wavelength $\lambda = c/f = 14.925 \text{ m}$), so the theoretical length of each dipole antenna should be around 7.46 m . The real length of the dipoles is 7.09 m as measured from tip to tip of the wire, because the finite diameter of the antenna wires and capacitive end effects require the antenna to be approximately 5% shorter to be resonant.

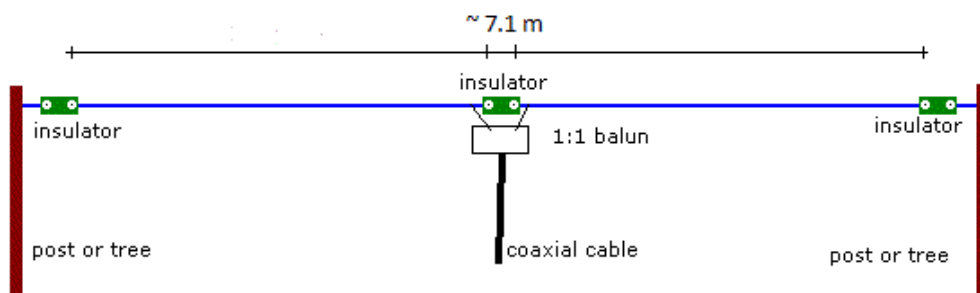


Figure 3.2: The constructing parts of a dipole antenna. The length of the dipole in the image favors the detection of radio waves at the frequency of 20.1 MHz.

The transmission line that we used to transfer the received signal from the antenna to the receiver is a coaxial cable. It consists of a central wire surrounded by a dielectric material inside of a braided copper wire covered with another layer of insulation. The central wire is called the core of the cable and the braided copper wire that surrounds the dielectric material its shield. Signals are conducted along the core and on the inside of the shield and travel from the antenna to the receiver. The transmission line is connected to the feed point of the antenna which, for a dipole antenna, is located at either side of the central insulator. The core of the coaxial cable is connected to one dipole wire and the shield to the other one.

The coaxial cable that we used as transmission line is designated as RG-59. It has an impedance of 75 ohms, an attenuation of 1.5 dB per 100 ft. at 20.1 MHz and a velocity factor of 0.66. The impedance is determined by the internal dimensions and geometry of the cable and is important to know it because the electronics of any system have to match in impedance to work properly. The attenuation is a measure of how much signal is lost due to wire resistance and dielectric losses in the transmission line and it should not exceed the value of 3 dB, which means that the maximum separation between the antenna and the receiver for our system should be 200 ft. The velocity factor is a measure of the speed of an electromagnetic signal moving through the cable and is given as a percent of the speed of light in vacuum.

In order to observe celestial radio sources crossing the sky with dipole antennas it is best to mount them with their wires running from east to west. In this case, the greatest gain of the antenna is located on the meridian plane of the observing site. The ground reflections produce an altitude asymmetry in the antenna pattern of the dipole and the altitude of maximum gain depends on the height at which the antenna wires are mounted. The position of the maximum gain point in the sky is lowered as we increase this height. So, the height of the antenna combined with the ground reflections makes its antenna pattern somehow more directional than the pattern of a single dipole in free space.

The directivity of a dipole antenna can be increased by adding a second, parallel dipole in a phased array. When these dipoles are connected in phase, they receive (or radiate) maximum power into two directions perpendicular to their connecting line. When they are connected in counter-phase, they receive (or radiate) maximum power on the direction of their connecting line. Any phase shift between these dipoles rotates the pattern in any angle we want, allowing us to target a source in the sky. This property of the phased array antenna pattern is based on the shift Fourier theorem and it is called electronic steering. In order to achieve this phase shift we combine the signals that both dipoles receive with a power combiner using different lengths of the coaxial cables which connect each dipole with the power combiner. The power combiner adds the signals from the two dipoles and feeds the resulting signal into the receiver.

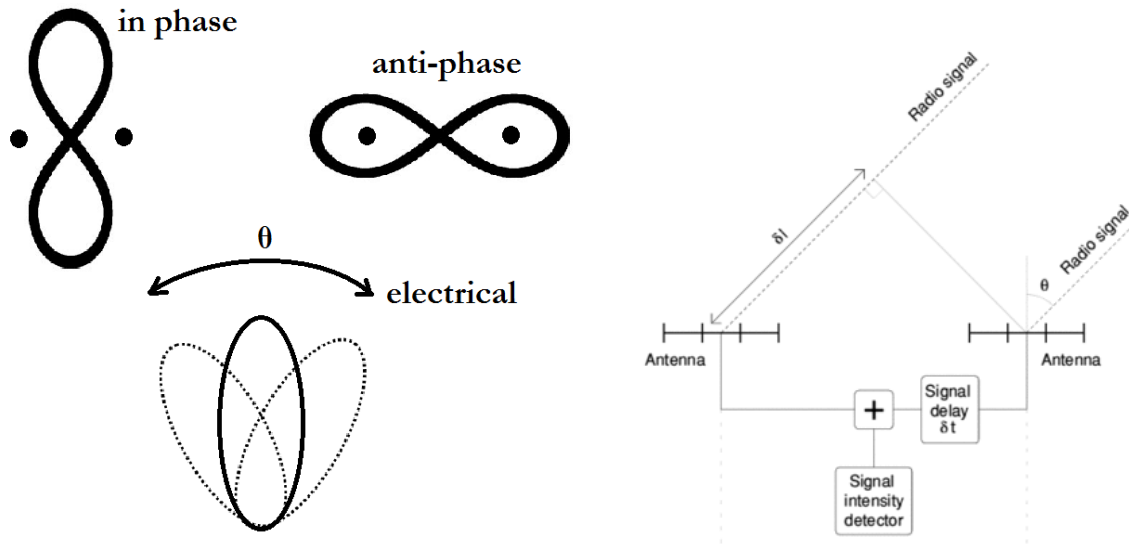


Figure 3.3: Electronic steering based upon phase-shifting between two or more dipoles. The phase-shift can be achieved with a signal delay between the two antennas as seen in the right image.

In the configuration of the antenna we constructed, there is an extra length of coaxial cable running from the south antenna to the power combiner, producing phase difference between the two signals of the dipoles and lowering the antenna pattern further to the south. In this way we can select the length of the phasing cable, as it is called, to change the altitude of the antenna beam and match it with the altitude of the sun for any time of the year. In other words we could describe this configuration as a meridian radio telescope. Furthermore, the use of two dipoles instead of one achieves twice the gain we get from the celestial radio signal.

The length of the phasing cable of the antenna we constructed and used is $\frac{3}{8} - \lambda$ (3.69 m), resulting in a 135° phase offset between the two dipole signals. The resulting antenna pattern has a strong south-facing gain lobe with an elevation of 35° . This elevation is ideal for observing Jupiter at the time when the experiment was conducted. In order to observe the sun, we used the configuration described above during winter but we removed the phasing cable during summer in order to turn the antenna beam closer to zenith.

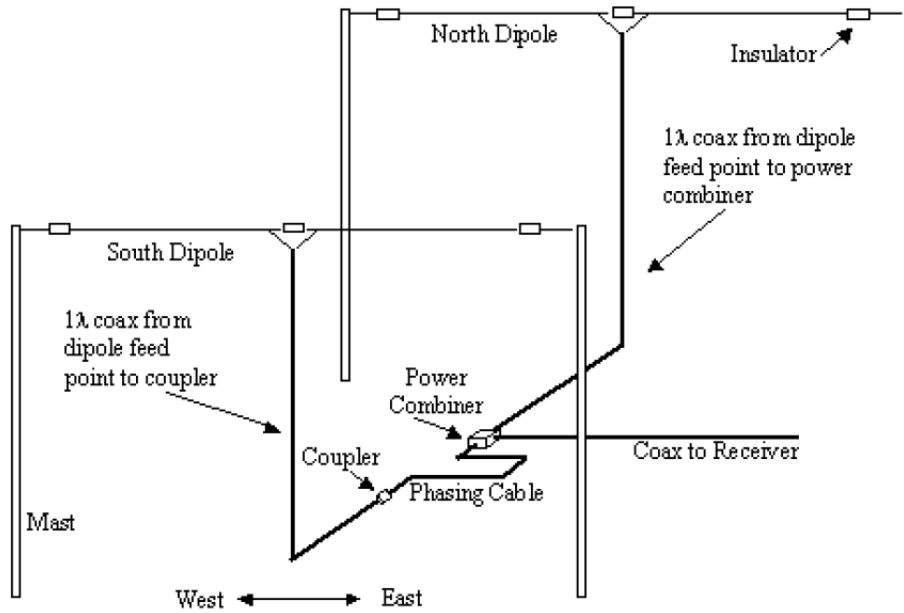


Figure 3.4: The antenna configuration of our low-frequency radio telescope.

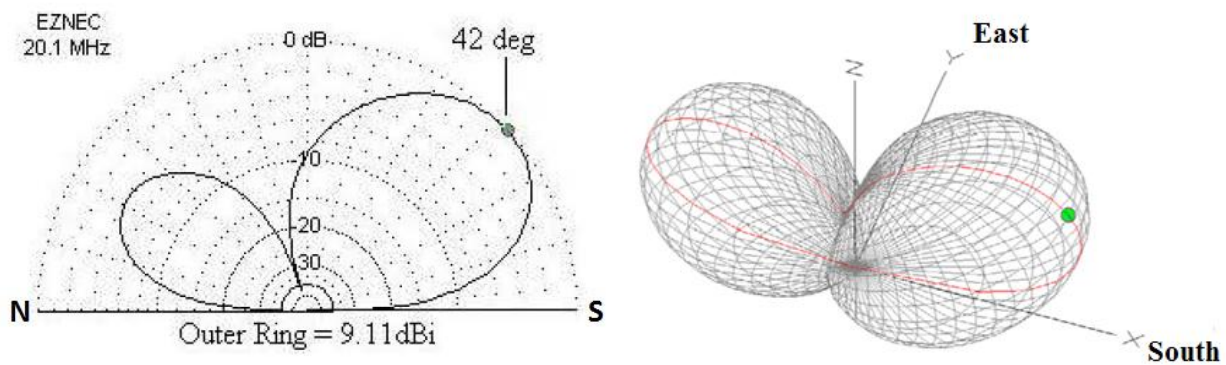


Figure 3.5: The antenna pattern of the radio telescope that we built. The turn of the main lobe to the south is a result of the added phase difference between the two dipoles.

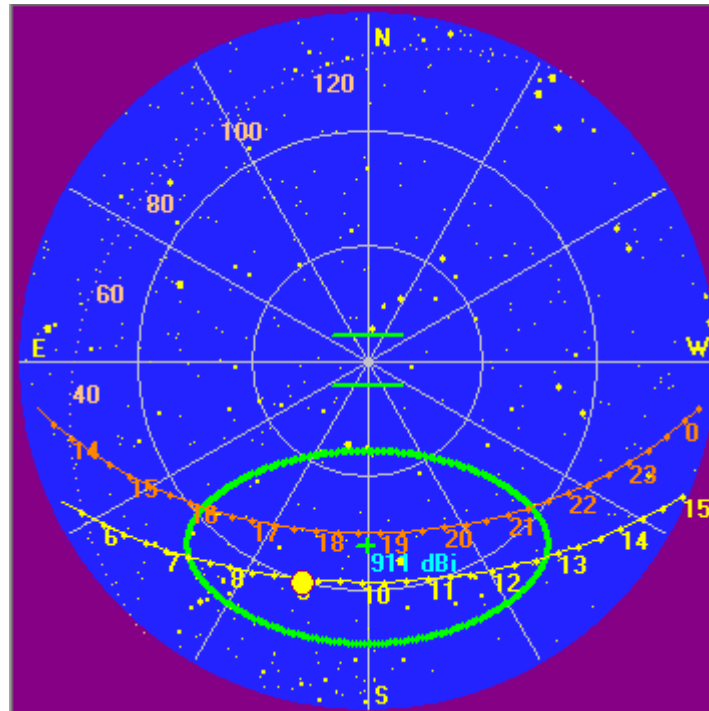


Figure 3.6: The position of the main beam of our radio telescope in the sky. The trajectories of the Jupiter and Sun can be seen as the orange and yellow lines respectively.

The phased dipole array which was constructed and installed for this project, is located right next to the Observatory of the Aristotle University of Thessaloniki. Its coordinates are $40^{\circ}37'50''.06$ North and $22^{\circ}57'33''.3$ East. Although the area is located near the center of the city, it was found to be very radio quiet. There weren't any strong interference at the observing frequency except for a shortwave radio station that was transmitting from far away and practically obstructed our observations for a couple of hours every day.

Detailed measurements using a theodolite showed that the separation between the dipoles of our antenna is about 4 m and their height is 4.57 m . The antenna pattern that we obtain using this antenna configuration with the phasing cable installed is shown in the Figure 3.5.



Figure 3.7: The antenna we constructed and used for our observations. The PVC masts that hold the two dipoles in place are clearly seen.



Figure 3.8: The two dipoles are parallel with each other and run in an East-West direction. The antenna feed-points of the two dipoles can be seen in the picture.

3.2 Receiver design and specifications

The receiver that was built for this thesis project is a shortwave superheterodyne receiver. The design is based on the Radio Jove project receiver and in fact most of the parts that were used to build it are purchased from the project's web page. The receiver has the ability to amplify the weak celestial radio signals that reach the antenna and convert them to audio signals of sufficient strength to drive headphones or a loudspeaker. The whole system is designed to operate over a narrow range of shortwave frequencies centered on 20.1 MHz.

The system's theory of operation is quite simple. When an electromagnetic wave coming from a celestial radio source, like the sun or Jupiter, reaches the wire of the dipole, a small radio frequency voltage appear at the antenna terminals. Then, the coaxial cable transfers the received signal to the antenna terminals of the receiver. When the antenna signal enters the receiver, it is filtered to reject strong out-of-band interference and then amplified using a junction field effect transistor (JFET) by a factor of ten. The circuitry that accompanies this JFET provides additional filtering of the incoming signal. The receiver input circuit is designed to develop a minimum of noise within the receiver which would affect the incoming signal and eventually the information that it carries.

The incoming radio frequency signals are down-converted in frequency to the range of audio frequencies. This conversion is performed by the local oscillator and the mixer of the receiver. The local oscillator generates a sinusoidal voltage wave form at a frequency close to the observing one, which is 20.1 MHz. The exact frequency value of the local oscillator is set by a tuning control in the front panel of the receiver. The mixer takes as input both the amplified radio frequency signal from the antenna and the local oscillator signal and it develops a new signal with a frequency value equal to the arithmetic difference between the local oscillator and the incoming signal frequency.

Following the mixer, the signal is fed to a low pass filter to eliminate interfering stations at frequencies close to the observing one. This filter is like a window with a width of a few kilohertz, through which we receive the celestial signals. In order to receive the weak signal that comes from Jupiter or the sun, the radio must be tuned to find a "clear channel" and interfering signals with a frequency in the vicinity of the center frequency must be rejected. This task is performed by the low pass filter.

The output audio signal of the mixer is very weak and needs to be amplified to drive headphones or a loudspeaker. This is the purpose of the audio amplifiers following the low pass filter. The output audio signal of the audio amplifiers is fed to two audio out ports on the back panel of the receiver. We connected a headphone set to the first port and the line-in channel of our computer's audio card to the second. This way the operator of the system can hear the signal and record it in real time on the computer's screen. Furthermore, using the appropriate software, we can process and store our observations both visually and acoustically.

To sum up for the receiver's theory of operation, it is useful to take a look at the following Figure which shows the receiver's block diagram. This Figure shows what happens to the celestial signal from the time it is received until it reaches our headphones.

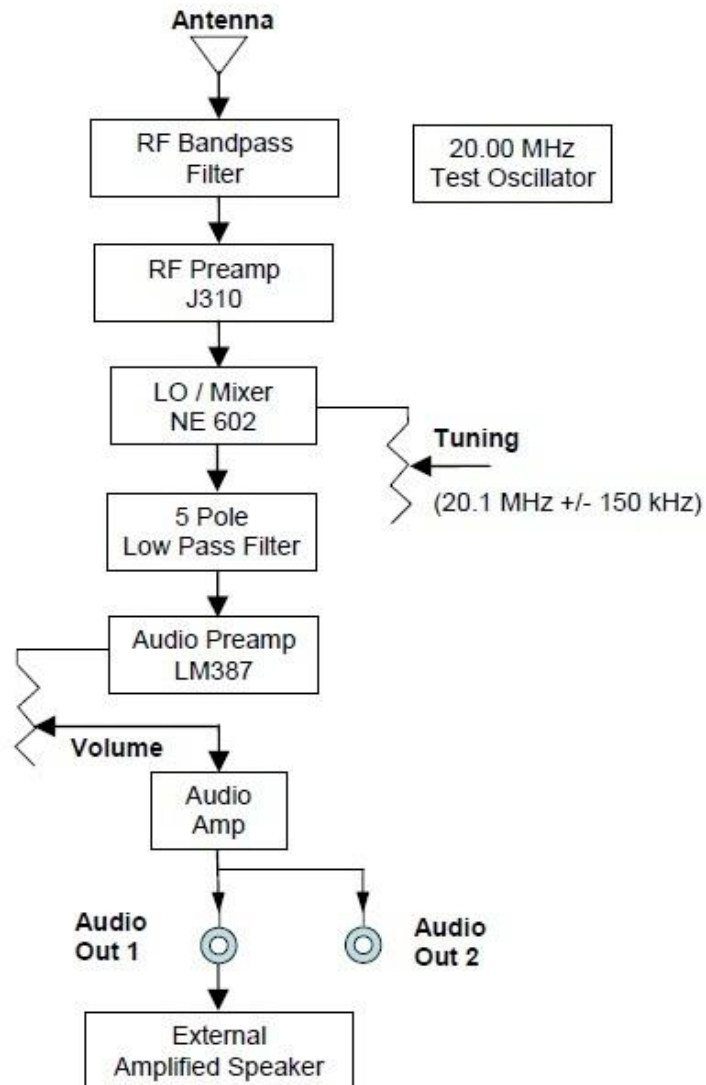


Figure 3.9: The receiver's block diagram.

The block diagram of the receiver shown above is useful in understanding signal flow and the tasks performed by the different parts of the receiver. The next level of detail is the receiver's schematic diagram. A schematic diagram is used to represent the wiring connections between all of the components of which our receiver consists. The schematic diagram of the receiver we constructed can be seen in Figure 3.10. On this schematic, the different part types are numbered sequentially. For example, inductors are numbered from L1 to L7, and resistors from R1 to R31.

Signal flow in the receiver's schematic shown in Figure 3.10 is as follows. The received signal from the antenna connector (J2) is fed into the resonant circuit L1, C2, C3 (bandpass filter) and then to the J-310 transistor (Q1), which amplifies it by a factor of 10. The output signal of the J-310 passes through another resonant filter (L3, C6) and then it is coupled to the resonant input circuit (L4, C9, C10) of the SA602 integrated circuit (IC1), which contains the local oscillator and the mixer of our receiver system. The frequency of the local oscillator is set by the variable inductor L5 and adjusted by the tuning control R7. The audio output from IC1 is filtered with the low-pass audio filter L6, L7, C20, C21, and C22. This audio signal is next amplified by the integrated circuit IC2 (an LM387) and its amplitude is controlled by the potentiometer R15. The final audio amplification is performed by the integrated circuit IC3 (another LM387), and the output transistors Q2 (2N-3904) and Q3 (2N-3906). The variable capacitors C2 and C6 and variable inductors L4 and L5 help us tune the receiver for operation at 20.1 MHz after its construction.

The various components of the receiver are mounted on a pc board and safely kept in a metal enclosure. The front panel of the receiver box contains the volume and tuning controls of the receiver and a LED which lights up when the receiver is in operation. On the rear panel there are the two audio outputs, the antenna terminal of the receiver and the power connector. The receiver requires 12 volts DC to operate and its current drain is approximately 60 mA. A representation of the pc board that holds the receiver components is shown in Figure 3.11.

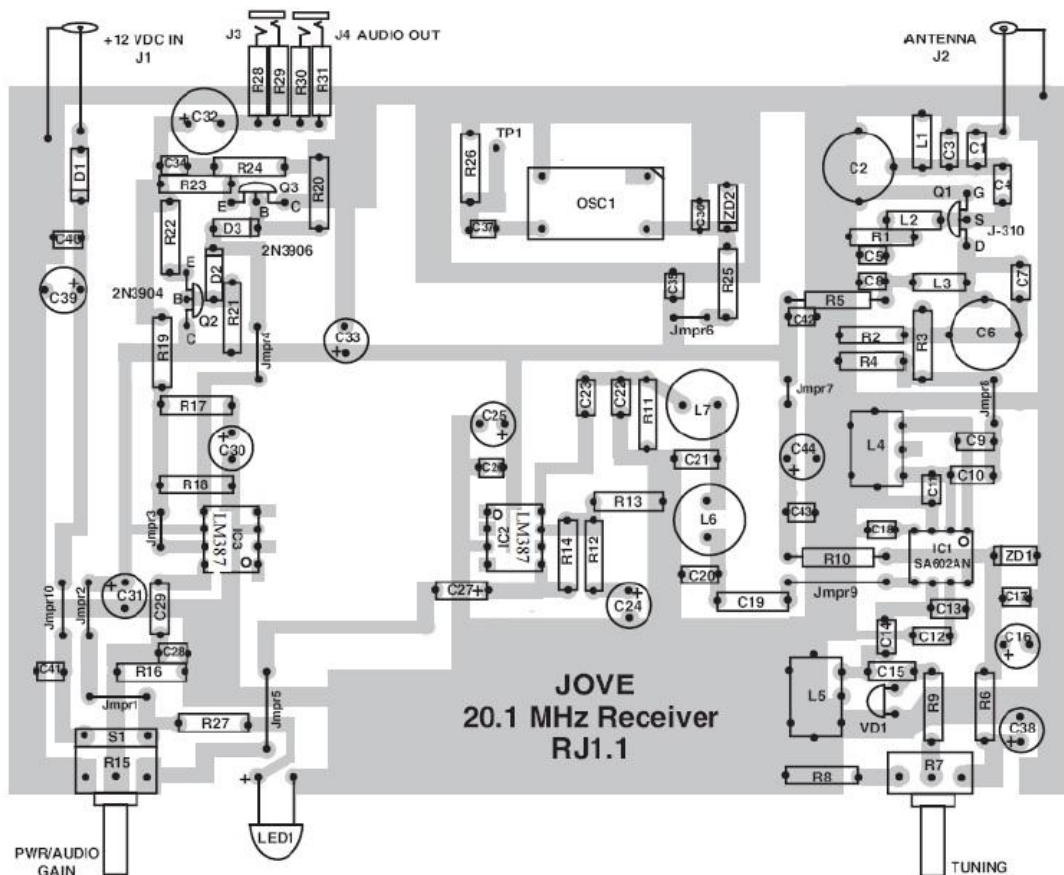


Figure 3.11: The pc board that holds the receiver's various components.



Figure 3.12: Views of the completed receiver.

After building the receiver, we aligned it properly to work at the frequency of 20.1 MHz. A first approach to the alignment and fine tuning of the receiver is done merely by hearing the audio output that it produces. Of course, the receiver needs to be plugged in and a headphone or a loudspeaker needs to be connected to one of the two audio outputs. The tuning of the receiver is done by a test oscillator which is represented as OSC1 in Figures 3.10 and 3.11. This test oscillator produces a sinusoidal signal at the frequency of 20 MHz and needs to be connected to the receiver circuit only when we fine tune it.

To align the receiver, we set the tuning control that is mounted on the front panel of the receiver to the 11 o'clock position. Then we carefully adjust the variable inductor L5 until a loud low frequency tone is heard through the speaker. By adjusting L5 to hear the tone, we are tuning the receiver to 20 MHz. The signal which we hear is generated in the crystal controlled test oscillator OSC1 built into the receiver. When the receiver tunes to 20 MHz with the knob set to the 11 o'clock position it will tune to 20.1 MHz with the knob centered on the 12 o'clock position. Next step is to obtain the maximum signal strength at the audio output. This is done by adjusting the variable capacitors C2 and C6 and the variable inductor L4 until we hear the tone loud and clear.

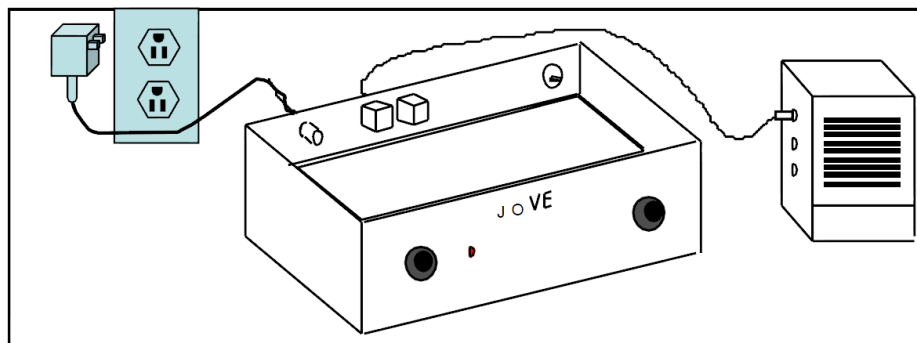


Figure 3.13: The tune-up of the receiver is done with the cover off and connected to the AC adapter and the amplified speaker.

The definitive test to check if the receiver is working properly is done with the help of the antenna. With no antenna connected, and the receiver's volume control set between the 12 and 2 o'clock positions, we hear a slight hissing sound in the headphones. With the antenna connected this hissing sound increases significantly. This is a proof that there is a radio signal that the antenna receives and the receiver successfully detects it. This test was performed right after the antenna construction and it was found that the system was working properly.

Finally, the technical specifications of the receiver as they are given by the bibliography or measured with the help of the staff and the instruments of the electronics lab at the Argelander Institute for Astronomy (AIfA) in Bonn are summed up as follows. The gain of the receiver depends on the setting of the volume control in the front panel of the receiver. With max clockwise gain setting the receiver's gain is > 100 dB. The radio frequency bandwidth was measured to be around 5 kHz and the noise figure is 6dB or better depending on how well the tune-up is performed.

3.3 Software

The program we used for data acquisition and storage is called Radio SkyPipe II. This software was designed by the Radio Jove project team and is used for Solar and Jovian observations by team members all around the world. Radio SkyPipe is a data collection program which allows sharing digitally sampled analog data in real-time over the internet or other TCP/IP connection but it may also be used as a standalone data collection utility which receives data either by sound card or via a simple analog to digital converter (ADC) connected to the computer. The online sharing of the data helps for the team members to communicate with each other and verify their observations.

Radio SkyPipe has three modes of operation: *Stand Alone*, *Client*, and *Server*. In *Stand Alone Mode* the PC acts as a data collection device, taking in data either through the sound card or an ADC. Data is displayed on a PC monitor that scrolls as new data is collected. After an observation is completed, the data file may be saved and recalled later for viewing or editing. *Server Mode* is an extension of the *Stand Alone Mode*. Data collected may be sent as it is collected via a TCP/IP connection to one or more remote PCs. In *Client Mode* the PC receives and displays data being sent from a Radio SkyPipe server, that is, from a PC running the same program in *Server Mode* at some remote location. We use Radio SkyPipe mainly in the *Stand Alone Mode* because the system is monitoring the sky and the data flow is running in a 24-hour basis.

With Radio SkyPipe II we are able to record and store our observations. During an observation Radio SkyPipe produces a real time graph of the power of the received signal. In the y-axis the power of the signal is recorded in arbitrary units, proportional to the power of the radio signal while in the x-axis runs the Universal Time (UT). The signal could also be heard through the speakers of the PC or the headphones directly connected to the receiver, aiding the identification of solar or Jovian emission.

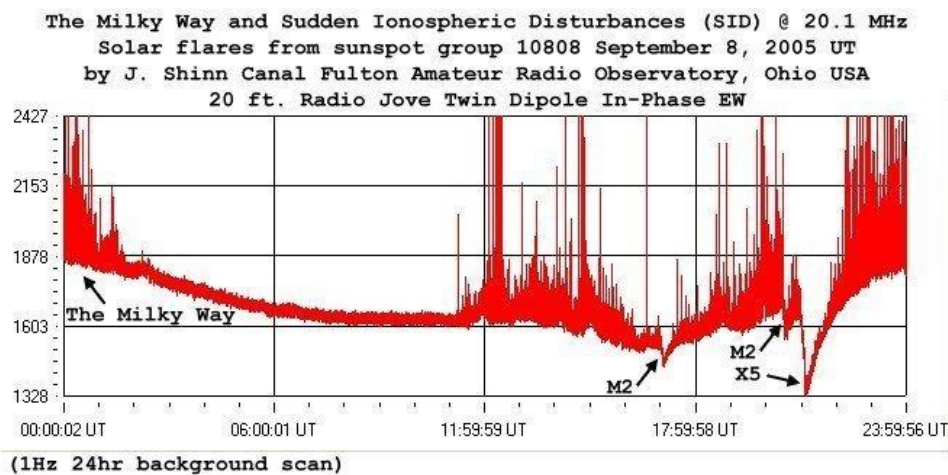


Figure 3.14: A Radio SkyPipe screenshot taken by another Radio Jove station.

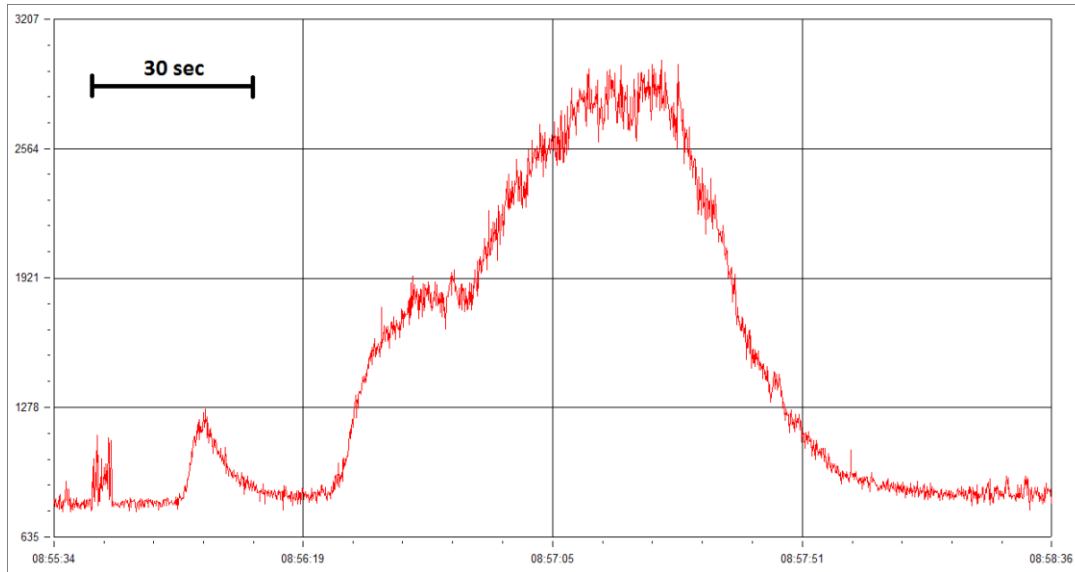


Figure 3.15: A solar radio burst as recorded by Radio SkyPipe installed on our station's computer.

A monitoring station produces a large number of files. That is the reason why these files should be stored in a practical way for future use. For the purposes of this thesis project we used the predefined logging system of Radio SkyPipe. The program uses a very sophisticated system. The date and time of the observation information can be retrieved from its file name. The file names start with the letters UT, meaning that the time information of the file is expressed in universal time, followed by twelve numerical characters. The first six numerical characters indicate the date of the observation in the form YYMMDD (Year-Month-Day) while the following six the starting time of the observation in the form HHMMSS (Hour-Minute-Second). In this way, merely by looking the file name, we can access the desired observation quickly. Furthermore the observation files are saved automatically in folders and subfolders which are named according to the month and day of the observation.

The observation files are binary files and have the extension *.spd which can be read only by the Radio SkyPipe program. If we want to process the raw data of the observation there are programs that can transform *.spd files to *.xls and thus process it any way we want using the Excel package of Microsoft Office suite. The *.xls output file is basically a two-column table which corresponds to an arbitrary number that expresses the signal power to an ascending series of numbers which express the time that is passing during the observation. Making a graph of this table reproduces the form of the observation that we take with Radio SkyPipe. Finally, Radio SkyPipe contains many options with which we can present and process our observations in many useful ways.

Another useful program that is offered with the Radio Jove project is Radio Jupiter Pro 3. This program takes the observer's coordinates as input and produces much information for Jovian observations as output. Radio Jupiter Pro uses the Jovian System III in correlation with Io's position to predict the most probable time for a Jovian radio burst to happen. Also, it can produce a year-long ephemeris for both the sun and Jupiter

which helps us find the best time of the year to observe Jupiter without the obscuring presence of the sun. The most useful screen of the program can be seen in Figure 3.16. This screen contains all the information needed to observe Jovian emission during the day that is displayed at the top of the window. It contains also the sunrise and sunset time, the time that Jupiter rises and sets for the observer's coordinates and finally a table which presents the best time period in which a Jovian burst is most probable to happen. Using Radio Jupiter Pro 3 we were able to roughly verify if the radio signals we received during some nights of my observations were coming from Jupiter or not.

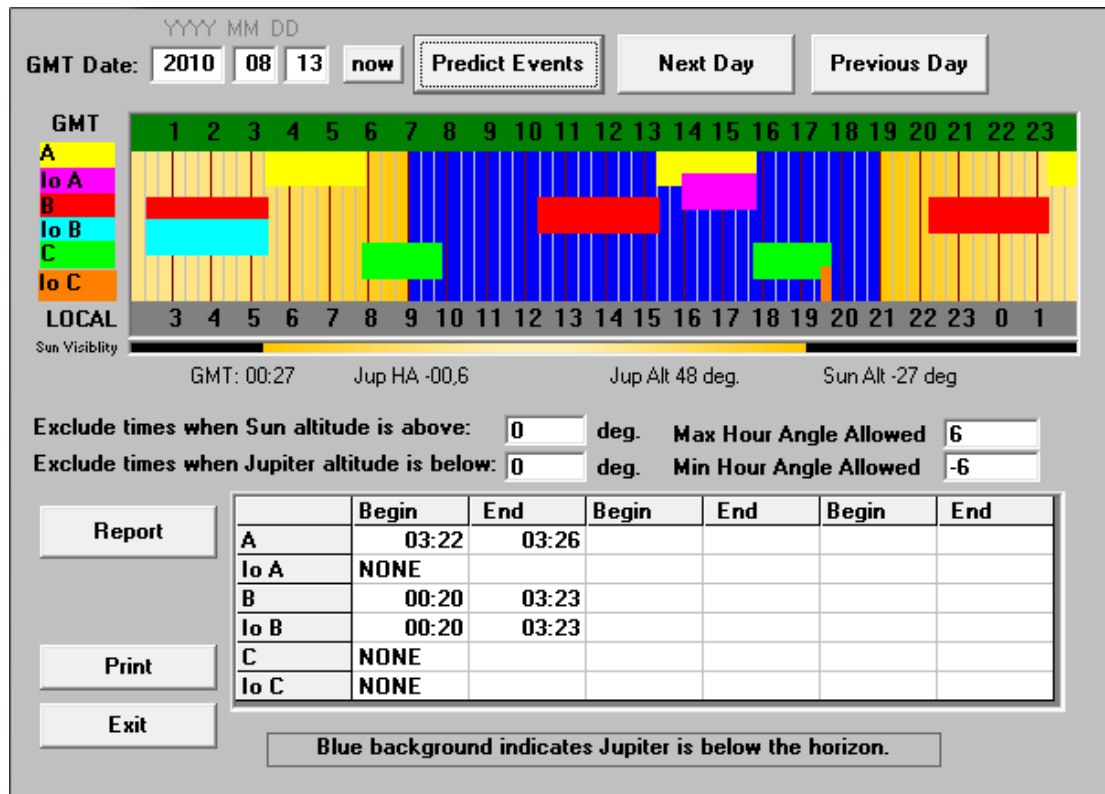


Figure 3.16: The prediction screen of Radio Jupiter Pro 3.

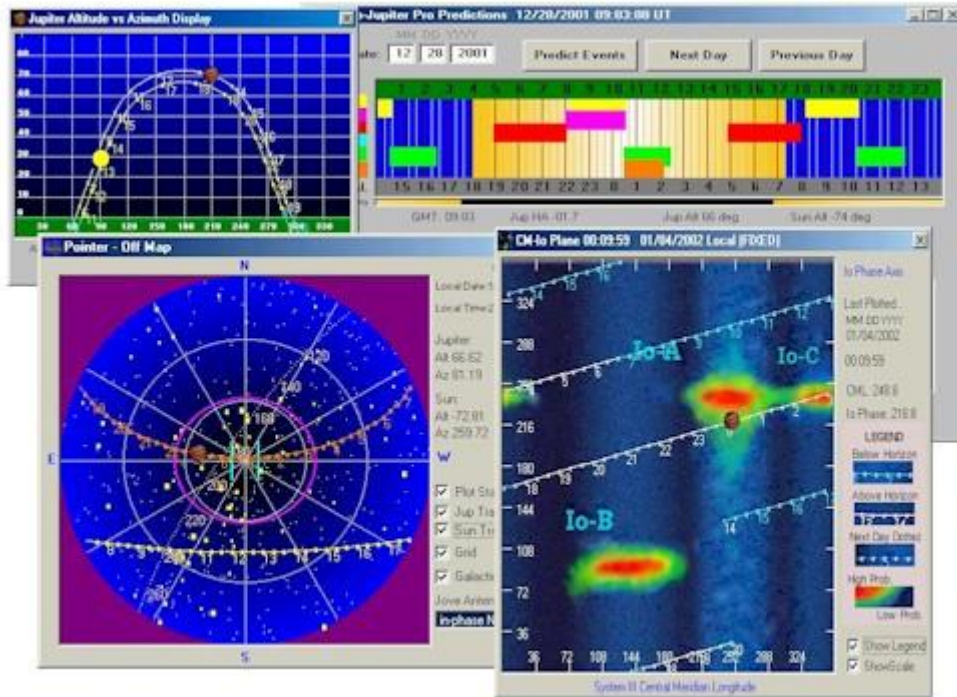


Figure 3.17: Radio Jupiter Pro 3 is a very useful program for the observation of solar and Jovian radio bursts.

The signals we receive from solar or Jovian bursts produce a certain type of sound at the computer's loudspeakers according to the type of the burst. Sometimes solar or Jovian bursts and some kinds of interference signals produce quite similar patterns in the graph of the observation. When this is the case, the most definitive way to verify whether we observed a solar or Jovian burst or interference is to hear the sound that was recorded at the time of the "burst". That is the reason why we used a third program for this thesis project. This program is called Loop Recorder Pro 2.06.

Loop Recorder Pro has the ability to record the sound of one audio channel of the computer's sound card in a 24-hour basis. We used this program to record and store the sound that was captured by Radio SkyPipe. This way an archive was made of both the observation graphical files and their sound. The sound files of the observations have duration of ten minutes each and are named in a practical way for quick reference. The names of the sound files contain both the date and start-time of the observation. They do not contain the end-time of the observation since all the sound files have a fixed duration of ten minutes. To be exact, the duration of the files is eleven minutes since it takes some time to save the previous sound file on the hard disk. The information that is obtained during this time isn't lost but stored in this extra overlapping minute of each file. Since the sound of the observations is in the form of noise, the sampling rate of the sound files is only 96 kbps.

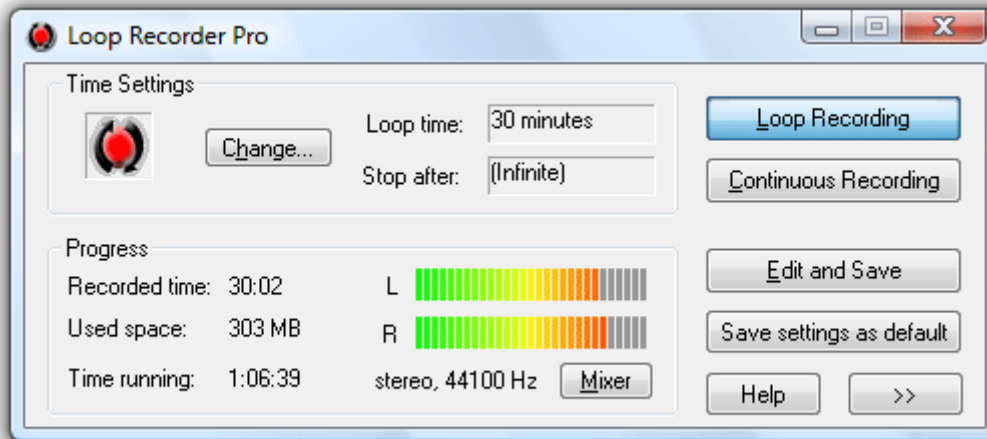


Figure 3.18: A screenshot of Loop Recorder Pro.

This setup of the system offers monitoring observations of the radio sky at 20.1 MHz with satisfactory results if it is installed in a relatively radio quiet site. We can observe solar or Jovian radio bursts and study their form in this narrow frequency channel around 20.1 MHz. A major disadvantage of the configuration of the system described so far is that it offers only qualitative and not quantitative results, meaning that we know when a burst happens and its shape but we cannot measure its power.

3.4 System calibration

The only way to overcome the system's disadvantage to obtain only qualitative results is to calibrate it. In fact, there are two parts of our system that we control in an arbitrary way. The first one is the tuning knob at the front panel of the receiver with which we select the receiving frequency of the system. There is no way to know the exact value of this frequency in the default design of the receiver. The second one is the display of the signal power at the screen window of Radio SkyPipe. It is expressed in arbitrary power units and according to theory it is mandatory to transform these units to antenna temperature if we want to obtain quantitative results.

3.4.1 Frequency calibration

The calibration of the tuning knob for us to know the exact receiving frequency was done with the help of the Electronics Lab of the Aristotle University of Thessaloniki and it was an idea of Professor Theodoros Laopoulos. The idea is quite simple. The tuning knob is basically a potentiometer which changes the value of the resistance of the resistor R7. This means that the output DC voltage value of the voltage divider formed by the resistors R6, R7 and R8 as seen in the circuit diagram of the receiver should be relevant to the receiving frequency of the system, since the potentiometer R7 is the tuning knob which selects the observing frequency. We can measure this output voltage with a multimeter located at the middle component lead of the potentiometer R7 and we can see how it changes as we turn the tuning knob.

Using a frequency generator we can generate sinusoidal electromagnetic signals with any frequency we want within the frequency range of the generator. In order to calibrate the system, we produced signals with frequencies between about 19.9 and 20.2 MHz. Then, using a simple antenna connected to the receiver we tried to detect these signals by turning the tuning knob. Then by measuring the DC voltage at the point we mentioned before we were able to make a table which correlates any received frequency, in the desired range, with a DC voltage output of the voltage divider R6, R7 and R8.

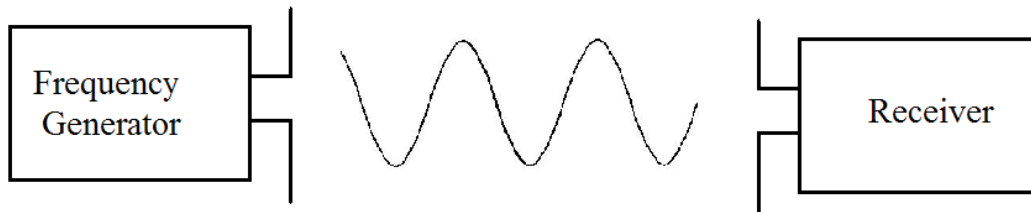


Figure 3.19: The calibration of the tuning knob is based in a very simple idea.

The calibration results are presented in the following table

Generated signal frequency (MHz)	DC voltage output of voltage divider (Volts)
19,874	0,98
19,881	1
19,891	1,09
19,901	1,18
19,912	1,29
19,921	1,38
19,932	1,49
19,944	1,62
19,951	1,69
19,962	1,8
19,97	1,9
19,981	2,01
19,99	2,11
19,998	2,19
20,007	2,29
20,016	2,4
20,025	2,5
20,033	2,6
20,042	2,7
20,051	2,81

20,06	2,9
20,068	3
20,077	3,11
20,086	3,21
20,094	3,3
20,102	3,39
20,111	3,51
20,119	3,6
20,127	3,69
20,135	3,79
20,144	3,91
20,153	4,01
20,162	4,11
20,17	4,2
20,177	4,29
20,189	4,42
20,195	4,5
20,207	4,63
20,212	4,71
20,221	4,81
20,228	4,89
20,239	5,01
20,248	5,12
20,257	5,22

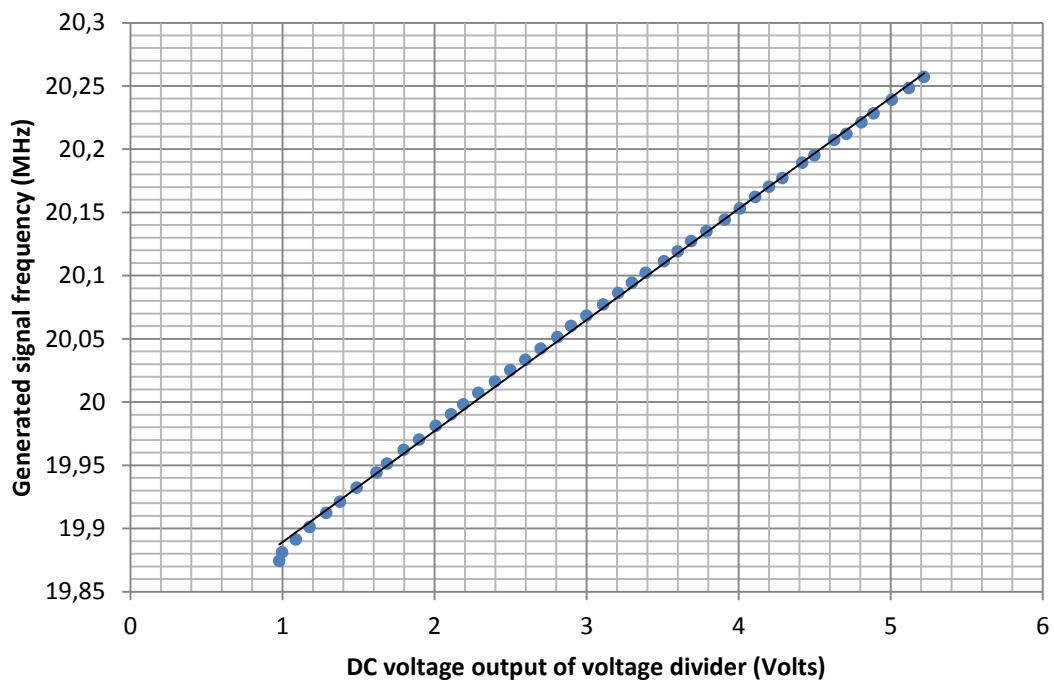


Figure 3.20: The plotted results of the calibration procedure.

As we see in the plot of the results in Figure 3.20, the function which correlates the receiving frequency to the DC voltage output of the voltage divider R6, R7 and R8 is linear and is given by

$$f(x) = 0.087x + 19.8$$

From this point on, we were able to select the receiving frequency of the system simply by measuring the DC voltage output of the voltage divider R6, R7 and R8. The devices we used for this calibration are the following: A Hewlett Packard 54601B (100 MHz) oscilloscope to view the generated signal, a Hewlett Packard 3325B synthesizer/function generator to generate the signals and a Hewlett Packard 34401A multimeter to measure the voltage. These devices were provided by the Electronics Lab of the Aristotle University of Thessaloniki.

3.4.2 The antenna temperature calibration

Next, we had to calibrate the Radio SkyPipe software in order to obtain our results in antenna temperature. In a Radio SkyPipe record, the horizontal axis is time and the vertical axis is expressed in arbitrary SkyPipe Units (SPU). The range of the vertical axis scale of the SkyPipe record is 32000 SPU when the sound card input is used. The signal trace plotted on the SkyPipe screen can be adjusted with both the receiver and the software volume control in Windows. Changing the values of these gains, we can move the trace up or down and also compress or expand it. There is no absolute point of reference. We usually set these gains to run the trace around 1000 SPU because in strong solar bursts the signal to noise ratio (SNR) can reach very high values. The units of the SkyPipe vertical scale are relative, arbitrary numbers. They are not physical units like volts, watts or degrees. In order to know the absolute strength of the received signals, we converted SkyPipe units into physical units with an absolute reference. To do this we used the calibrated noise source, RF2080 C/F, provided by the Radio Jove project.



Figure 3.21: The calibrated noise source RF2080 C/F.

The RF2080 calibrated noise source generates a radio frequency noise signal similar to the noise received by a shortwave receiver located at a very radio quiet site. The typical level of noise expected at such a quiet receiving site is of the order of 25 thousand degrees of Kelvin. This level of noise is called galactic background because it is generated by relativistic electrons spiraling in the galactic magnetic field.

According to theory, the power of a noise signal transferred to the receiver is described by the following equation

$$P = kBT$$

where P is the power in watts, k is the Boltzmann's constant ($1.38 \cdot 10^{-27} \text{ J/K}$), B is the receiver bandwidth in Hz and T is the noise source temperature in K. In a radio-quiet receiving site with the bandwidth of our receiver ($\sim 5 \text{ kHz}$) the power from the galactic background transferred to the receiver by our antenna corresponds to a 25 thousand degrees noise source.

The RF2080 C/F unit contains both a calibrated noise source and a bandpass filter around the frequency of 20.1 MHz. The bandpass filter in the RF2080 C/F unit is used to reduce or eliminate strong interference signals delivered to the receiver by international broadcasting stations. The unit is installed between the antenna and the receiver and requires a power supply of +12 volts to operate. The unit contains only one switch, which controls the power and also selects the source of the signal that the receiver detects. When the unit's switch is at the OFF position, the antenna is connected to the receiver. When it is at the ON position, the calibrated noise source signal is routed to the receiver while the antenna's signal is isolated. The bandpass filter has a loss of approximately 1.5 dB on the signal power. Therefore, the noise source temperature that corresponds to the signal power that the receiver detects from the RF2080 C/F unit is not 25 thousand degrees but rather 17.7 over a frequency range of $20.1 \text{ MHz} \pm 100 \text{ kHz}$ because of this filter's loss.

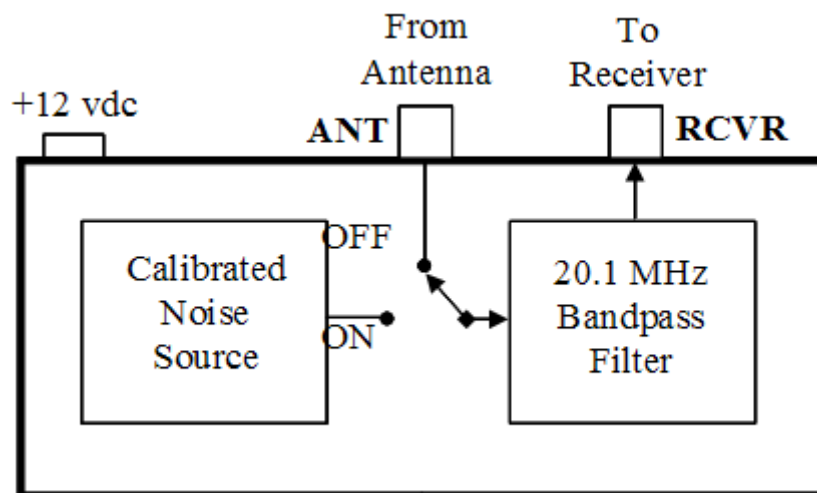


Figure 3.22: ON and OFF selections of the calibrated noise source RF2080 C/F.

In version 2.0 or later of the Radio SkyPipe software, SPU are proportional to the power of the received signal. If the input power doubles the SPU also double. From the last equation, we can deduce that SPU are also proportional to the temperature of the noise source, so using the RF2080 C/F unit as a noise source of known temperature, it is possible to convert SkyPipe units into antenna temperature units.

In order for the calibration to be done right, the receiver and also the computer's sound card should exhibit linear operation over a wide range of input signal strengths. The relationship between the input and the output signal of the system can be seen in the Figure 3.23. Up to an input level of about 15 units we see that the receiver demonstrate linear operation. This stops for higher input levels, where the output can no longer follow the input and the receiver reaches its saturated region. From this point on, the receiver's output power and voltage have reached their maximum level. This means that the receiver's output signal will not change at all when the input signal is increased. If the linear region of the receiver is wide enough, we can calibrate the system at a single point and use a simple equation to create the proper vertical scale for all other input signals. In the ideal case we would calibrate the receiver's operation at many different input signal temperatures, well up into the saturated region. However, in order to save time and money we used a single-temperature calibrator. If we set the gains as it is suggested in the calibrator's manual, this calibration method should allow us to measure the antenna temperature of solar and Jovian bursts to an accuracy of ± 1 dB, except in the saturated region of the receiver.

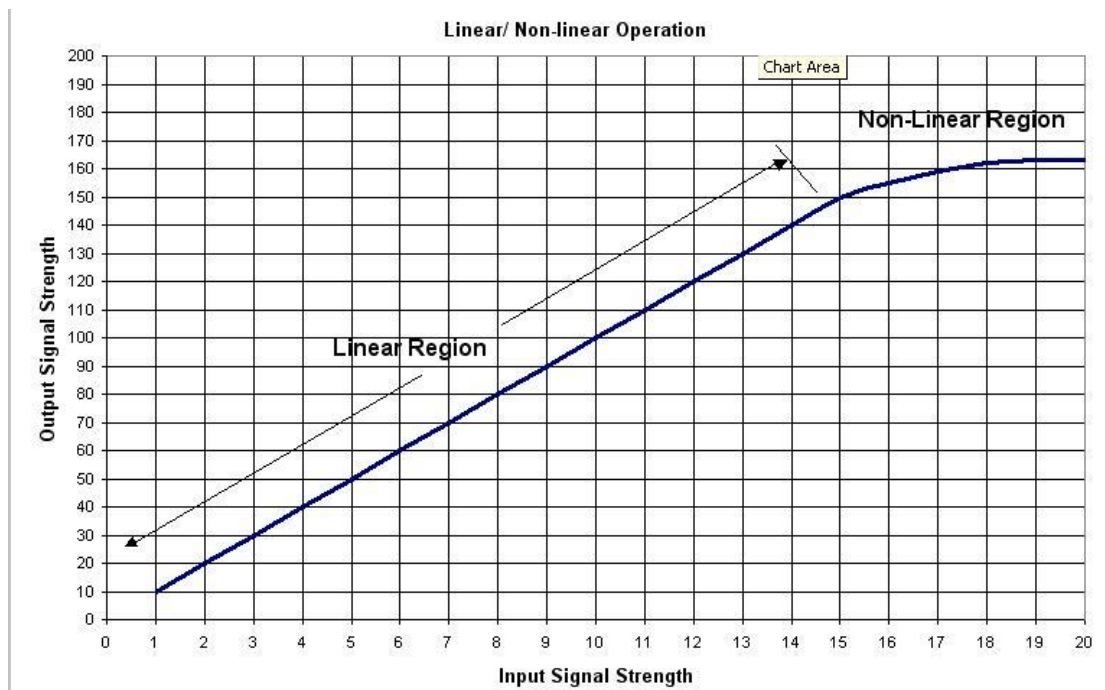


Figure 3.23: Linear and non-linear regions of operations of our receiver.

In order to calibrate the vertical axis of Radio SkyPipe software, we installed the RF2080 C/F noise source between the antenna and the receiver (Figure 3.24). We used a

short jumper coaxial cable between the RF2080 C/F and the receiver. Then we adjusted the volume control on the receiver to the 12 o'clock position, we routed the receiver's output signal to the computer's soundcard input and launched Radio SkyPipe. There, under the menu Tools, we run the Calibration Wizard.

The Calibration Wizard is a subprogram of Radio SkyPipe which calculates the cable losses according to the system configuration and automatically scales the vertical axis in units of antenna temperature with the help of the RF2080 C/F noise source. The input information that is required is the antenna type we use (single or dual dipole), the coaxial cable type, its length between the power combiner and the receiver and the calibrator's noise signal temperature. As mentioned before we use a dual dipole antenna, the coaxial cable is RG-59 and it has a length from the power combiner to the receiver of $5 \cdot \frac{\lambda}{2} = 24.65 \text{ m}$. The calibrator's noise signal temperature is 25 thousand degrees. The Calibration Wizard calculated the loss of the cables to be 2.25 dB from the antenna terminals to the receiver and using the calibrated noise source signal of the RF2080 C/F unit, which has a temperature of 25 thousand degrees, it scaled the vertical axis of Radio SkyPipe in antenna temperature.

From this point on we were able to obtain and describe our data in a quantitative way, using the antenna temperature at the antenna terminals. The temperature of the background noise for our receiving site was found to be around 50 thousand degrees. According to theory this corresponds to a very radio-quiet site and is almost equal to the galactic background noise level generated by relativistic electrons spiraling in the galactic magnetic field. We can also understand that this is a very low background noise level from the fact that relatively strong solar bursts can exceed 200 thousand degrees in antenna temperature at these frequencies.

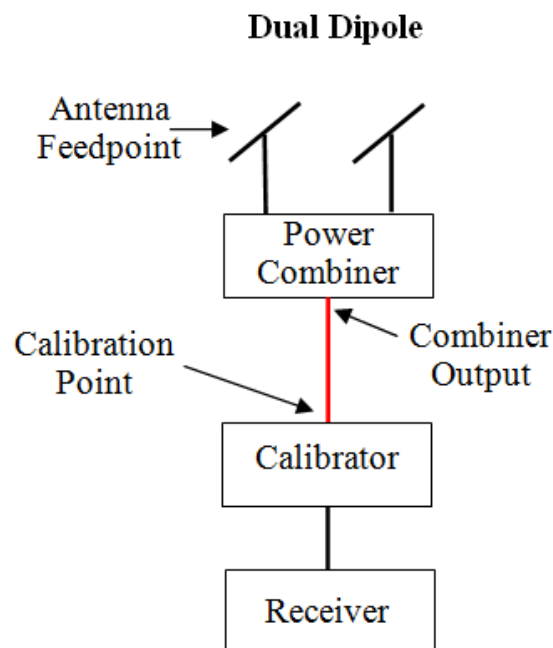


Figure 3.24: The system configuration we used for the calibration of Radio SkyPipe.

Chapter 4

Observations and Results

4.1 Verification of an observation

So far, we have described the system that we built for this thesis project and the potential target radio sources that it can detect in the radio sky. The antenna setup at the observing site finished in the beginning of June 2010 (Figure 4.1). During this month we tested the antenna and the receiver of the telescope and we also conducted some first observations at random time periods during some days to see if everything was working correctly. These observations also helped us check for local or distant interference and understand if the observing site is radio quiet since the RF2080 C/F calibrator wasn't purchased yet.



Figure 4.1: The first observations were conducted with a portable station which we would set up next to the antenna. The masts holding the antenna dipoles can be seen in the background.

By the end of June it became clear that a monitoring station should be installed to record the observations all around the clock. The reason for the round-the-clock monitoring is that solar flares are not predictable and it is difficult to start the system every sunrise and stop it every sunset or use it only at nighttime when Jupiter's radiation could be detected. The round-the-clock monitoring station also helps to find periodical patterns of local or distant interference and thus maybe understand their origin. Guided by these thoughts we proceeded to the installation of the monitoring station. The antenna signal was transferred by a 24.65 m coaxial cable ($5 \cdot \lambda/2$) into the Observatory of the Aristotle University of Thessaloniki where the receiver was installed permanently (Figure 4.2). The receiver was connected to a Personal Computer's sound card and also the required software was installed on the PC's hard drive.

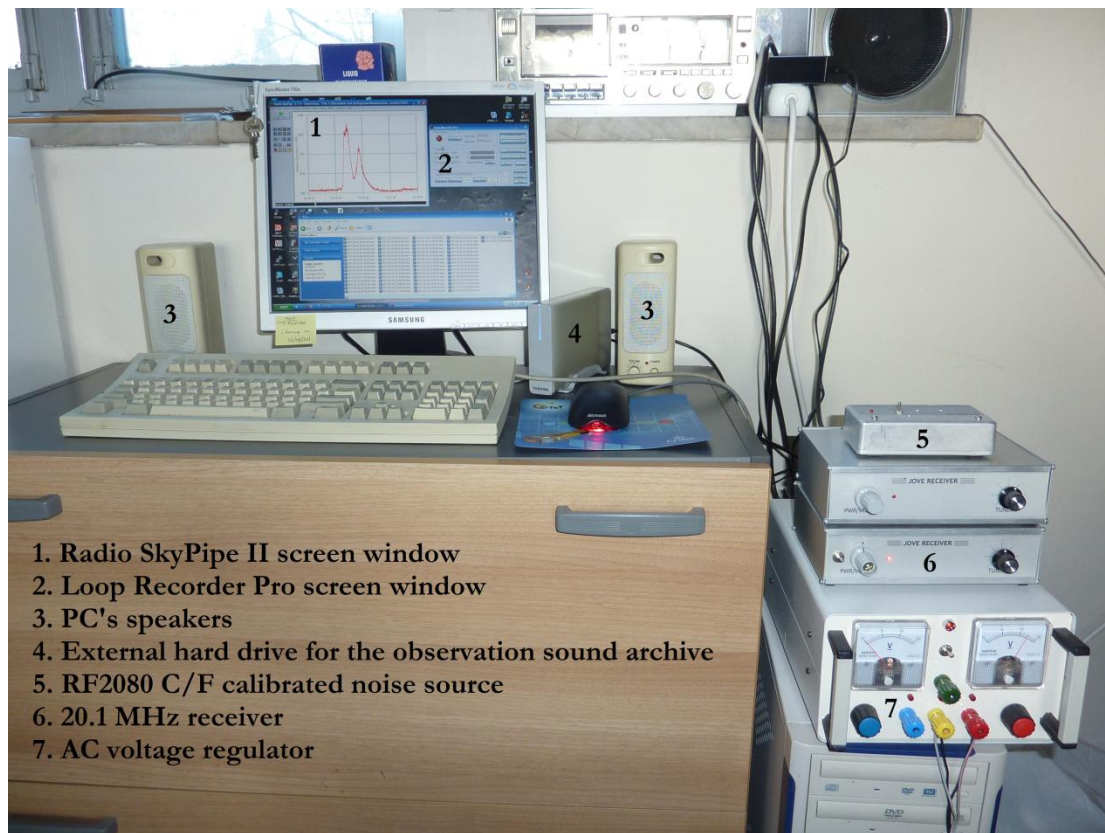


Figure 4.2: The monitoring station permanently installed in the Observatory.

The observations archive consists of the Radio SkyPipe and the Loop Recorder Pro records. A single SkyPipe record duration is 24 hours from the midnight of a day until the midnight of the next one. The Loop Recorder Pro records duration is 11 minutes each, ten of which are present on a single record and one is overlapping with the starting minute of the following record. The file names of these records are named in a practical way as mentioned in the previous chapter for quick access. On the 5th of July 2010 the system started to archive the Radio SkyPipe files first with 3-hour long records and later with records of 24-hour duration. These long records helped in the study of local and distant interference and also in the determination of the background noise level of the observing site.

After a month of observations it became clear that in order to distinguish between solar activity and pure terrestrial interference, an archive of the sound records of our observations should be kept. The sound of each observation turned out to be a definitive aiding tool in the identification of the signal source. The sound that solar bursts produce at the computer's speakers is characteristic and many examples of it can be found online either on the web site of the Radio Jove project or on other web pages which refer to low frequency solar observations. The sound of local interference can vary greatly in its forms but when it is detected it usually has a very precise periodicity, a large signal to noise ratio and in most cases doesn't last for long. Distant interference was also detected especially in the early afternoon hours when the radio telescope detected the signal of a broadcasting shortwave radio station.

The recording and archiving of the large sound-files demanded the installation of an external hard drive on the system's PC. The size of a SkyPipe record for one day is about 12 MB while the size of a sound record for eleven minutes is about 7.5 MB. The installation of the hard drive and the monitoring of the observations' sound started on the 6th of August 2010. After that date, we were able to identify if a signal's source was terrestrial or extraterrestrial simply by searching our archive and listening to the observation sound. The monitoring of the sky hasn't stopped since then except in a few cases, when various problems (usually hardware) showed up, which were usually solved immediately or in the matter of a couple of days at the most. Finally, the RF2080 C/F calibrator was installed on 11/01/2011. After that date our data is properly calibrated and our measurements are expressed in Kelvin of antenna temperature.

The second step in the verification of the signal's source is the correlation of our observations with similar observations from other low frequency observing stations around the world (Figure 4.3). If the source is extraterrestrial, our Radio SkyPipe records should also be monitored by some other stations on Earth and also the sound that our signal produces should be similar. There are many low frequency stations around the world and almost all of them use the Radio Jove project antenna and receiver. Some of these stations publish their successful observations on the Radio Jove Data Archive web site in many forms, like *.jpeg, *.spd and *.wav when sound is available. The web page of the Radio Jove Data Archive is <http://jovearchive.gsfc.nasa.gov/> and it contains a clever search machine for the acquisition of the desired observation (Figure 4.4). Not all the potential solar bursts that we observed were verified by other Radio Jove stations. Although many more seem to be real events we consider as absolutely valid only those verified by other stations.

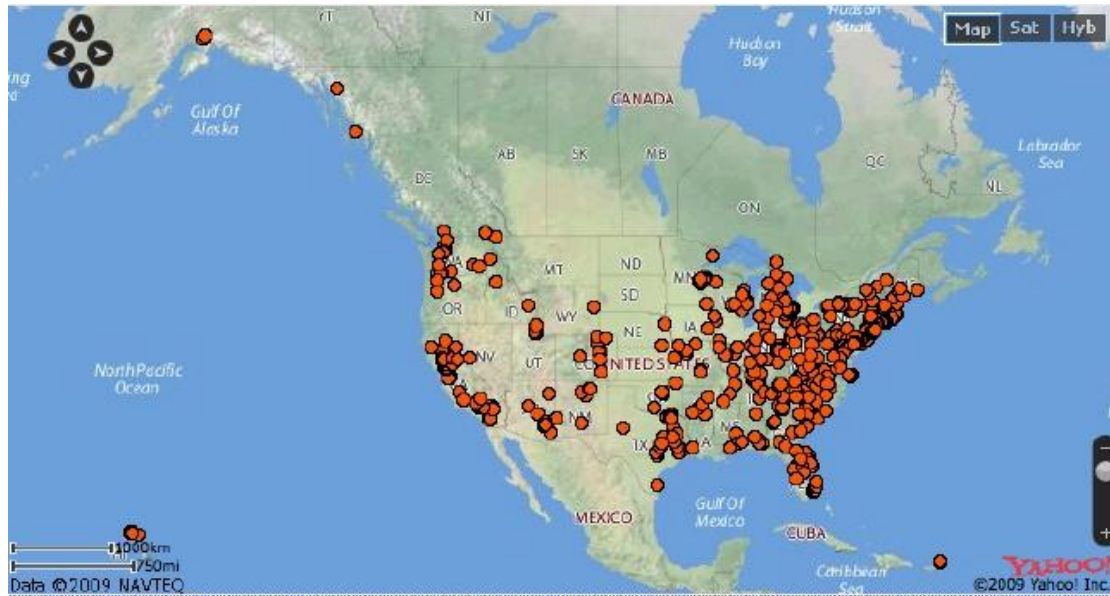


Figure 4.3: The distribution of purchased (not necessary operating) Radio Jove stations in U.S.A.

Finally, the last step for the verification of an observed radio burst as a solar flare was done by checking solar observations in other wavelengths. Flares are multi-frequency phenomena and can be detected on the whole range of the electromagnetic spectrum. We used the data of the Solar Dynamics Observatory (SDO) satellite to acquire a visual image of the flare (Figure 4.5) and the data of the GOES 14 satellite of the National Oceanic and Atmospheric Administration (NOAA) to see if there was an increase in the soft X-ray flux density during the time of the observed radio burst (Figure 4.6). In this way we verified that some of the radio bursts we received at 20.1 MHz were indeed the result of a strong solar flare.

Data Products Key										
 Image File Available  SkyPipe File Available  Text File Available  Sound File Available										
FIRST_NAME	LAST_NAME	SCHOOL/OBS	START_DATE	START_TIME	STOP_DATE	STOP_TIME	OBJECT	STORM_TYPE	FREQUENCY	DATA PRODUCTS
Dave	Typinski	AJ4CO Observatory	01/20/2011	1748	01/20/2011	1752	Sun	Unknown	20.1	  
Dave	Typinski	AJ4CO Observatory	01/20/2011	1748	01/20/2011	1752	Sun	Unknown	18-24	 

Figure 4.4: An example of a Solar radio burst report published on the Radio Jove Data Archive web site.

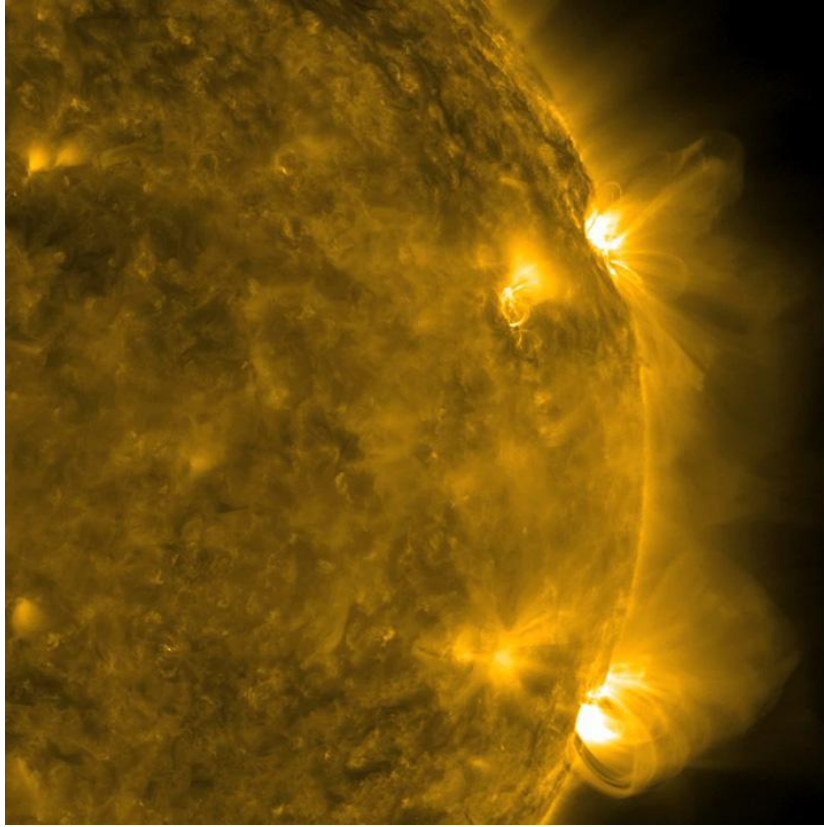


Figure 4.5: SDO has the ability to take high-definition images of the sun. This picture shows two active solar regions.

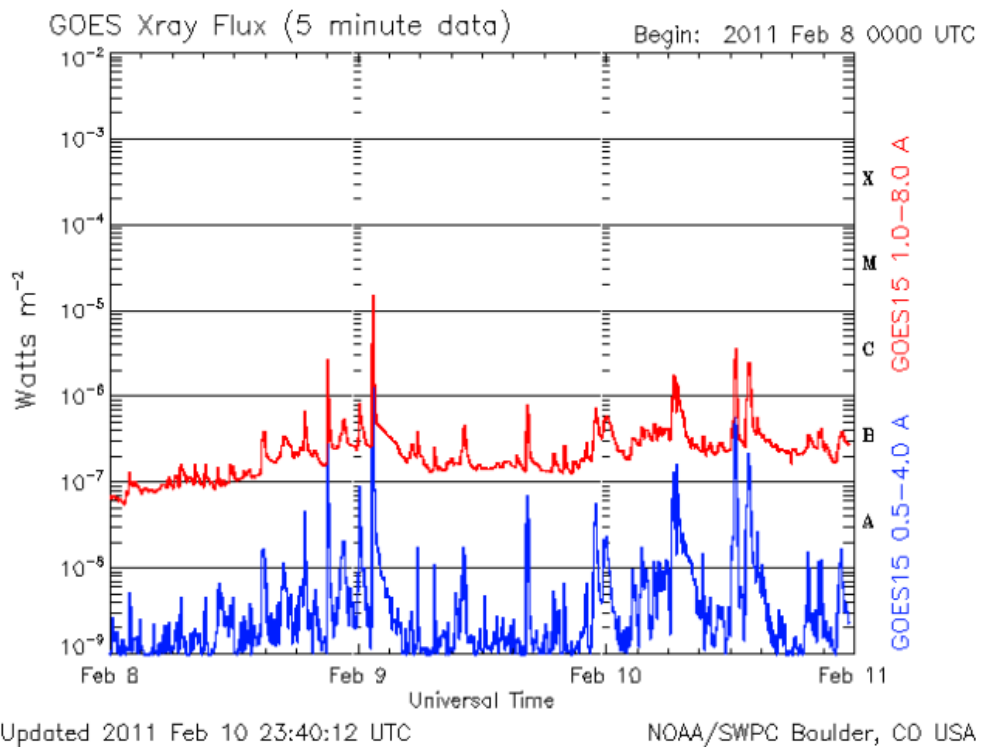


Figure 4.6: NOAA's satellite, GOES 14, monitors the soft X-ray flux density of the sun. The red line corresponds to wavelengths between 1-8 Å while the blue one to 0.5-4 Å.

4.2 Sources of interference

The results described in this diploma thesis refer to the observations we conducted from the beginning of July until the end of October 2010. The system continues the monitoring of radio signals until now and more observations are ready for further analysis. The low background noise levels (~ 50000 degrees) allow the detection of extraterrestrial signals but, except of the use of a narrow filter, there is no method to mitigate interference. During these four months we successfully observed some solar and Jovian radio bursts but we also observed too much interference, local or distant. These interference events can be divided into two categories, the natural ones and these that are caused by manmade devices.

Natural interference includes the physical phenomena on Earth that emit radio signals at low frequencies. The most frequent natural interference that was detected by the radio telescope was caused by thunderstorms, local or distant. At first, when we observed spikes at the SkyPipe record during some nights, we thought that they were caused by Jovian radio emission. However, after checking the Radio Jupiter Pro program, no Jovian emission was predicted for these nights. The answer came from the local weather reports that showed that during these nights local thunderstorms were present in a radius of 200 km around the observing site. The definitive verification of this thunderstorm interference came when we observed the SkyPipe record in real time when a local thunderstorm was present. Every time we saw lightning, a spike showed up in the SkyPipe record. Up to now we have not been able to identify any other natural interference in our records.

Manmade interference are caused by low-power devices such as microwave ovens, computers, printers, disk drives, CRT monitors, mobile phones, TV broadcasting, satellites, wideband metal detectors and other lab equipment that can emit signals strong enough to be detected by a nearby antenna. Low frequency radio signals can be also emitted by poorly-shielded power generators or cars' ignition near the observing site. Although we didn't conduct any detailed study to identify the sources of these local interference sources, it was found that they didn't affect our observations because they were very short in time. The only source of such interference that we might have identified is the motor that opens and closes the dome of the Observatory. Often when the motor was initiated, a spike showed up in the SkyPipe record.

The most important manmade interference that we recorded every day was a strong international broadcasting shortwave radio station. This station belongs to the 13m shortwave band. The signal of this station was extremely strong preventing the detection of even strong solar bursts when it was present. We received the radio station broadcast for a certain period of time every day. During this period we could not accept as valid any solar bursts that happened to take place. The radio station interference lasted from about 09:30 until 15:00 UT every day. During this interval we could clearly hear voices and music!

After some online search and using the information that we could hear from the broadcast, it was found that the radio station was the International Mediterranean Radio broadcasting from Morocco at 21.7 MHz. We suppose that the fact that we could hear the station at the frequency of 20.1 MHz is due to the ionosphere's electron density at that point of the day which was able to reflect the signal from the station and send it back to our radio telescope. The International Mediterranean Radio has two antennas of 250 kW each to transmit its signal. During the broadcast no extraterrestrial signal could be detected resulting in a couple of useless observing hours every day (Figure 4.7).

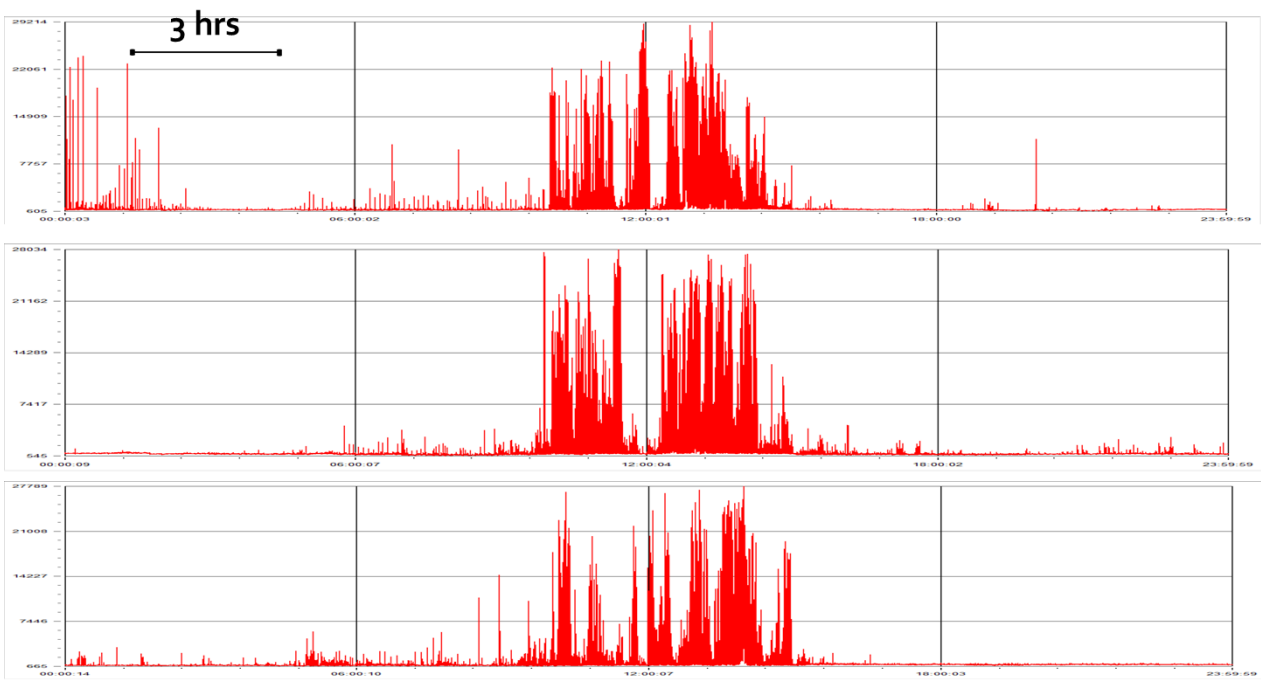


Figure 4.7: The Radio SkyPipe records of three successive days from top to bottom. The middle part of each record is strong interference from a shortwave radio station in Morocco. Solar radio bursts have much smaller signal to noise ratio. The spikes in the top left were caused by a local thunderstorm.

After the installation of the RF2080 C/F calibrator and its narrow band filter, this interference was mitigated at large.

4.3 Solar observations

From the start of July until the end of October 2010 we observed more than 20 potential solar radio bursts, 15 of which were verified by other low frequency observing stations around the world. Three of these bursts were also verified by observations in other wavelengths and specifically by the SDO and GOES 14 satellites in visual and X-rays respectively. Some of these bursts are described below in detail.

On the 1st of August 2010 a strong solar flare was observed on the photosphere of the sun. On that day, the record we obtained with Radio SkyPipe showed a big raise of the radio noise between 14:15 and 14:19 UT. This signal was caused by a type III radio burst that happened on the sun and it was also reported by NOAA. The signal to noise ratio (SNR) of the observed burst was ~ 35 . The calibrator wasn't installed at the time but

if we consider that the background noise level was measured to be around 50 thousand degrees, the peak of the burst should correspond to an antenna temperature of $\sim 260 \cdot 10^3$ K.

The observed burst was verified by the corresponding observation of Hawk's Nest Observatory at Pennsylvania, USA. This observatory uses the same equipment as ours for low frequency solar observations. The sun was low in the horizon for that Observatory at the time of the burst occurrence, meaning that it was almost outside the main lobe of the radio telescope. This resulted in an observation with smaller SNR than ours for which the sun was inside the main lobe of our telescope. This is a proof that the side-lobes of the telescope have smaller gain than its main lobe. The two observation records can be seen in Figure 4.8.

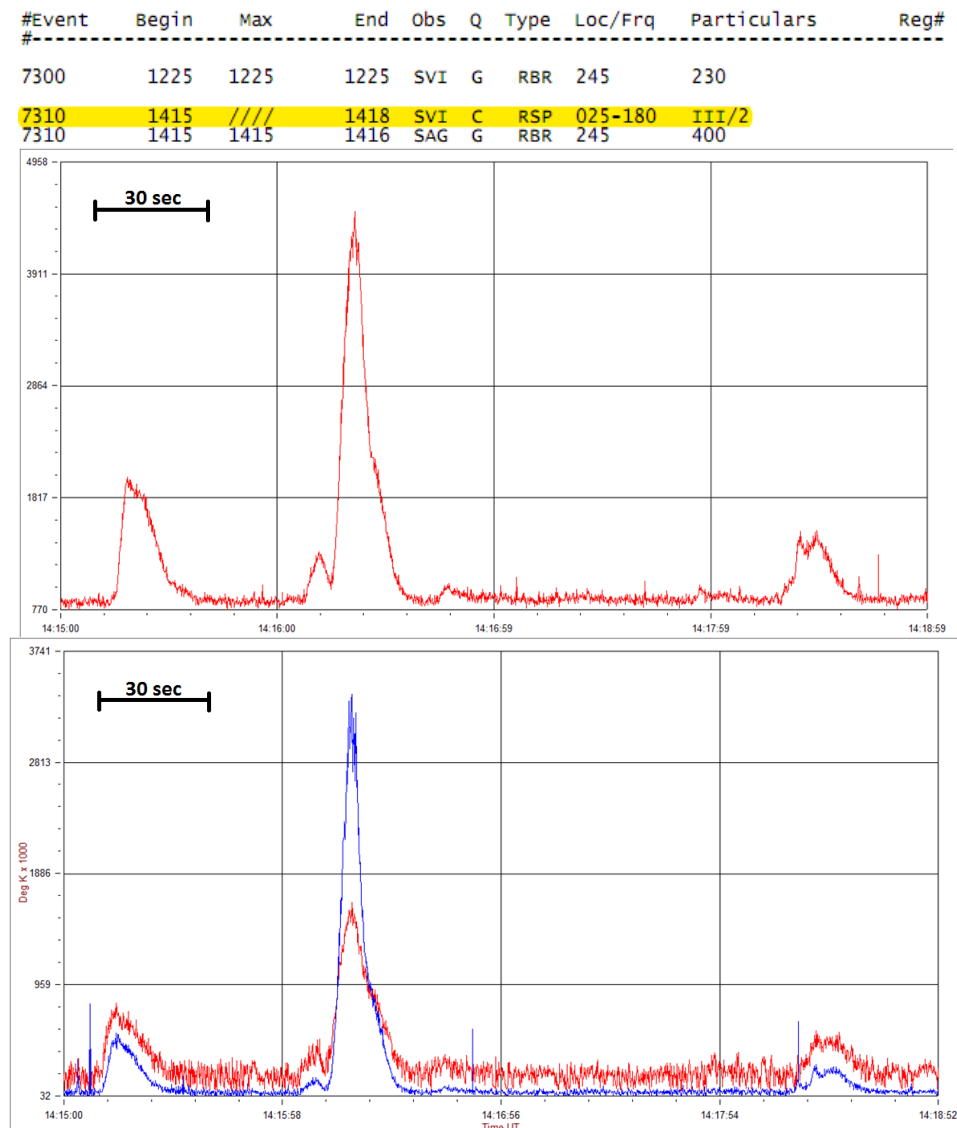


Figure 4.8: The solar burst of the 1st of August 2010. Our SkyPipe record is in the top and the one of Hawk's Nest Observatory at the bottom. The red line corresponds to 20.1 MHz radio waves received by a Radio Jove dual dipole antenna. It is clear that we have a much sharper observation because the sun was located inside the main beam of our radio telescope while it was located inside a side lobe of Hawk's Nest Observatory telescope. The blue line corresponds to 20.1 MHz again but another type of antenna is used (Yagi). The NOAA's report of the event can be seen in the top of the picture.

Another successful solar observation that we conducted is that of the 17th of October 2010. NOAA's report of that day showed that a strong flare (C1.7) occurred on the sun followed by radio bursts of type III and V near the sunspot region 1112. The report as well as the soft X-rays flux density of that day recorded by the GOES 14 satellite can be seen in Figure 4.9. The flare was also visible by the SDO satellite as a sudden increase in the intensity of the photosphere (Figure 4.10). Our SkyPipe record of this flare can be seen in Figure 4.11. The SNR of the burst was ~ 47 and the antenna temperature at the peak of the burst was ~ 185 thousand degrees.

Event	Begin	Max	End	Obs	Q	Type	Loc/Frq	Particulars	Reg#
6790 +	0826	0830	0833	G14	5	XRA	1-8A	B1.7 4.8E-05	1112
6800 +	0852	0859	0908	G14	5	XRA	1-8A	C1.7 1.1E-03	1112
6800 +	0855	////	0856	SVI	C	RSP	025-180	III/1	1112
6800 +	0856	////	0858	SVI	C	RSP	025-180	V/2	1112
6800 +	B0906	U0907	A0928	SVI	3	FLA	S19W31	SF ERU	1112

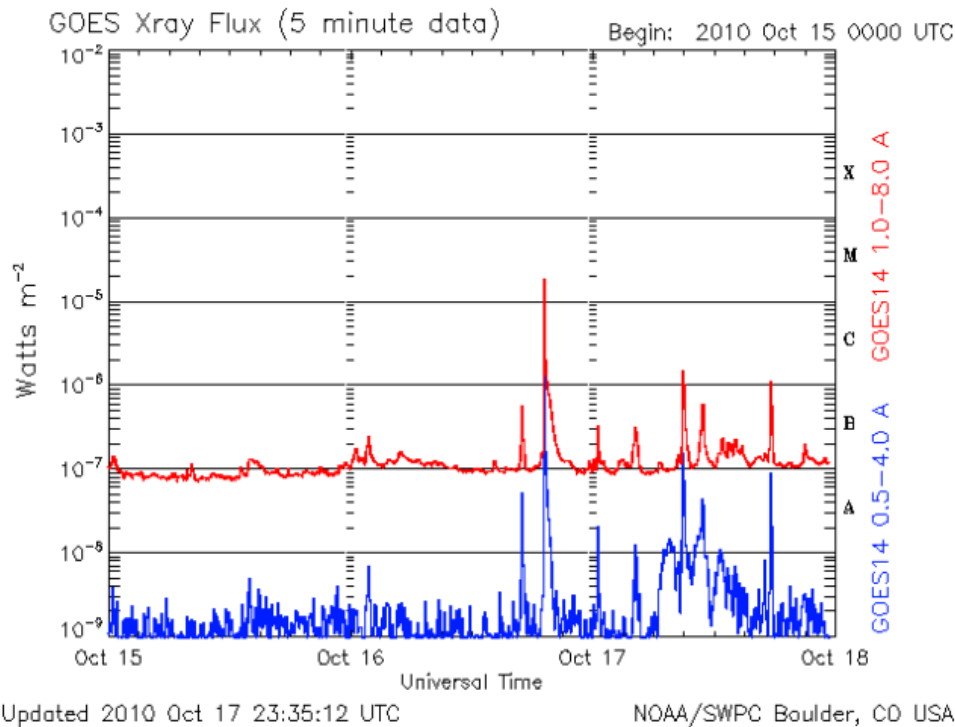


Figure 4.9: NOAA's report and the soft X-ray flux density of the event on the 17th of October 2010. The report includes both the X-ray and the radio bursts which are highlighted. The event is expressed by the first spike between Oct 17 and Oct 18 in the X-ray flux density plot at the bottom.

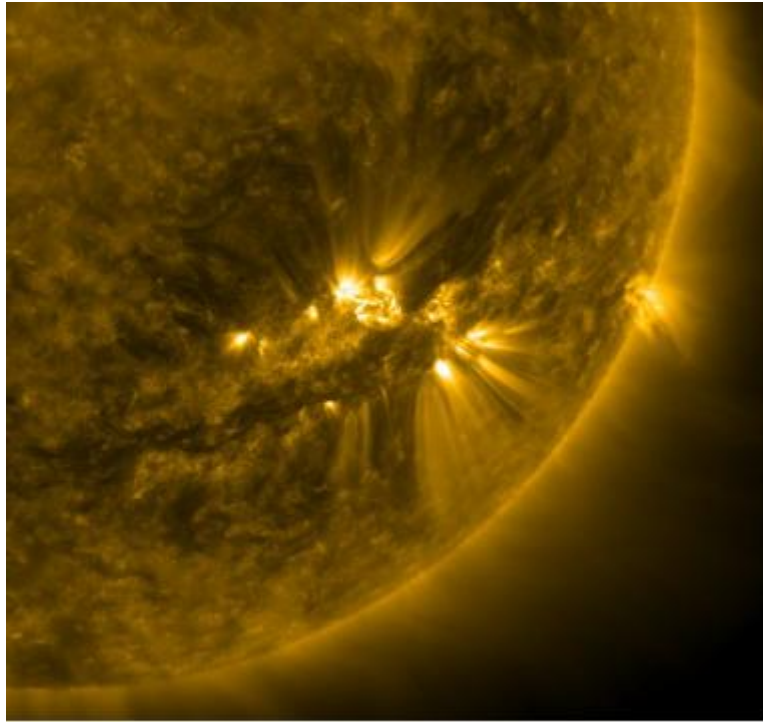


Figure 4.10: A picture of the active region 1112 at 08:48 UT on the 17th of October 2010, observed by the SDO satellite.

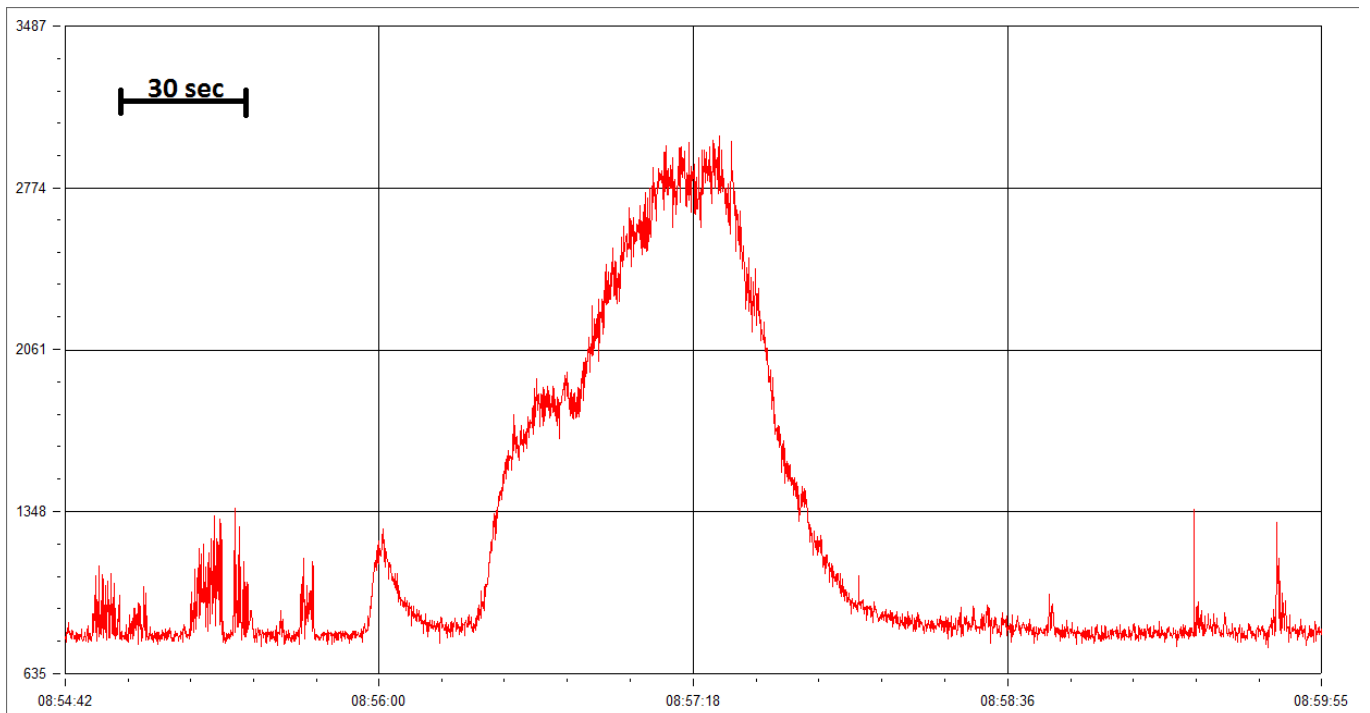


Figure 4.11: Our SkyPipe record of the event on the 17th of October 2010.

The best solar observation reduced so far for the thesis is the one on the 14th of August 2010. That is because we have both the observation's graphical pattern acquired by the Radio SkyPipe program and its sound recorded by Loop Recorded Pro. It is a strong solar flare (C4.4) followed by a radio burst of type II near the sunspot region 1099. NOAA's report and the plot of the soft X-rays flux density of that day can be seen in Figure 4.12. The event was also recorded by the SDO satellite in a beautiful sequence of pictures (Figure 4.13). The type II radio burst that we recorded lasted about 5 minutes and its graphical pattern can be seen in Figure 4.14. The SNR of our recording of the burst was ~ 62 and the antenna temperature at the peak of the burst pattern was $\sim 240 \cdot 10^3$ K.

#Event	Begin	Max	End	Obs	Q	Type	Loc/Frq	Particulars	Reg#	
2540 +	0938	1005	1031	G14	5	XRA	1-8A	C4.4	9.9E-03	1099
2570	0939	1000	1030	SVI	3	FLA	N11W53	SF	ERU	1093
2540 +	0941	0959	1110	SVI	3	FLA	N17W52	SF	ERU	1099
2540	0952	////	1009	SVI	C	RSP	30-80	II/1	406	1099

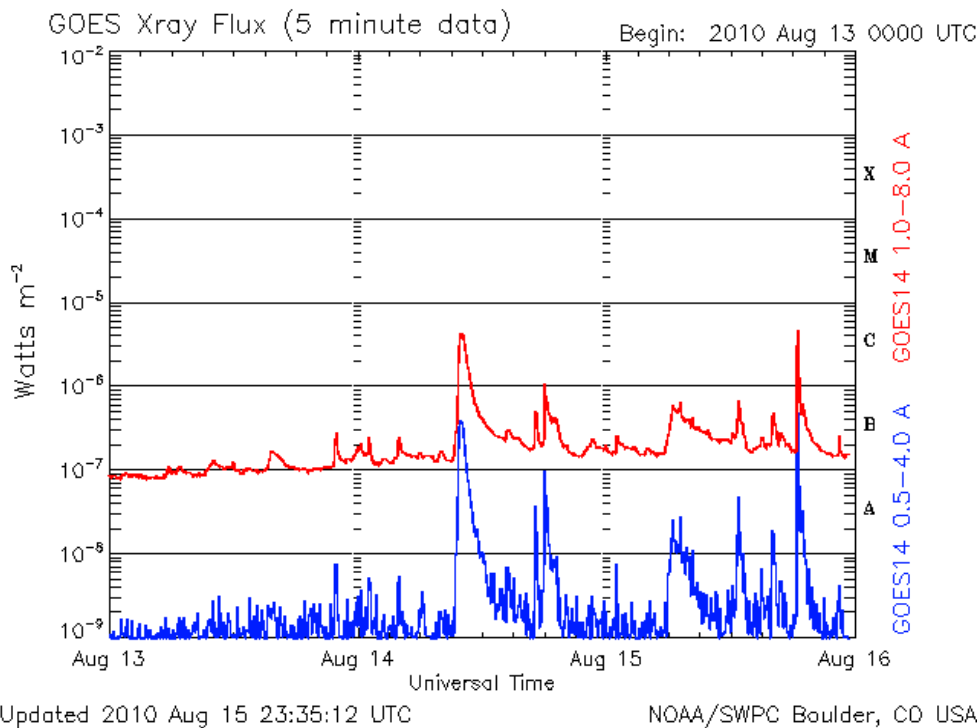


Figure 4.12: NOAA's report and the soft X-ray flux density of the event on the 14th of August 2010. The report includes both the X-ray and the radio bursts. The event is expressed by the big raise of the red line between Aug 14 and Aug 15 in the X-ray flux density plot at the bottom.

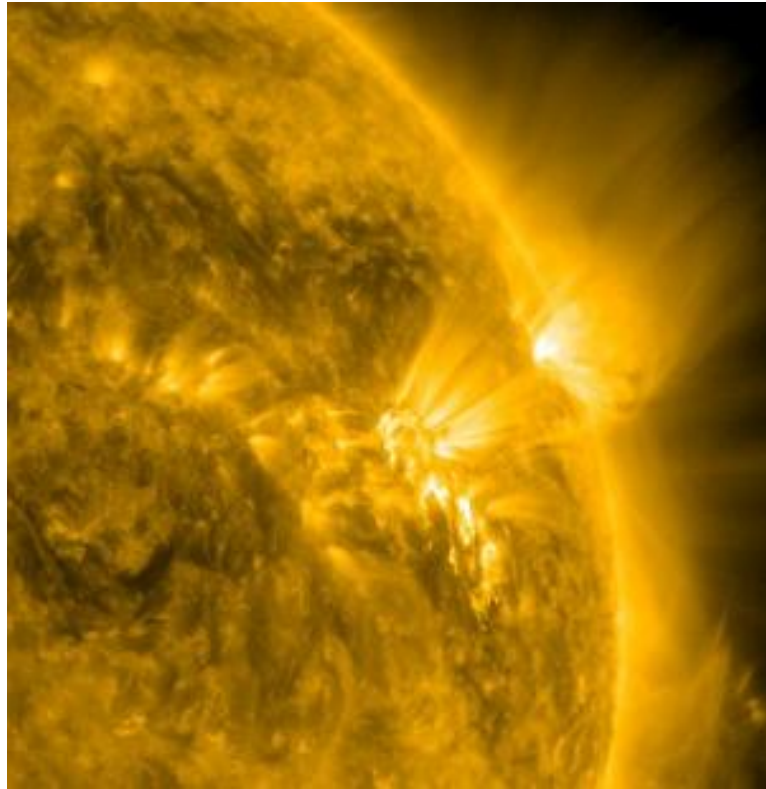


Figure 4.13: A picture of the active region 1099 at 10:00 UT on the 14th of August 2010. It was taken by the SDO satellite.

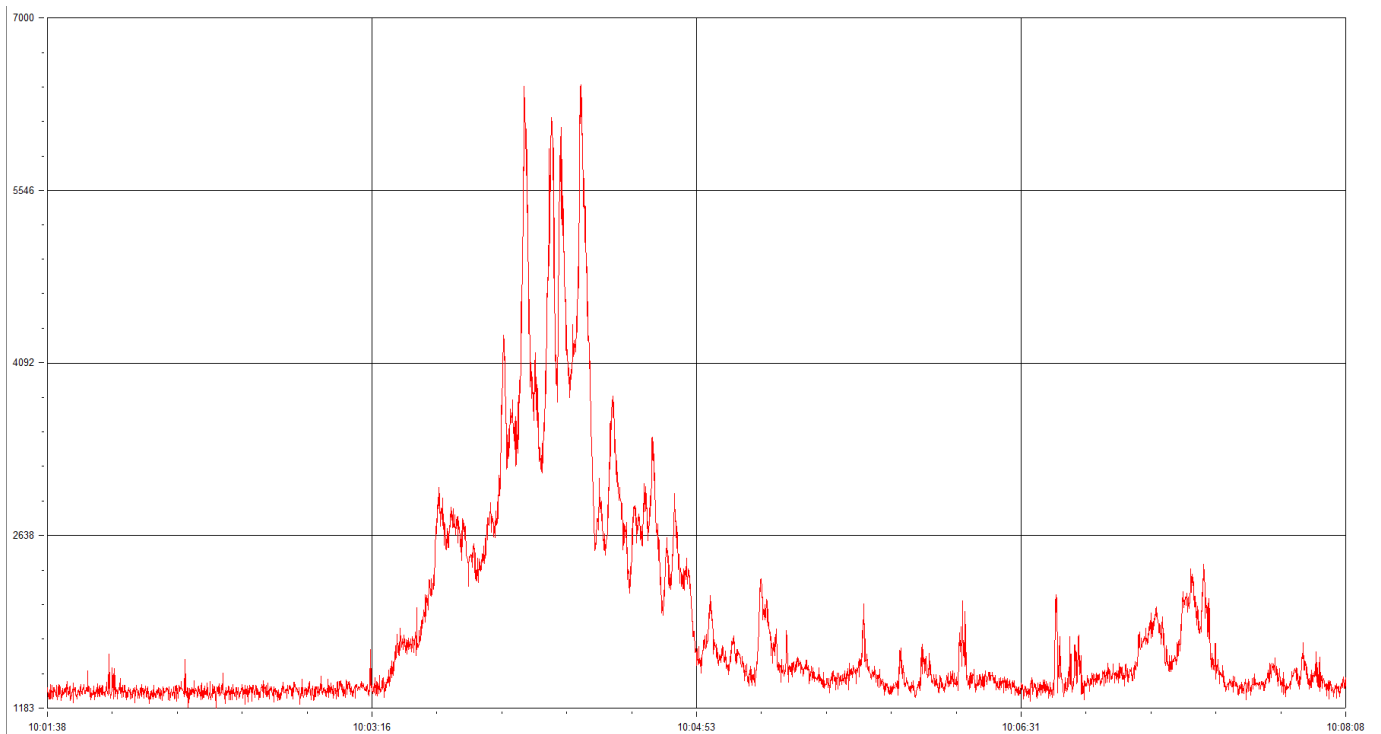


Figure 4.14: Our SkyPipe record of the event on the 14th of August 2010.

Some other verified solar radio bursts accompanied by their pattern can be seen in Figures 4.15 – 4.18. The verification of these observations was done by NOAA’s reports of the radio and X-ray bursts.

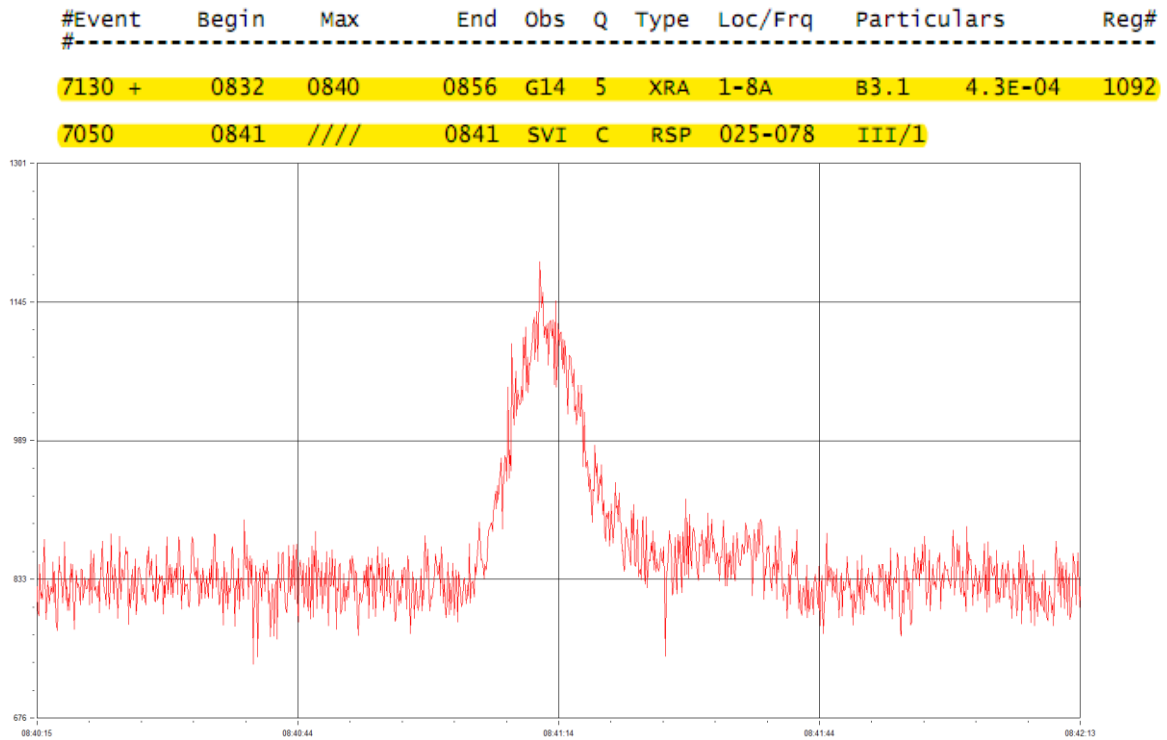


Figure 4.15: A type III solar radio burst as recorded on the 31st of July 2010. The SNR is ~18 and the maximum antenna temperature $\sim 71 \cdot 10^3$ K.

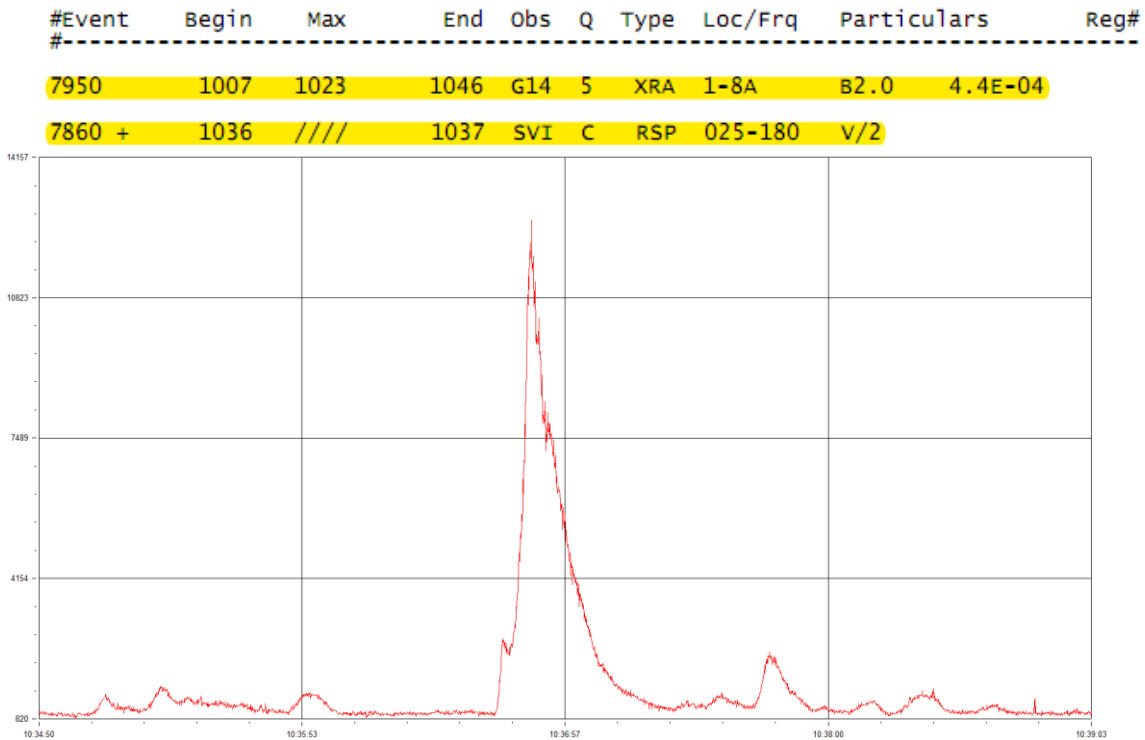


Figure 4.16: A type V solar radio burst as recorded on the 3rd of August 2010. The SNR is ~131 and the maximum antenna temperature $\sim 632 \cdot 10^3$ K.

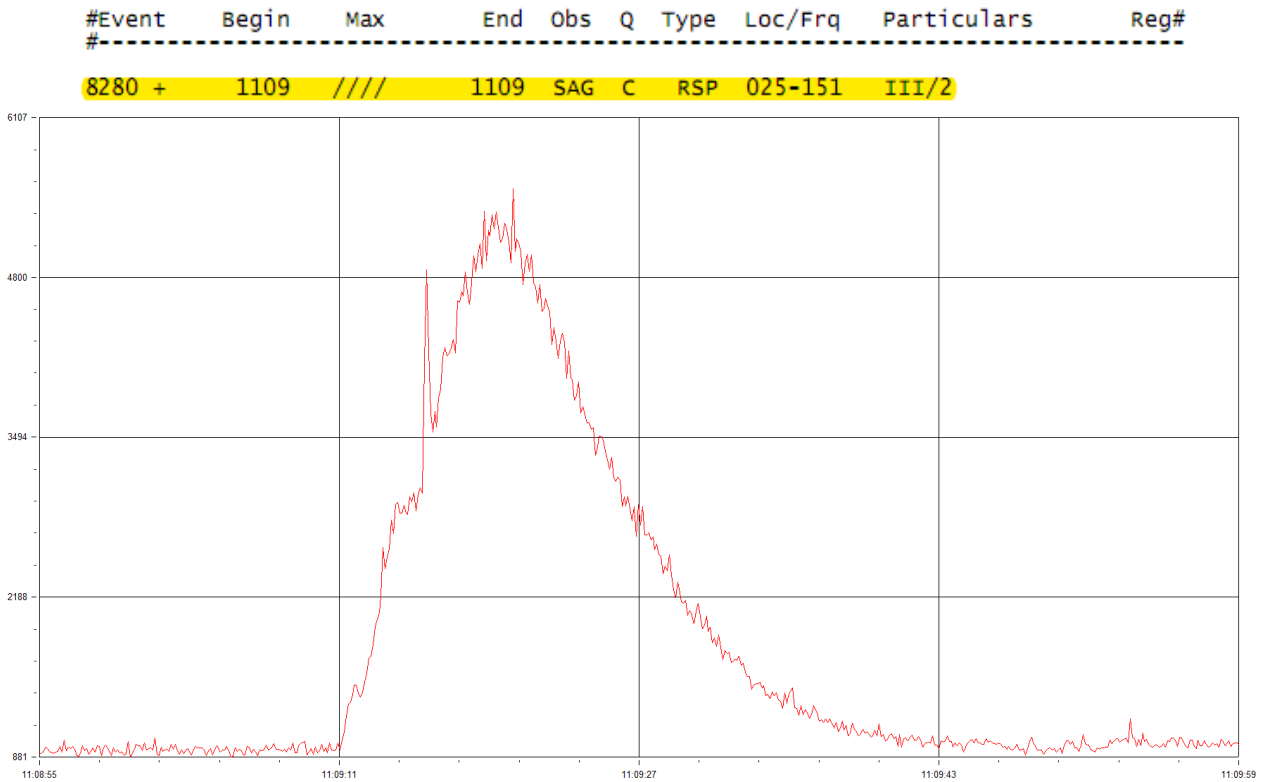


Figure 4.17: A type III solar radio burst as recorded on the 5th of August 2010. The SNR is ~ 92 and the maximum antenna temperature $\sim 292 \cdot 10^3$ K.

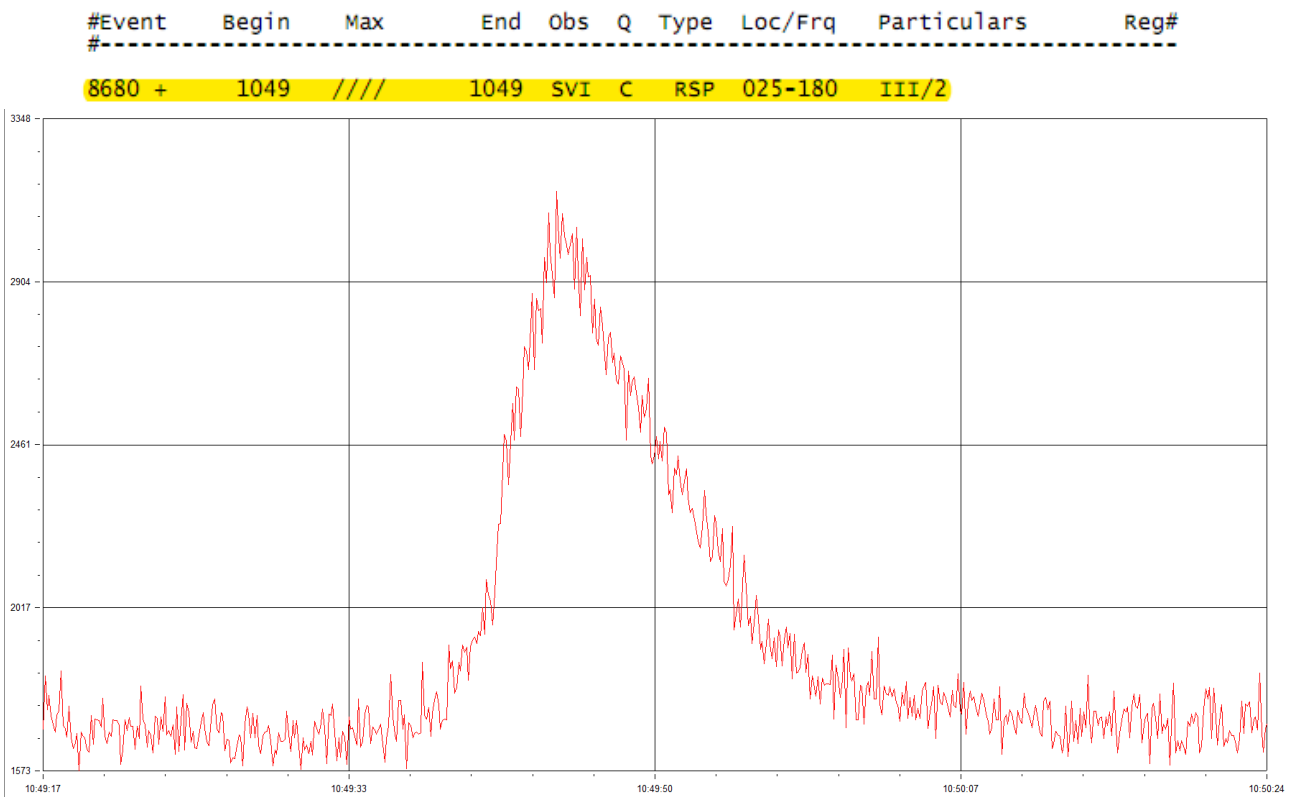


Figure 4.18: A type III solar radio burst as recorded on the 9th of August 2010. The SNR is ~ 25 and the maximum antenna temperature $\sim 93 \cdot 10^3$ K.

4.4 Jovian observations

The radio quiet observing site that we set up our antenna offers us the opportunity to observe Jovian decametric radiation during some nights. Jovian radio burst verification has an advantage and a disadvantage compared with that of a solar radio burst. The advantage is that the time when these bursts occur is not entirely unpredictable like the solar bursts. These bursts occur mainly when Io happens to be at a certain Jovian longitude (see §2.5). The program we used to verify if some nighttime spikes in the SkyPipe graphs were produced by Jovian bursts is the Radio Jupiter Pro 3, provided by the Radio Jove project. This program can predict Io and non-Io Jovian radiation for a given date.

The disadvantage is that the Jovian emission cannot be detected at frequencies higher than 40.5 MHz and we couldn't verify the observations with observations in different wavelengths. The method we used for the verification of our Jovian observations except for the Radio Jupiter Pro predictions is by comparing our observations with similar observations around the world at 20.1 MHz through the Radio Jove Data Archive web page. The problem is that there aren't many Radio Jove stations in Europe and the archived Jovian observations from stations in the USA could not be detected from our observing site because of the large time difference. Finally, the verification of a Jovian observation can be done by its sound which is characteristic for Jovian L and S bursts. Sound samples of L or S bursts can be found again online.

A successful Jovian observation that was also verified by a Radio Jove station at Nice, France is that of the 13th of August 2010. The Radio Jupiter Pro program predicted Io-B radiation for the first hours of that day, between 00:20 and 03:23 UT (Figure 4.19). The Radio SkyPipe records of that period of time for our station and for Nice can be seen in Figure 4.20. The spikes of the observation are Jovian Io-B radiation and this can be verified by the sound they produce. That sound is similar to the one recorded at the Nice station which was also published in the Radio Jove Data Archive web site. The observation, from its sound pattern, can be classified as an S burst. It should be mentioned that not all predicted Jovian radiation can be detected, because its occurrence depends on many different factors not all of them known yet and fully understood.

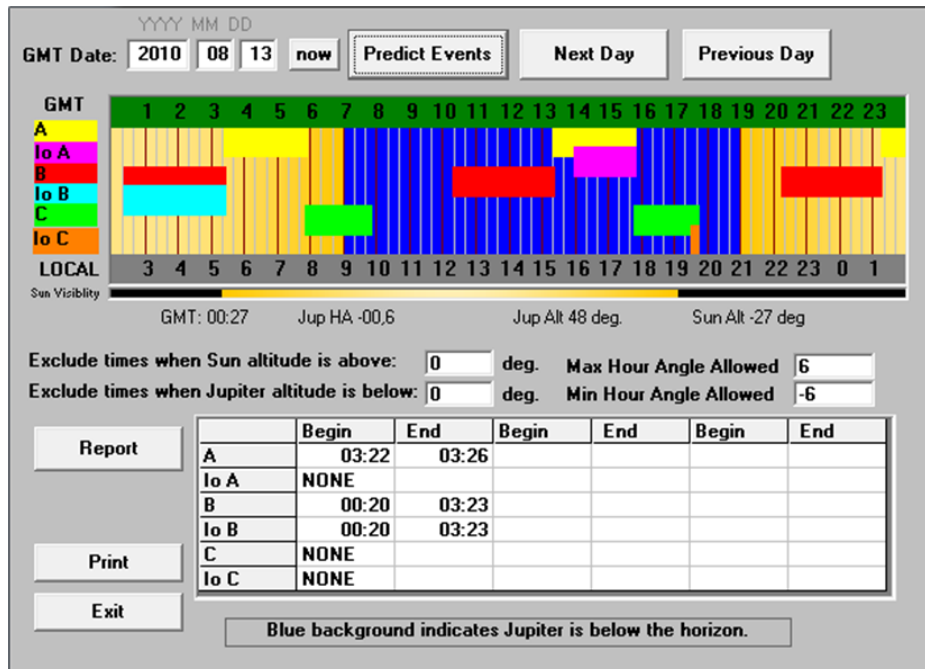


Figure 4.19: The prediction of Radio Jupiter Pro for Jovian Io B radiation on the 13th of August 2010.

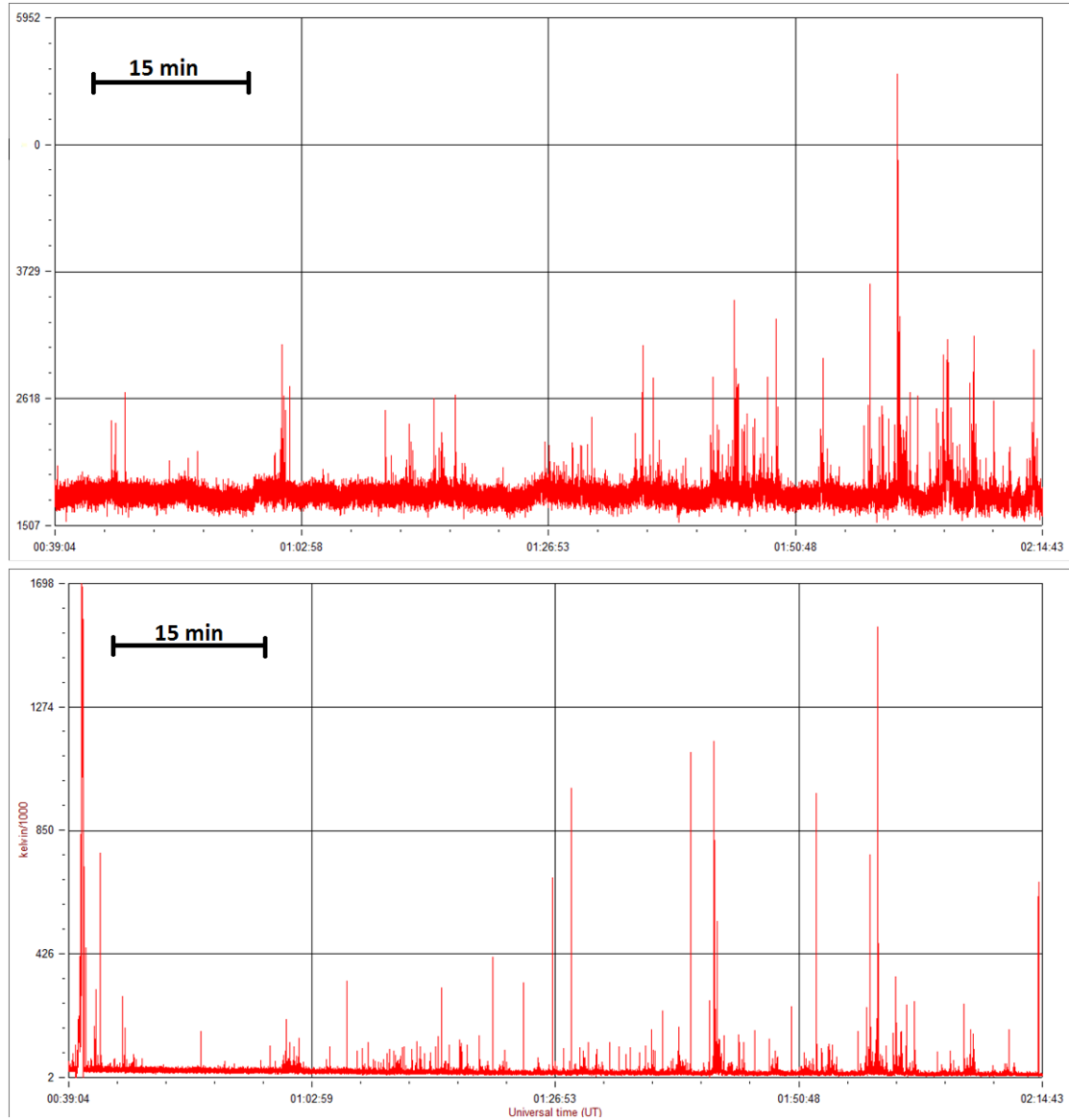


Figure 4.20: The Jovian Io B bursts of the 13th of August 2010. Our SkyPipe record is in the top and the one of Nice's Observatory at the bottom. Both the observatories use similar equipment.

4.5 Conclusions

The goal of this Diploma thesis was the construction and installation of a low frequency radio telescope working at the frequency of 20.1 MHz and based on NASA's Radio Jove project design. Furthermore, a monitoring station was set up in the Observatory of the Aristotle University of Thessaloniki for the continuous observation of the radio sky. To sum up the results of the project:

1. We set up a dual dipole phased array antenna in a “meridian telescope” design for the observation of the sun and Jupiter (Figure 4.21).
2. We constructed a radio receiver working at 20.1 MHz with the help of the Electronics Lab of the Argelander Institute of Astronomy of the Friedrich Wilhelm University of Bonn.
3. We set up a monitoring station at the Observatory of the Aristotle University in Thessaloniki, Greece which consists of a dual dipole phased array, a 20.1 MHz radio receiver and a dedicated computer with the necessary software installed.
4. We calibrated our system to know the exact observing frequency with the help of the Electronics Lab of the Aristotle University of Thessaloniki and also we calibrated the system to produce the results in antenna temperature with the help of the calibrated noise source RF2080 C/F.
5. We observed many solar radio bursts and verified these observations with other projects that monitor the sun, like NASA's Solar Dynamics Observatory (SDO) – Figure 4.22 and the GOES 14 satellite (Figure 4.23) of the National Oceanic and Atmospheric Administration (NOAA). The verification also included comparison of our observations with similar observations conducted by other low frequency radio telescopes around the world.
6. We observed some Jovian radio bursts and verified these observations with others, mostly low frequency European radio observations posted in the Internet.
7. We have created a large archive of observational data from the beginning of July 2010 until February 2011. The monitoring station continues to observe and archive data which are in the process of being reduced.

8. Furthermore, the signal is converted to audio in order to exclude radio interference.

The monitoring station built for this Diploma thesis project is encouraged to remain in the Observatory for further radio observations to be conducted also by other Astronomy students of the Physics Department of the Aristotle University of Thessaloniki. An interesting advancement of the equipment would be a setup of a second dual dipole antenna for the conduction of interferometric observations at 20.1 MHz, or at a different, higher frequency, in order to calculate spectral indices and exclude narrow band interference.

The current equipment is also an educational tool for Radio Astronomy. It can be used by students to learn the basics of Radio Astronomy by studying radiowaves from Jupiter and the sun. In fact, Radio Jove project offers a number of lesson plans for this purpose. Students can also learn the operation of a radio receiver by studying the receiver built for this project. This radio telescope offers a hands-on experience for students interested in radio astronomy to conduct their own observations of the radio sky and also understand how a radio telescope works, because they can see and study its electronics in detail.



Figure 4.21: During the setup of the antenna in the backyard of the Observatory.

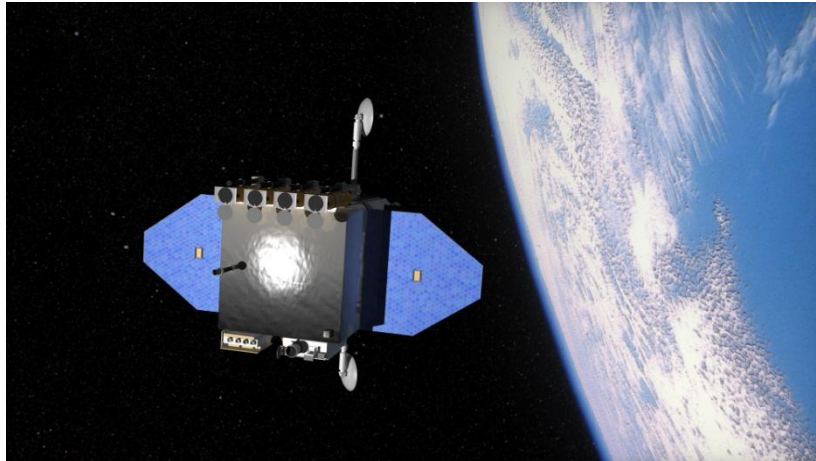


Figure 4.22: The satellite of the NASA's SDO project.



Figure 4.23: The GOES 14 satellite of NOAA. A picture of its construction can be seen on the left.

Bibliography

1. *NASA's Radio JOVE Project*. [Online] <http://radiojove.gsfc.nasa.gov/>.
2. *Fringe Dwellers - Simple Radio Interferometry*. [Online] <http://fringes.org/>.
3. *SpaceWeather.com*. [Online] <http://www.spaceweather.com/>.
4. *SpaceWeatherLive.com*. [Online] <http://www.spaceweatherlive.com/>.
5. *NOAA's Solar Events Report*. [Online] <http://www.swpc.noaa.gov/ftpmenu/indices/events.html>.
6. *SDO | Solar Dynamics Observatory*. [Online] <http://sdo.gsfc.nasa.gov/>.
7. *Hawk's Nest Radio Astronomy Observatory*. [Online] <http://home.comcast.net/~starmanjb/dual.html>.
8. *Nice Observatory*. [Online] <http://rulivas.pagesperso-orange.fr/documentation.htm>.
9. *Radio JOVE Data Archive*. [Online] <http://jovearchive.gsfc.nasa.gov/>.
10. *Solar Monitor*. [Online] <http://www.solarmonitor.org/>.
11. *Thessaloniki Lightning Detection Station*. [Online] http://www.sv2bzq.gr/hystory_weather/stormvue.html.
12. [Online] http://en.wikipedia.org/wiki/Dipole_antenna.
13. *LOFAR*. [Online] <http://www.lofar.org/>.
14. *RadioJove at the International Space University*. [Online] <http://astro.u-strasbg.fr/~koppen/RJove/>.
15. *National Radio Astronomy Observatory (NRAO)*. [Online] <http://www.nrao.edu/>.
16. *Max Planck Institute of Radio Astronomy*. [Online] <http://www.mpifr-bonn.mpg.de/>.
17. *Argelander Institute for Astronomy*. [Online] <http://www.astro.uni-bonn.de/>.
18. *Section of Astrophysics, Astronomy and Mechanics of the Aristotle University of Thessaloniki*. [Online] <http://www.astro.auth.gr/>.
19. **Flagg, Richard S.** *JOVE RJ1.1 Receiver Kit Assembly Manual*. [Online] 2010. http://radiojove.gsfc.nasa.gov/telescope/rcvr_manual.pdf.
20. **Team, Radio JOVE Project.** *Radio JOVE RJ1.2 Antenna Kit Assembly Manual*. [Online] December 2004. http://radiojove.gsfc.nasa.gov/telescope/ant_manual.pdf.

21. **Associates, RF.** *RF 2080 C/F Manual*. [Online] January 2010.
radiojove.gsfc.nasa.gov/telescope/RF%202080%20Manual.doc.
22. **Seiradakis, John H.** *Introduction to Radioastronomy*. Thessaloniki : Planetario Publications, 2009. ISBN: 978-960-89049-7-2.
23. **Kraus, John D.** *Radio Astronomy*. Delaware, Ohio : Cygnus-Quasar Books, 1986. Library of Congress Catalog Card Number: 86-70011.
24. **Klein, Ulrich.** *Radio Astronomy: tools, applications and impacts*. Bonn : Argelander Institute of Astronomy, 2006.
25. **Wilson, Thomas L., Rohlfs, Kristen and Huttemeister, Susanne.** *Tools of Radio Astronomy*. Berlin, Heidelberg : Springer-Verlag, 2009. ISBN: 978-3-540-85121-9.
26. **French, Robert S.** An Urban Radio Telescope for Jovian and Solar Emissions at 20.1 MHz. *Swinburne Astronomy Online*. [Online] November 2009.
<http://rfrench.org/astro/papers/P143-HET608-RobertFrench.pdf>.
27. **Atiani, Samer.** *Bachelor Thesis: Constructing a Radio Interferometer*. Guilford College : s.n., 2006.
28. *Report of a simple 2-Element Solar Radio Interferometer at Bleien Observatory.*
Monstein, C. and Meyer, H. Zurich : Physics, Astronomy and Electronics Work Bench, 2006.